

# Vented gas and dust explosions

*External explosions*

**Mads-Jørgen Klausen**



**Master thesis submitted as part of the degree**  
Master of Science in Process Safety Technology

UNIVERSITY OF BERGEN

[01.06.2016]



# Abstract

The use of explosion venting is a widely applied safety measure, mitigating the effects of an internal gas and dust explosion. Implementation of this safety measure does however not eliminate all risks and hazards associated with these explosions. By venting an internal explosion to the outside one introduces hazards to the areas surrounding the vented enclosure. A theoretical study of vented explosions, along with the relation between the internal and external explosion, has been performed identifying the characteristics and effects of these.

Applicability and limitations when using empirical expressions for predicting external phenomena associated with vented explosions has been discussed. Representing an alternative prediction method, the use of the CFD software FLACS to accurately predict explosion characteristics has been investigated. This has been achieved by simulating previous experimental work. Evaluation of obtained predictions has been performed discussing the ability to represent similar events, values and processes as those recorded experimentally. A possible approach for obtaining agreeing predictions has been assessed. The use of CFD for simulating scenarios as those investigated has shown to be promising, however, a continued investigation of these results is necessary due to strong sensitivity observed for fundamental simulation settings.

*Keywords:* Vented gas explosions, vented dust explosions, external explosions, CFD, Dust-Ex



# Acknowledgment

I would like to express my gratitude to the following:

My supervisors: Kees van Wingerden, Bjørn Johan Arntzen and Jon-Thøger Gjøvåg Hagen, for awakening my interest for the subject, your guidance and for encouraging me when my motivation has been low.

Helene Hisken for taking the time to discuss occurring topics, and providing valuable advice.

Gexcon AS for allowing me to carry out my thesis in collaboration with them, and to benefit from their expertise and knowledge.

My family, especially my parents, Inger Johanne and Gjert, for unconditional and continued support.

My girlfriend, Siv Grinde, for care and support, especially since circumstances normally should require you to be the recipient of this.

My employer, FLO MARKAP STA for allowing me to take time off work to pursue a master's degree. It would have been considerably more difficult if I had not been granted this opportunity.

To my fellow students, for sharing good experiences, both educational and social.

## Nomenclature

$a$	- acceleration [m/s <sup>2</sup> ]
$A_v$	- vent area [m <sup>2</sup> ]
$(dP/dt)_{max}$	- maximum rate of pressure rise [bar/s]
$E_r$	- equivalence ratio [-]
$F$	- force [N]
$l_s$	- turbulence length scale [m]
$L_{f, max}$	- maximum flame length [m]
$m$	- mass [kg]
$n$	- number of moles [-]
$P_{max}$	- maximum pressure in unvented vessel [bar, mbar, kPa]
$P_{red}$	- pressure in vented vessel [bar, mbar, kPa]
$P_{red, max}$	- maximum overpressure within vented chamber [bar, mbar, kPa]
$P_{r, max}$	- pressure at any distance, $r$ , from the vent, where $r$ is greater than $R_s$ [bar, mbar, kPa]
$P_{stat}$	- pressure in which vent panel releases [bar, mbar, kPa]
$P_{s, max}$	- maximum external overpressure [bar, mbar, kPa]
$P_{vf}$	- dispersion pressure, pressure applied for dispersion of dust [bar, mbar, kPa]
$r$	- external distance from vent opening [m]
$R_s$	- the distance from the vent, at which the maximum external overpressure occurs [m]
$RTI$	- relative turbulence intensity [-]
$U$	- characteristic velocity [m/s]
$V$	- volume of vessel [m <sup>3</sup> ]
$\lambda$	- equivalence ratio [-]

## Abbreviations

CAD	- Computer-Aided Design
CASD	- Computer Aided Simulation Design
CFD	- Computational Fluid Dynamics
DESC	- Dust Explosion Simulation Code
Eq	- equation
FLACS	- Flame Accelerator Simulator
L/D	- length to diameter relation
No	- number
LFL	- lower flammability limit
UFL	- upper flammability limit

# Table of content

1	Introduction .....	1
1.1	Background .....	1
1.2	Explosion in process industries .....	2
1.2.1	Definition of gas and dust explosion .....	2
1.2.2	Relevance to which industries .....	2
1.2.3	Gas and dust explosions .....	3
1.2.4	Necessary circumstances for explosion to occur .....	4
1.2.5	How to avoid explosions or reduce consequences .....	7
1.2.6	Vented explosions .....	8
2	Theory and previous work .....	12
2.1	Earlier, historical work .....	12
2.1.1	Work by Wirkner-Bott, St. Schumann and M. Stock .....	12
2.1.2	Work by Crowhurst, Colwell and Hoare .....	15
2.1.3	Work by Cooper, Fairweather and Tite .....	17
2.1.4	Work by Harrison and Eyre .....	20
2.1.5	Work by van Wingerden .....	22
2.1.6	Work by Colwell .....	24
2.2	Applicability of empirical expressions .....	25
2.2.1	Comparison of expressions .....	27
3	Software & simulation setup .....	32
3.1	FLACS .....	32
3.2	Background for using FLACS .....	33
3.3	Procedures for FLACS-simulations .....	33
3.3.1	Pre-processing .....	34
3.3.2	Running of simulation .....	36
3.3.3	Post-processing .....	36
4	Gas explosions .....	37
4.1	Setup gas simulations .....	37
4.1.1	Setup of experiments by Harrison and Eyre .....	37
4.1.2	Setup of experiments by van Wingerden .....	42
4.1.3	Setup for varying test volume .....	46
4.1.4	Setup of tests varying vent sizes .....	50



4.2	Results and discussion.....	50
4.2.1	Results simulations of experiments by Harrison & Eyre .....	50
4.2.2	Results simulations of experiments by van Wingerden.....	60
4.2.3	Results simulations of tests volume .....	65
4.2.4	Results simulations of tests vent size .....	70
4.2.5	Key findings – gas explosions.....	74
5	Dust explosions.....	76
5.1	Setup dust simulations.....	76
5.1.1	Setup of experiments by Wirkner-Bott.....	76
5.1.2	Setup of experiments by Colwell .....	82
5.2	Results and discussion.....	86
5.2.1	Results simulations of experiments by Wirkner-Bott.....	86
5.2.2	Results simulations of experiments by Colwell .....	93
5.2.3	Key findings – dust explosions.....	98
6	Conclusions .....	101
7	Recommendations for further work.....	103
	References .....	104



# 1 Introduction

## 1.1 Background

When evaluating risks and hazards associated with explosions, the aspects of the explosion most often considered damaging are the generation of excess pressures and the heat release caused by combustion. Several measures are available to mitigate the explosion, one of these being reduction of overpressure by explosion venting. As explosion venting is a relatively inexpensive safety barrier based on simple principles, it has been applied as a safety measure for several decades. Although reducing the hazard levels, the implementation of such measure do not completely eliminate the hazards associated with explosions. As the principle of explosion venting is based upon release of excess pressure from a confined area, the vented flow can introduce hazards in the area directly outside the vent. Amongst others, these hazards can represent propagating blast waves, expelled flames or toxic releases in the external area surrounding the vent. During the 1980s and 1990s a greater understanding of the external hazards associated with explosion venting was gained through multiple studies of the phenomena. In the 1980s Harrison and Eyre [1] conducted an experimental investigation, documenting and describing the external pressure development being caused by an external combustion of expelled gas. This study also described a connection between this external explosion and the internal combustion process and pressure development.

Historically, the assessment of external hazards associated with explosion venting has been based on empirical expressions, derived from experimental data obtained through studies of the vented explosions. These studies have often been based on a limited amount of experimental scenarios, resulting in the developed methods only being valid for similar conditions as those applied in the experiments. The limited applicability of the prediction methods can be improved by performing additional experimental studies varying the initial conditions of the scenario, and updating the empirical expressions accordingly. Such continued modification of the empirical expressions will result in a broader applicability, however, it is assumed that the increasing range of validity subsequently would result in reduced accuracy for the predicted values.

The last couple of decades the development in the field of numerical simulations and Computational Fluid Dynamics (CFD) has been in great change and the progress has been enormous. This progression is closely connected to the rapid development within computer technology and subsequently increased in computational capacity. When compared to experimental values the predictions obtained by numerical methods and CFD are of greater accuracy than what seen before. Thereby providing a useful tool in the assessment of risks and hazards introduced by vented explosions.

The use of CFD is already an important tool in evaluation of explosion risks and hazards, and the increased accuracy and cost savings associated with the use of such tool suggest it to be used even more in the future. It is however important to remember that all physical aspects of an explosion are not completely understood, and that the numerical methods developed to represent these phenomena often are based on assumptions and simplifications. As all CFD-tools are based on such numerical methods, one must keep in mind that the applicability of a CFD-tool is not without limitations. To be able to understand limitations in the simulations and to further develop and improve the software, it is important to validate simulations by comparing them with experimental results, and subsequently update the software model when greater understanding is achieved.

The objective of this thesis is consequently to identify the characteristics of external explosions caused by vented explosions, and to investigate the possibility of accurately predict the development of these external explosions by the use of CFD software. The assessment will be performed, simulating experimental work and comparing the obtained values to the experimental recordings.

## **1.2 Explosion in process industries**

### **1.2.1 Definition of gas and dust explosion**

There have been many attempts to formulate a definition of an explosion as a phenomenon. Studying literature one can find a wide variety of definitions. When looking at different areas of research and different industries it can be seen that the understanding of an explosion can vary a lot, and that even within the same field of research the definitions diverges. In addition to different basis and background, the lack of agreed terminology can also be a source to varying definitions. Despite this possibility of individual understanding one can however draw a main conclusion - the definition of an explosion is, to some extent, based upon the part of the explosion that is of relevance to the person who is providing the definition. In the following an attempt will be made to define an explosion from a process safety engineer's point of view:

A technical understanding of an explosion can be defined as the sudden release of a large amount of energy due to an exothermal chemical reaction. Or more precise a chemical reaction between oxygen and a combustible substance resulting in a violent release of energy in the form of heat and pressure.

### **1.2.2 Relevance to which industries**

The danger of explosions is of relevance to most industries where gas and/or dust can form an explosive atmosphere, either intentionally as part of the handling or refinement process, or accidentally as a

consequence of an unforeseen and undesirable event. The case of gas explosions is most often associated with petroleum industries, but can also occur within manufacturing of paints and other chemical industries. A risk of gas explosions can even be present for handling and storage of biological materials, as decomposition of such can cause generation of combustible gases.

Dust explosions in process industries are primarily related to facilities handling and processing organic dusts such as feeds and grains, coal, peat, metals and plastic powders. However, facilities producing pharmaceuticals and powder paint can also be affected.

According to Eckhoff [2] accidental gas or dust explosion represent a risk in the following industries:

- Oil and gas industry
  - On- and offshore facilities for production of oil and gas
  - Oil and gas refineries
  - Transport and storage systems, such as pipes, tanks, etc.
- Petrochemical, chemical and metal production
  - Petrochemical production of chemicals and plastics
  - Pharmaceuticals, pesticides, and fertilizer
  - Manufacturing of paint and dye
  - Production and handling of pulverized metal and plastics
  - Manufacturing of food and feed products
  - production of paper, cellulose, and other extracts from wood
- Mechanical processing and handling
  - Mills and storage for feed and grain
  - Sawmills, or other mechanical wood refining
- Speciality industries such as production of explosives, pyrotechnics and similar

### **1.2.3 Gas and dust explosions**

Gas and dust clouds share many similar characteristics when it comes to ignition and combustion properties. As stated by Eckhoff [2], once generated, the characteristics for explosive mixtures of gas and air or dust and air are quite similar. Defined limits of flammability, laminar burning velocities, influence of turbulence and effect of initial pressure on maximum explosion pressure are alike for the two types of explosions. According to Eckhoff [2] these similarities might be the reason for the wrongly

established perception that the hazards represented by the different types of explosions are the same. He points out that there are essential differences between the types of explosive clouds. For gas mixtures, propagation of flame and explosion is only possible when the mixing ratio of the gas cloud is within the limits of flammability. In other words, a gas mixture above or below these limits will not ignite without change in concentration. With regards to propagation of explosions, similar upper and lower limits can be found for mixtures of dust and air. However, settled dust or a dust deposits representing a higher concentration than that able to propagate an explosion can still be able to propagate a flame. The reason for this is the relatively large size and shape of the dust particles causing air to be trapped between particles. Contrary to combustion of dust/air mixtures, this type of combustion is not to be regarded as an explosion, but a slow burning smouldering combustion.

Explosive clouds of gas or dust also differ in the duration of their presence. In a confined homogenous mixture of gas and air, the small size of the gas molecules results in intermolecular forces to be the dominant, causing the mixture to stay homogeneous with time [2]. For dust clouds on the other hand, the considerably larger size of the dust particles causes their movement to be controlled by other forces such as gravity. The formation of a dust cloud is reliant on the external force causing the dust to disperse. The existence of the cloud is in turn dependent on the duration of dispersal, along with other external effects affecting both dispersal and settling. Consequently, the susceptibility to external forces causes the dispersed dust to settle with time, in turn resulting in the explosive atmosphere to disappear.

Another major difference between gas and dust explosions is the formation or origin of the two. A gas explosion is typically a result of a leakage or undesired event, where the surrounding area offer some sort of confinement allowing the generation of an explosive atmosphere. Contrary to gas explosions, a dust explosion will usually occur inside a process unit, as the concentration of a combustible dust cloud is largely reliant on confinement. Although occurrence is most common inside process units, the possibility of a dust explosion is not limited to such scenarios.

#### **1.2.4 Necessary circumstances for explosion to occur**

For combustion to take place the presence of certain elements is required. Looking at an “ordinary” combustion there is a need for a *combustible matter*, *oxygen* and an *ignition source*. To most these elements are recognised as the three parts of the fire triangle shown in Figure 1.

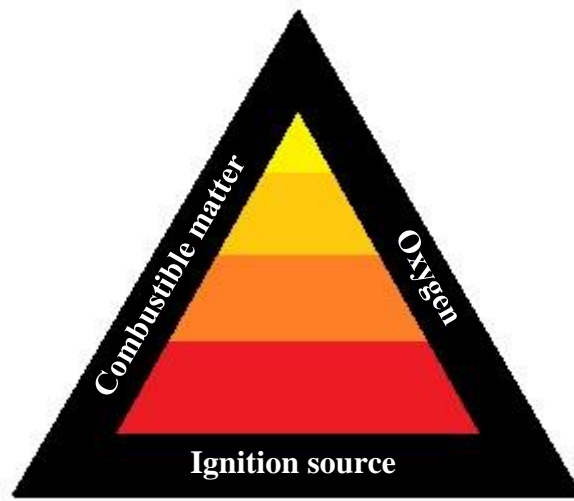


Figure 1: Fire triangle

There are a number of substances that can represent the combustible element in an explosion. Typical fuel sources are gases, mists and sprays (often consisting of hydrocarbons), dusts and of course conventional explosives. Except for the latter a common denominator for these are that they need to be mixed with oxygen or another oxidizer, and that the mixture has to be within the limits of flammability for the mixture to ignite. Dependent on the fuel source represented in the cloud or explosive atmosphere, there is also a requirement for some degree of confinement. As the way of mixing, and the lifespan of a gas cloud compared to a dust cloud, is very different, the dependency on confinement is of most importance when looking at dusts. The reason for this is due to the way the fuel forms an explosive atmosphere, described in section 1.2.3. As the dust particles do not mix with oxygen on a molecular level, as for formation of gas clouds, the dust is more effected by surrounding forces and conditions. Due to this susceptibility to external forces such as gravity, the dust cloud is instantly upon formation subject to settling and dilution. If confined the dust will still settle, however an explosive atmosphere will sustain as long as the source of the dispersion of dust is maintained. The confinement of a dust cloud will in other words, reduce the effect of external forces, thus resulting in the duration of the cloud to be sustained somewhat longer. Compared to dust clouds, the intermolecular connections associated with gas clouds are stronger and not equally affected by surrounding forces. The gas cloud is however prone to dilution, and consequently some level of confinement is still required to sustain an explosive atmosphere. Consequently, for an explosion to occur there is a requirement of *mixing/dispersion* and *confinement*, in addition to combustible matter, oxygen and ignition source. Together these five combine to the five sides of the explosion pentagon, seen in Figure 2.



Figure 2: Explosion pentagon

## Level of magnitude

For both gas/air- and dust/air-mixtures, there are factors affecting to which extent the mixture is able to propagate an explosion, and the severity of such a propagation. Similar for explosive mixtures of gas or dust is that these have upper and lower flammability limits with regards to fuel to air ratio. Within these limits the mixtures are able to propagate combustion and explosion. A lean mixture with fuel to air ratio below the lower flammability limit (LFL) will not have sufficient fuel to be able to propagate combustion. A rich mixture with fuel to air ratio above upper flammability limit (UFL) contains too little oxygen to support propagation of an explosion.

For gases the main influencing factors are chemical composition of the gas, and the mixing ratio of gas to air (equivalence ratio ( $\lambda$ )). The influencing factors of dust are a bit more complex. Effecting the severity of a reaction is dust characteristics such as moisture content, particle size, agglomeration, and the concentration of the dust cloud. In addition, as the basic nature of a dust cloud is dependent on dispersion of the dust by some external force, the turbulence associated with such a dispersion will influence the rate of combustion, in turn the severity of the explosion.

Taking into consideration the amount of factors influencing the reactivity of a dust, there has been attempts to find a single measure expressing the explosion characteristics of a dust. Presented as Eq. 1.1 is the *cube root law* and the definition of  $K_{St}$ . According to Eckhoff [3] this relation was introduced by Bartknecht in the 1970's, and claimed it to be "a specific dust constant" confirmed by various experimental test with different dusts and in vessels of numerous volumes.



$$(dP/dt)_{max}V^{1/3} = constant = K_{St} \quad (1.1)$$

$$(dP/dt)_{max} - \text{maximum rate of pressure rise per time [bar/s]}$$

$$V - \text{volume of vessel [m}^3\text{]}$$

As can be seen in Eq. 1.1, the  $K_{St}$ -value is based upon the maximum rate of pressure rise within a specified volume. By multiplying the maximum rate of pressure rise with the cubic root of the vessel volume, the  $K_{St}$ -value becomes volume independent. The rate of pressure rise is dependent on the combustion rate, which in turn is highly dependent on the level of turbulence within the mixture. Turbulence level is however not taken into consideration in the expression. It can therefore be argued that  $K_{St}$ -value represents an inadequate expression for a dust/air mixtures reactivity as it does not consider vessel geometry, dispersion system, ignition delay and other factors influencing the level of turbulence upon ignition. The expression is assumed to be applicable only for similar conditions as those applied to the experiments used to classify the dust. Consequently, there is a disagreement with regard to  $K_{St}$  representing an adequate measure for reactivity, as the expression on its own does not consider level of turbulence present [3].

### 1.2.5 How to avoid explosions or reduce consequences

To avoid an explosion, it is necessary to remove one of the elements required for combustion to take place. By removing the ignition source, the oxygen or the combustible matter itself the chain is broken and combustion is not able to propagate. In process industries the ideal approach to this, is by designing the process in a way that does not allow simultaneous presence of one or the either of these three - a principle called *inherent safety*. The best way to achieve this is by implanting such a mind-set early in the design of the process plant. Although representing best practice, such a focus is not always implemented sufficiently early in the design phase, or in some cases just not possible. Consequently, for many process plants the safety assessment of the process is initiated with parts of the process facilities or sometimes the entire plant already designed.

Although not implemented in the fundamental philosophy of the design, preventing explosions by removal of either combustible matter, ignition sources or oxygen can still be achieved. This can be done by implementation of various technical and organizational safety measures. Such a technical measure can for example be the implementation of a centralized control system, detecting and monitoring different parameters of relevance with regard to explosion safety. Typical examples of such parameters are pressure, temperature, gas or dust concentration, amongst many others. Based on evaluation of the levels of the monitored parameters, the control system can shut down parts of, or the entire process should critical conditions occur.

Should the design of the process plant for some reason make it impossible to implement an inherent design philosophy, the implementation of consequence reducing measures are most likely required to achieve a satisfactory safety level. Such measures are based on either implementing measures ensuring that the structural strength of the process unit is sufficient to withstand the impact of an explosion, or to limit the extent of an explosion by preventing propagation. Often a combination of both can be the best approach. The protective measures can again be divided into active or passive measures. An active measure relies on registration of change in one or multiple parameters of the process to activate the counter measure reducing propagation. An example of such a measure is an explosion suppression system - a system based on a pressurised extinguishing agent, which is released upon e.g. pressure rise or increase in temperature. An automatic suppression system can typically be used to knock down an initiated explosion, or to reduce the extent of an explosion by hindering propagation in pipes or channels. Other examples of active measures are quick acting isolation valves, triggered by pressure rise or registration of another undesired condition in the process plant. The isolation valves come in many different designs, all intended to prevent propagation of flame and explosion.

Passive measures may also be triggered based on an undesired change in the process, however the nature of these measures are not reliant on activation. Examples of such are valves applying pressure dependant poppets, closing pipe connections upon increased pressure, and 90° or 360° pipe bends fitted with burst panels thereby preventing continued propagation. Protective means are also often associated with structural measures intended to increase the structural strength of one or several process units. In the case of measures ensuring sufficient structural strength, an example of a passive measure is application of reinforced construction. Implementation of added structural strength may however be an expensive safety measure. Instead of constructing a device strong enough to withstand an internal explosion, a safety measure preventing explosion pressures exceeding the critical limits of the device is implementation of a pressure relief panel, burst panel or explosion vent.

## **1.2.6 Vented explosions**

### **Description of principle**

Explosion venting is a widely used safety measure when it comes to explosion protection in process industries. The concept of explosion venting is based on reducing the maximum explosion pressure generated inside an enclosure, typically a process unit, to a level below the critical pressure which exceeds the structural strength of the vessel. The reduction of internal pressure is accomplished by implementing an orifice in the enclosure, allowing the overpressure generated by combustion or explosion to be ventilated to the surroundings. Doing so one avoids a pressure build-up inside the enclosure, thereby discontinuing the escalating nature of an explosive combustion and the pressure

build-up associated with confined combustion. Dependent on the nature of the process inside the enclosure, the orifice may or may not be covered by a vent panel. This cover can for example be in the shape of a hinged door or a weaker panel, depending on what is regarded as suitable for the process unit in question. In addition to requirement for adequate sizing of the vent, the release or rupture pressure of the vent cover has to be sufficiently low, allowing the cover to open upon pressure rise. In this way avoiding pressure build-up approaching the tolerance limit of the enclosure.

The graph in Figure 3 serves as a good illustration of the effect of a pressure relief vent. The internal pressure development of a confined explosion within a vessel, is illustrated by the curve “A”. The maximum pressure reached in the unvented vessel,  $P_{max}$ , is represented by the peak value of this curve. When introducing a pressure relief vent with static release pressure,  $P_{stat}$ , the development of the pressure build-up changes characteristics. The rate of pressure increase after the venting starts is lower, as is the “new” maximum internal pressure,  $P_{red}$ , of the vented enclosure. The reduced pressure build-up and the maximum internal pressure,  $P_{red}$ , of the vented explosion is a result of two competing processes. As for the confined explosion, the combustion inside the vented enclosure causes a volume production due to the increased volume of combustion products. Increased volume inside a closed vessel in turn leads to an increased pressure. However, for the vented explosion a volume reduction is initiated when the relief vent opens at  $P_{stat}$ , consequently causing the pressure build to decrease.

- $P_{max}$  – maximum pressure in unvented vessel
- $P_{red}$  – pressure in vented vessel
- $P_{stat}$  – pressure in which vent releases

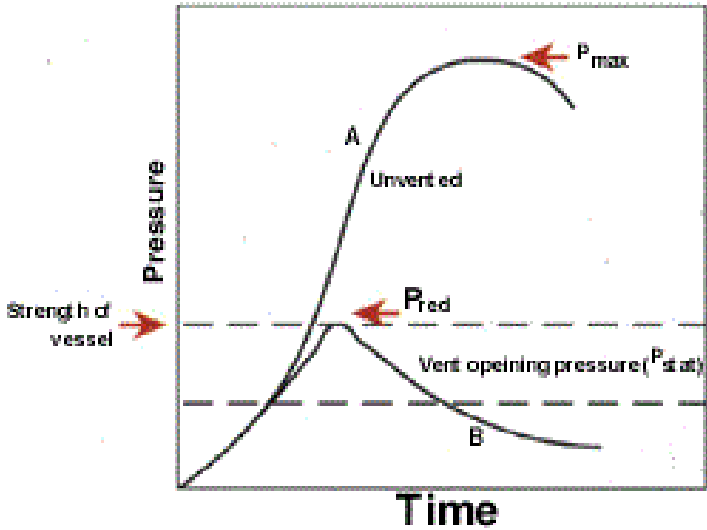


Figure 3: Pressure characteristics vented explosion, FlowSeal Engineering [4]

## External explosion

As explained in the previous section, the principle of explosion venting is to avoid damaging internal pressures by venting increased volume to the surroundings. This reduces the rate of volume production inside the enclosure, consecutively reducing the pressure build-up.

The venting process can be divided into phases, the first one being pressure build-up before venting. This phase is initiated when ignition of the enclosed gas or dust cloud propagates combustion, causing the pressure to rise (Figure 4-a). When this pressure reaches the release pressure of the vent panel, the vent opens and the venting phase starts. In the initial stage of the venting phase, the growing volume of combustion products forces the flame front inside the enclosure forward, causing it to push the combustible gas or dust cloud in front of the flame and out of the vent opening (Figure 4-b). The venting of such combustible mixtures will cause a flammable and turbulent cloud to form outside the vent. If the concentration of the expelled cloud is within the limits of flammability, the cloud can be ignited as the internal flame propagates further and reaches the outside of the vent opening (Figure 4-c). If the combustible cloud outside the vent opening is of sufficient size and concentration to propagate an explosion, an *external explosion* will be the outcome (Figure 4-d).

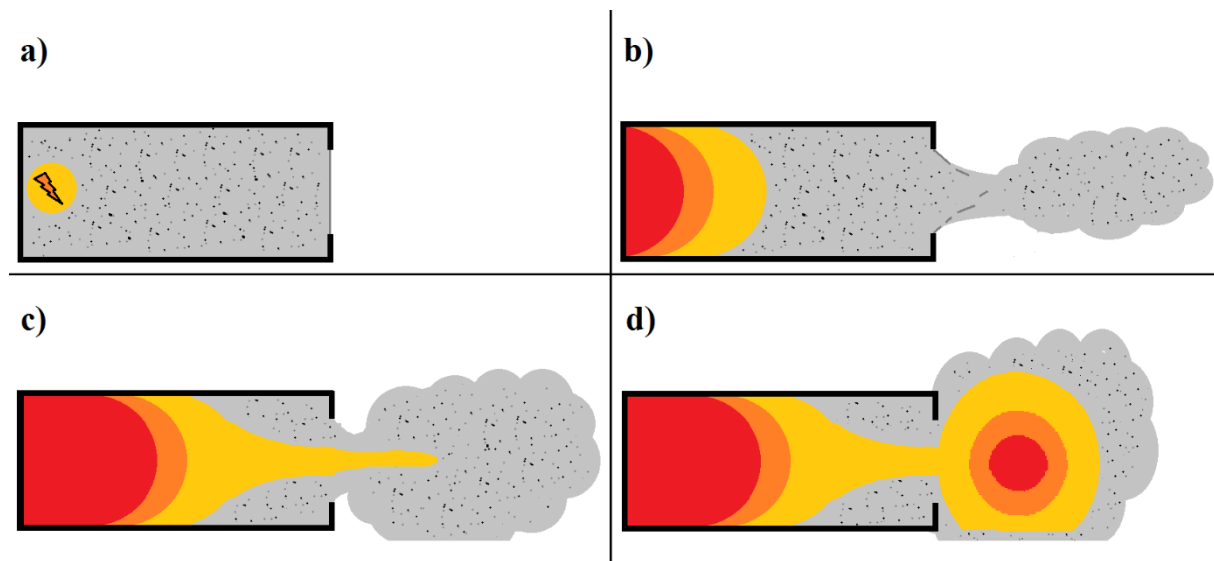


Figure 4: External explosion: graphic illustration of the basic principles

When looking at vented dust explosions the external explosion can in some cases be mistaken to be a *secondary explosion*. Differencing the two is the origin of the dust contributing to the explosion outside the enclosure. Contrary to an external explosion, the dust propagating the flame in a secondary explosion is accumulated outside the enclosure prior to the venting of excess pressure (Figure 5-a). Such dust deposit can be a result of small leaks, spilling, etc. in combination with insufficient cleaning routines.

In case of a secondary explosion the external dust deposit is twirled up as a result of the blast wave associated with the *primary explosion* (Figure 5-b), propagating out of the enclosure either through an existing opening or as the vent panel gives in to exceeding internal pressure. The dust cloud generated by this blast wave is in turn ignited as the flame front propagates out of the enclosure (Figure 5-c), causing an explosion outside the enclosure (Figure 5-d).

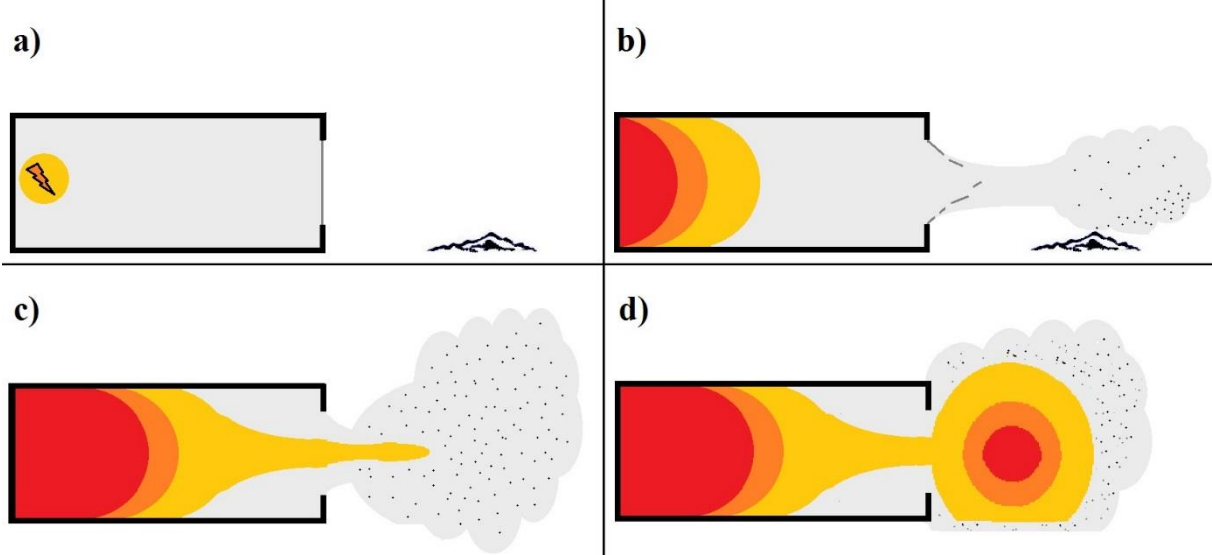


Figure 5: Secondary explosion: graphic illustration of the basic principle. Illustrating the external dust deposit forming a dust cloud, subsequently ignited by the ejected flame.

## 2 Theory and previous work

### 2.1 Earlier, historical work

In the following chapter the results of an extensive literature study will be summarized. The literature study performed extends beyond that referred to in this chapter, considering only references with direct relevance to the subjects discussed in this thesis. Publications referred primarily include studies investigating various aspects of a vented explosion.



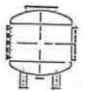

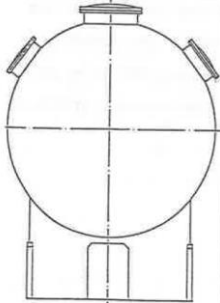
#### 2.1.1 Work by Wirkner-Bott, St. Schumann and M. Stock

In 1992 Wirkner-Bott, St. Schumann and M. Stock [5] published a paper on flame and pressure effects from ventilated dust explosions. The paper was based on a comprehensive experimental test program consisting of multiple test series of vented dust explosions. The experiments were carried out in a wide variety of vessels of different volumes and shapes, and with different vent areas and static release pressures. Vessels with volumes from 0,3 m<sup>3</sup> to 250 m<sup>3</sup>, of cylindrical shape and with L/D between 1,0 and 1,8 were used.

The 250 m<sup>3</sup> vessel was equipped with three vents panels to account for the structural strength of the vessel, the remaining vessels were only equipped with one vent. For the vessels of size 0.3 m<sup>3</sup> and 1.0 m<sup>3</sup> the vent panel was located on the side/end wall, venting the explosion in a horizontal direction. The vent openings in the vessels of volumes 10 m<sup>3</sup>, 60 m<sup>3</sup> and 250 m<sup>3</sup> were located in the top of the vessels, thus venting the explosion in an upward direction. To record explosion pressures Wirkner-Bott et al. [5] used pressure transducers located both inside and outside the vessels. The external transducers were positioned in the centre line of the vent opening, mounted on a mast at a distances of 2 m, 4 m, 6 m, 8 m, 10 m, 12 m from the vent irrespective of the volume of the vented vessel. Additional details of experimental setup are presented in Table 1.

The type of dust used in the test program was a powder of maize starch with a  $K_{St}$ -value of 200 bar m/s, and a wheat flour with  $K_{St}$  of 140 bar m/s. However, to simulate a dust with other explosion properties Wirkner-Bott et al. [5] delayed the ignition time when using maize starch with a  $K_{St}$  value of 200 bar m/s. The rationale for this was to decrease the initial turbulence level in the dust air mixture in an attempt to produce a dust with a reactivity equal to a  $K_{St}$  of 100 bar m/s.

Table 1: Characteristics of vessels used in the experiments by Wirkner-Bott et al. [5]

Vessel	V [m <sup>3</sup> ]	V <sup>2/3</sup> [m <sup>2</sup> ]	L/D [-]	Dust dispersion, Reservoir	P <sub>stat</sub> [mbar]	A <sub>v</sub> / V <sup>2/3</sup> [-]				
	0.3	0.45	1.8	1 ring nozzle 1 reservoir: 3 dm <sup>3</sup> P <sub>vf</sub> : 20 bar	180				0.3	
250-275							0.19	0.3		
	1.0	1.0	1.0	1 ring nozzle 1 reservoir: 5,7 dm <sup>3</sup> P <sub>vf</sub> : 20 bar	160				0.3	
200					0.07	0.1		0.3		
230-250							0.15		0.45	
290								0.3		
440-460							0.15	0.3		
	10	4.64	1.0	1 ball nozzle 1 reservoir: 50 dm <sup>3</sup> P <sub>vf</sub> : 20 bar	200	0.08		0.14		
500					0.08		0.14			
	60	15.33	1.5	12 ring nozzles 12 reservoirs: 12,3 dm <sup>3</sup> P <sub>vf</sub> : 20-24 bar	100			0.13		
	250	39.69	1.0	10 ball nozzle 10 reservoirs: 50 dm <sup>3</sup> P <sub>vf</sub> : 20 bar	100			0.16		

The purpose of their work was to investigate external effects, concentrating on external pressure development and the characteristics of the external flame. The connections between the internal and the external explosions were also of interest. The ultimate objective of the research of Wirkner-Bott et. al. [5] was to find relations allowing them to develop expressions predicting the characteristics of the external explosion. By systematically analysing and processing the measured characteristics of the external explosions for the variety of vessels, Wirkner-Bott et. al. [5] developed the following empirical expressions as a suggestion on how to predict the external effects of vented dust explosions.

Maximum external overpressure:

$$P_{s,max} = 0,2 \cdot P_{red,max} \cdot A_v^{0,1} \cdot V^{0,18} \quad (2.1)$$

$P_{s,max}$  = Maximum external explosion overpressure [bar]

$A_v$  = Vent area [m<sup>2</sup>]

$V$  = Vessel volume [m<sup>3</sup>]

$P_{red,max}$  = Maximum overpressure within test chamber [bar]

Maximum flame length in meters, emitted from the vent opening:

$$L_{f,max} = 8 \cdot V^{1/3} \quad (2.2)$$

The distance,  $R_s$ , in meters from the vent, at which the maximum external overpressure occurs:

$$R_s = 0.25 \cdot L_{f,max} \quad (2.3)$$

Pressure,  $P_{r,max}$ , at any distance,  $r$ , in meters from the vent, where  $r$  is greater than  $R_s$ :

$$P_{r,max} = \left(\frac{R_s}{r}\right)^{1.5} \cdot P_{s,max} \quad (2.4)$$

The empirical expressions suggested by Wirkner-Bott et al. [5] were however not without limitations. The experiments in which the expressions were derived from were based on a limited number of volumes using dusts with specific chemical and explosion properties. Consequently, the expressions are only applicable when evaluating vented dust explosions similar to those included in the experimental study. The validity of the empirical equations is therefore limited to scenarios corresponding the following conditions:

- Dust of category St.1<sup>1</sup> according to VDI Guideline 3673: 1992, also described in VDI 3673: 2002 [6]. The German national standard VDI 3673 has now been withdrawn. Equivalent standards are the European standards EN 14034-1 [7] and EN 14034-2 [8]
- Strength of vessel,  $P_{red} \leq 1$  bar
- Vent release pressure,  $P_{stat} \leq 0.1$  bar
- Vessel volume  $\leq 10000$  m<sup>3</sup>

---

<sup>1</sup> St.1 > 0 to 200 bar m/s, St.2 > 200 to 300 bar m/s, St.3 > 300 bar m/s



## 2.1.2 Work by Crowhurst, Colwell and Hoare

In 1995, D. Crowhurst, S. Colwell and D.P. Hoare [9] published an article discussing the external effects of vented dust explosions and comparing their findings to those of Wirkner-Bott et al. [5]. Their work was based on an experimental test program of vented dust explosions in a steel enclosure where utilising a partition wall allowed tests to be conducted in enclosure volumes of 20 m<sup>3</sup> and 40 m<sup>3</sup>. The enclosure is illustrated in Figure 6.

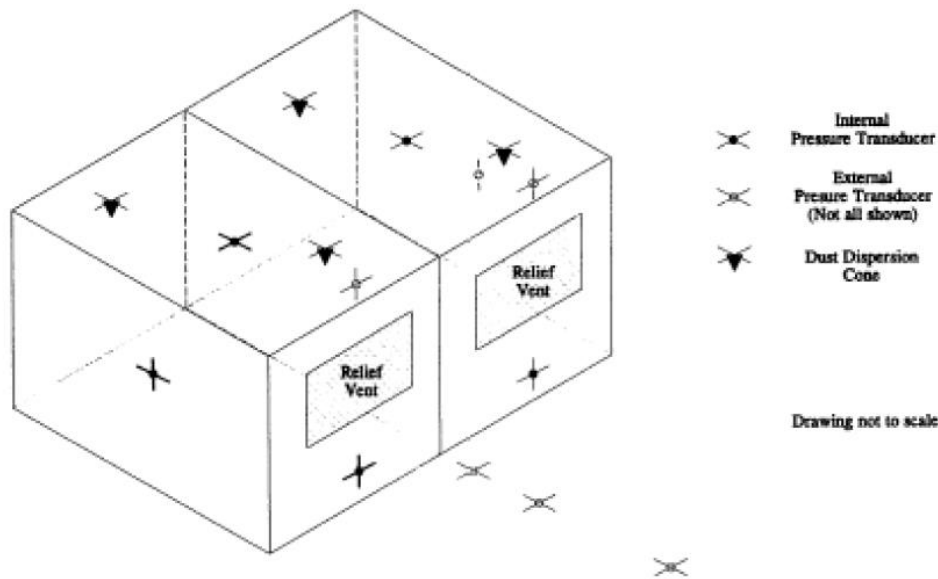


Figure 6: Experimental setup used by Crowhurst et al. [9]

The objective of their work was to investigate the blast effects and external flame characteristics of vented dust explosions using Kellingley coal and maize starch. Classification of the dusts and determination of explosion characteristics was done using a standard 20-litre sphere test.

In their work Crowhurst et al. [9] systematically recorded pressure development both inside and outside the test chamber. On the inside the pressure transducers were located in the roof of the enclosure, while one the outside the transducers were located on the centre line of the vent at distances of 0.5 m, 2.5 m, 3.75 m, 5.0 m, 7.5 m, 10.0 m, 15.0 m and 20.0 m. In addition, the experiments were documented by use of both regular and high speed video.

The characteristics of the external explosions were evaluated and Crowhurst et al. [9] suggested that the external explosions could be categorized in two main types:

- *Type 1* representing the strongest external explosion, typically caused by a large vent area or by a low vent release pressure, in combinations with ignition on the opposite side to the vent opening. These circumstances caused large amounts of unburnt dust to be showed in front of the internal flame front

and to be ejected out of the vent opening. The ejected dust cloud was in turn ignited when the flame ejected from the vent opening.

- *Type 2* was characterized by a long flame jet discharging from the vent opening. This type of external explosion was associated with a reduced vent area and increased level of turbulence within the enclosure.

When comparing their own experimental results to values obtained by using the empirical expressions (Eq. 2.1 - 2.4) proposed by Wirkner-Bott et al. [5] , Crowhurst et al. [9] found their own experimental results to deviate some from those predicted by the empirical expressions. For maximum external pressures they found the predictions to agree with a slight overestimation, while the predicted pressure decay with distance from the vent was found to represent an underestimation compared to the experimental findings. For the external flame length Crowhurst et al. [9] found the values obtained by using Eq. 2.2. to represent an under prediction compared to the flame lengths observed during the experiments, both the average and the peak lengths. Based on their findings Crowhurst et al. [9] suggested the following modifications to the empirical expressions suggested by Wirkner-Bott et al. [5]:

Maximum external overpressure:

The expression suggested by Wirkner-Bott et al. for prediction of maximum external overpressure, was found to represent an appropriate estimation. The empirical expression, referred to as Eq. 2.1 therefore remained unchanged.

$$P_{s,max} = 0,2 \cdot P_{red,max} \cdot A_v^{0,1} \cdot V^{0,18} \quad (2.1)$$

Maximum flame length in meters, emitted from the vent opening:

$$L_{f,max} = 10 \cdot V^{1/3} \quad (2.5)$$

The distance,  $R_s$ , in meters from the vent, at which the maximum external overpressure occurs:

$$R_s = 0.2 \cdot L_{f,max} \quad (2.6)$$

Pressure,  $P_{r,max}$ , at any distance,  $r$ , from the vent, where  $r$  is greater than  $R_s$ :

$$P_{r,max} = \left(\frac{R_s}{r}\right) \cdot P_{s,max} \quad (2.7)$$

Although not stated explicitly in their publication [9], as the alternative expressions suggested by Crowhurst et al. are modified versions of the original expressions [5], these are assumed to be valid for similar scenarios as those studied by Wirkner-Bott et al. described in section 2.1.1.

### 2.1.3 Work by Cooper, Fairweather and Tite

The development of pressures in vented gas explosions in near-cubic vessels was investigated by M.G. Cooper, M. Fairweather and J.P. Tite [10] during the early 1980s. The focus of their work was the development of internal pressure when applying vents of low failure pressure, to vented gas explosions in otherwise empty enclosures. Cooper et al. performed extensive analysis explaining the different physical phenomena causing pressure rise inside the enclosure. In their investigation of cause for internal pressure rise, Cooper et al. [10] describe phenomena of interest both with regard to internal pressure build-up, and of significance for the external explosion. This in turn indicating a connection between the internal and external development. The work of Cooper et al. [10] is therefore regarded as a suitable basis for analysing the internal pressure development.

The research of Cooper et al. [10] was mainly based on data collected from an experimental test program conducted in steel vessels of cubic or cuboidal shapes with volumes of 0.76 m<sup>3</sup>, 2.55 m<sup>3</sup>, 2.41 m<sup>3</sup>, 1.70 m<sup>3</sup> and 0.68 m<sup>3</sup>. After filling the vessels with a desired concentration of fuel-air mixture, ignition was initiated at the centre of the vessels. All the vessels configurations allowed for the explosion vents to be mounted in the centre of at least one of the side walls. For further details of the vessels please see the referred article [10]. The overpressure developed inside the vessels were measured by two piezoelectric transducers mounted in the vessel sides. In addition to registration of pressure development by transducers, one of the vessels were also equipped with a clear polycarbonate window allowing observation of the combustion process inside the vessel.

When analysing the experimental data Cooper et al. [10] identified a clear pattern for pressure build-up inside the vessels. The characteristic pressure development is displayed in Figure 7. They found that a typical pressure to time profile for the type of explosions investigated showed four main pressure peaks.

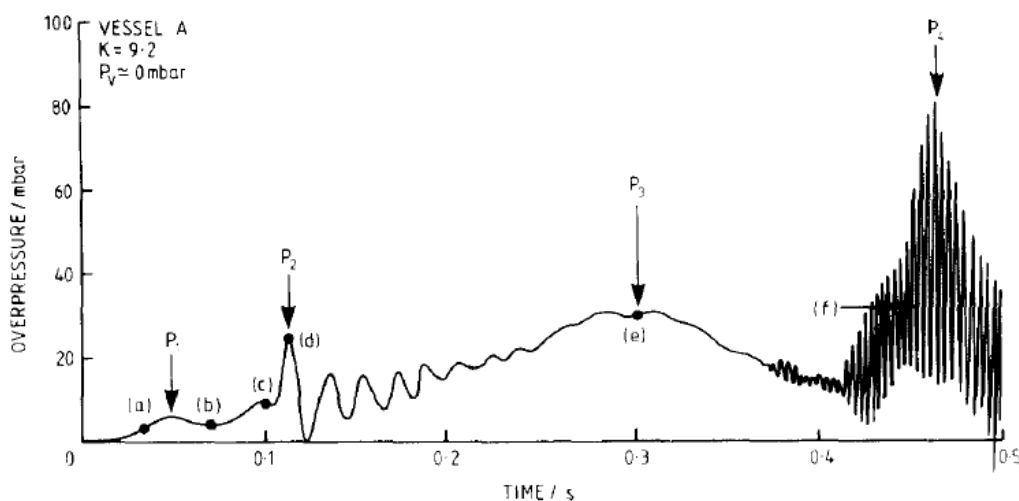


Figure 7: Typical pressure time profile recorded by Cooper et al. [10]

After ignition the first pressure peak identified,  $P_1$ , was found to be associated with the rupture of the vent panel. Prior to the vent rupturing the pressure inside the vessel increased due to the growing volume of the combustion products generated by the explosions. Upon rupture of the vent panel, the flow rate out of the vent exceeded the rate of volume production caused by combustion, in turn resulting in a slight decrease in pressure. After the pressure has decreased some, an increasing rise in pressure can again be seen. Cooper et al. [10] explains this increase to be a result of the volume production exceeding the volume flow out of the vent. An increased distortion of the flame surface was also observed, believed to be caused by outflow of unburned gases in turn stretching the flame towards the vent opening. When reaching the vent opening the expelled flame allowed burnt gas of lower density to be expelled from the vessel. This venting of burnt gas was believed to cause the ventilation of excess pressure to temporarily exceed the volume production caused by combustion. In Figure 7 this can be seen as a minor decrease in internal pressure. The second pressure peak,  $P_2$ , was by Cooper et al. attributed to the external explosion occurring when the flame ejected from the vent opening ignited the previously expelled unburnt gas. The peak is assumed either to be a result of the external explosion propagating back into the enclosure, or due to a reduction of flow out of the vent caused by the blast wave from the explosion choking the outflow. After this Cooper et al. [10] observed the start of ventilation of burnt gases to agree with the initiation of Helmholtz oscillations. The oscillations were observed as repetitive unified motion of the pockets of gas, moving back and forth in the direction of the vent opening. These oscillations occurred as a result of the internal excess pressure being vented out, generating an internal pressure slightly lower than the pressure on the outside, in turn causing the air to be drawn back into the enclosure. During this phase the burning rate was believed to be amplified by the turbulence generated between outflow of burnt gas and the gas remaining within the vessel. This in turn gave rise to volume production caused by combustion, resulting in increased internal pressures. Cooper et al. [10] also referred to the work of G.I. Taylor and pointed out that the flow of two gases of different density can become unstable when the interface between these are accelerated towards the denser one, known as both Taylor- and Rayleigh-Taylor instabilities. From this Cooper et al. stated that the fluid motion caused by the Helmholtz oscillations consequently could give rise to such Taylor instabilities. The third pressure peak,  $P_3$ , was attributed to when the flame front reached the walls of the enclosure leading to a reduction in volume production, causing the pressure to drop. The fourth pressure peak,  $P_4$ , was by Cooper et al. [10] described as an oscillatory pressure peak *“generated when pressure waves resulting from the combustion process couple with the acoustic modes of the vessel and set up sustained oscillations”*. These coupled oscillations were believed to cause a rapid increase in the combustion rate as a result of a larger flame area. According to Cooper et al. [10] it was believed that this acoustically enhanced combustion process was connected to combustion of pockets of unburnt gas. However, Cooper et al. stated that peaks such as these could rarely generate in actual situations.

Further in their studies Cooper et al. [10] proceeded by adjusting parameters such as vent area and vent release pressure to investigate which influence these factors had on the earlier observed phenomena. By increasing the vent release pressure Cooper et al. [10] observed two dominant pressure peaks. The first peak being  $P_1$  and the second to be  $P_4$ . It was believed that increased release pressure of the vent panel caused the combustion within the vessel to increase resulting in the origins and magnitude of  $P_3$  to be reduced, thus merging it with the increased  $P_1$ . The reduction or disappearance of  $P_3$  was by Cooper et al. [10] explained to be caused by the onset of peak  $P_4$  proceeding those of  $P_3$ .

It was observed that an initial decrease in the vent area caused an increase in the pressures recorded as peak  $P_2$ . However, with a continued decrease of the vent area  $P_2$  was observed to decrease due to the smaller vent area restricting the flow of gas through the vent, in turn reducing the magnitude and effects of the external explosion. Influence of reduced vent area on the peaks  $P_3$  and  $P_4$  were explained to be caused by the restricted venting associated with a smaller vent area, causing pressure build-up by combustion to be more severe.

Finally Cooper et al. [10] compared their findings to explosions in practical situations. Evaluating their theory, they found the four dominant pressure peaks to not always be represented in practical situations. It was believed that the influence of parameters such as gas composition, vent release pressure, vent area and shape of the vessel not always sustained the phenomena associated with the different pressure peaks. Variations in the same parameters were also believed to cause the character of the combustion and venting process to change, causing some of the peaks to merge together. The magnitude of  $P_1$  was believed to depend mainly on the release pressure of the explosion vent. The peak  $P_2$  was, as already mentioned, believed to be caused by the ignition of an unburnt combustible cloud on the outside of the vessel. A situation normally associated with internal ignition initiated far from the vent opening, causing large amounts of unburnt gas to be expelled from the opening. The third pressure peak,  $P_3$ , was recognised to appear in scenarios where a vent panel of insufficient size, but with low release pressure was fitted to a large vessel or enclosure. If the vessel was empty the pressure build-up was due to the pressure difference across the vent opening, while if the vessel contained obstacles turbulence generated during venting could cause a larger pressure peak. According to Cooper et al. pressure peak  $P_4$ , was always associated with explosion venting in large empty vessels. Although not investigated by Cooper et al, with relation to presence in actual situations it is appropriate to mention that the appearance of acoustically enhanced combustion, peak  $P_4$ , is not observed for vented dust explosions [11]. This is assumed to be due to the dampening effects of the dust, hindering the generation of a propagating acoustic wave.

## 2.1.4 Work by Harrison and Eyre

An extensive study of the phenomena of external explosions was performed by A.J. Harrison and J.A. Eyre [1] during the early to mid-1980s. Their investigation was based on an experimental series of vented gas explosions carried out in an enclosure of 30 m<sup>3</sup>. The enclosure was equipped with interchangeable plates to be mounted on the end wall of the enclosure, allowing utilisation of various vent areas during the tests. An illustration of the experimental setup presented in Figure 8.

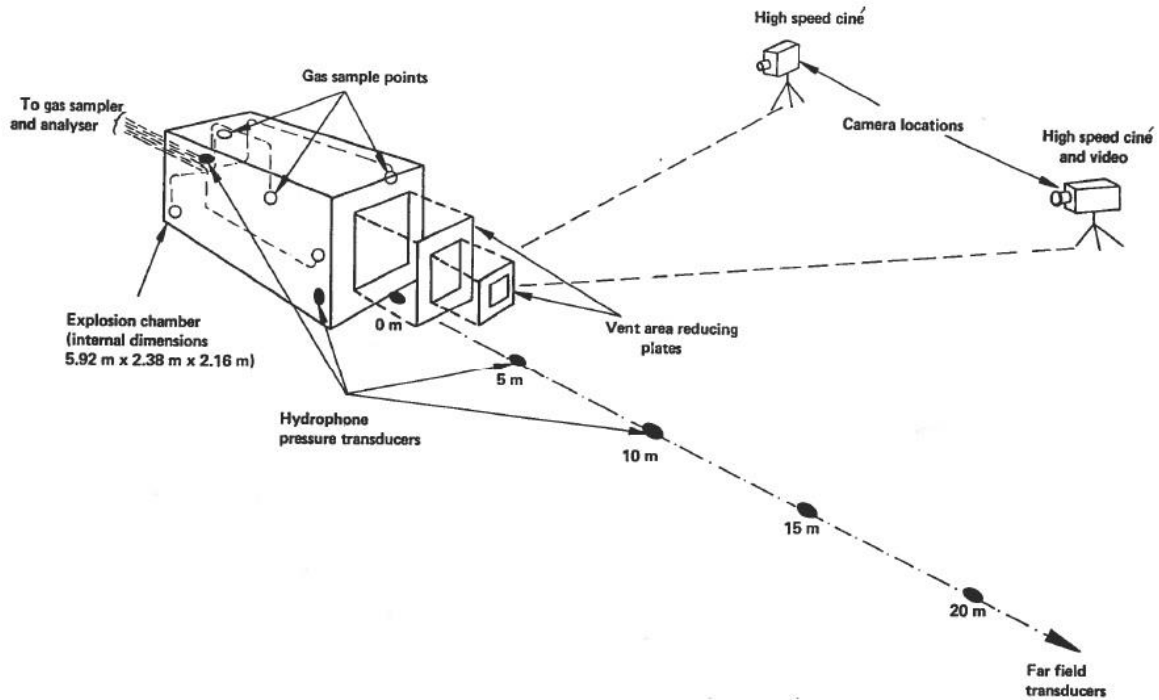


Figure 8: Experimental setup, Harrison and Eyre [1]

To form a basis for evaluation, pressures developed inside and outside the enclosure were recorded using pressure transducers, along with high speed filming of the area outside the vent. The two transducers on the inside of the enclosure were mounted in the centre of the rear wall and on the side wall, just above the ground. On the outside of the chamber the transducers were mounted immediately on the ground outside the vent, and at intervals of 5 m in the centre line of the vent opening.

Harrison and Eyre [1] stated that at the time, most methods for prediction of vent area and vented explosion pressures were either empirical expressions based on specific experimental conditions, or numerical solutions of simplified equations for the production and loss of volume. Recommendations for application of the latter being conservative, thus leading to over dimensioning of vent area and in some cases representing an unnecessary high cost. The objective of their study was therefore to investigate the effects influencing the external explosion, subsequently giving a greater understanding

of the phenomenon, in turn useful when evaluating the need for explosion venting and sizing of vent area.

To be able to evaluate the importance of influencing factors Harrison and Eyre [1] varied parameters such as vent area, gas type and concentration (stoichiometry) and position of the ignition source. They found that the external pressure was a result of an external explosion, and not a consequence of internal pressure emerging from the enclosure. Also observed was the occurrence of the peak external pressure prior to the internal pressure peak. The external explosion was also observed to influence the development of the internal pressure build-up. According to Harrison and Eyre [1] the external explosion can influence the internal combustion process in three ways:

- Reduction of the pressure gradient across the vent opening, by choking outflow of excess pressure caused by internal volume production. This is stated to be the primary source of influence [1].
- An acoustic pressure wave generated by the external explosion can cause both an increase and a decrease in internal pressures when propagating in through the vent.
- Negative phases introduced by the external explosion, triggering instabilities in the system.

When effected by the external explosion Harrison and Eyre stated that it could not be expected that the pressure prediction methods of that time would apply since they solely were based on the internal combustion.

Evaluating results from tests applying various ignition locations, Harrison and Eyre [1] concluded that ignition at the far end of the enclosure, opposite of the vent caused a higher overpressure than for ignition initiated at the centre of the enclosure. It was also observed that the external explosion associated with rear wall ignition was more violent than for central ignition. It was suggested that the difference in internal pressures between rear wall and centrally ignited explosions not only were a result of the higher external pressures associated with rear ignition. Also believed to influence the pressure build-up associated with rear wall ignition, was the later start of venting of burnt gas and the increased acceleration of the flame due to it propagating along the entire length of the enclosure.

When investigating the experimental setup with different vent areas but otherwise alike, Harrison and Eyre [1] found the shape of the external flame, and the speed in which the flame emerged from the opening to vary dependent on the size of the vent. For larger vents the flame appeared as a jet for only a few metres, before it propagated in all directions, forming a spherical fireball. The external flame observed for experiments applying a vent of smaller area was observed to be in the shape of a prolonged jet flame. The velocities of the ejected flame observed with the latter configuration was much higher

than when applying a vent of larger area. The effects of the external explosion on the internal was found to be of influence in the case of larger vents, and to be less significant for vents of smaller areas. This assumption was based on observations of the internal pressure caused by combustion to be lower compared to the external pressures when applying a large vent, whilst for smaller vents the internal pressure exceeded the pressures registered in the external explosion. Also assumed to be of influence was the larger vent area allowing a larger pressure wave to propagate into the enclosure. The size of the vent area was also observed to have an impact on the blast wave generated by the external explosion. It was observed that the vent of medium size provided the conditions supporting generation of the most severe far field blast wave.

### **2.1.5 Work by van Wingerden**

To contribute to a greater understanding of the effects influencing the development of vented explosions, van Wingerden [12, 13] performed a series of methane-air explosion in a vented enclosure. The tests were conducted investigating the effects of variations of the area and configuration of the vent, location of ignition source, gas concentration and introduction of an obstacle in the direction of the flow.

The experiments were conducted in a concrete bunker with the dimensions 4.0 m x 3.7 m x 2.6 m, giving a volume of approximately 38.5 m<sup>3</sup>. The enclosure was open in one end, allowing the utilization of various vent areas. As shown in Figure 9, the system used for varying the vent area comprised of six steel beams placed at different heights, crossing the opening of the enclosure. The vent opening was varied by sliding one or several solid walls between the beams, allowing vent openings of various configurations. To retain the gas and to investigate the effect of various vent release pressures, several layers of polyethylene sheeting was covering the vent opening.

Internal pressure development was registered by three pressure transducers mounted in the ceiling and walls of the concrete bunker. The internal flame and explosion development were filmed using a high speed camera. External pressure development was registered by three transducers located normal to the vent opening, at distances 0 m, 7.5 m and 17.5 m. A camera was located outside, aimed at the vent opening, registering flame emerging from the opening.





*Figure 9: Front view enclosure, van Wingerden [13]*

Analysing the experimental results for centrally ignited explosions in vented empty enclosures, van Wingerden found a characteristic internal pressure-time profile consisting of two dominant pressure peaks. The first peak was associated with the release of the vent cover, while the second assumed to be a result of oscillatory combustion. The combustion induced oscillations were observed to be enhanced by an acoustic wave generated during the combustion, resulting in a high overpressure. The second pressure peak was usually observed to represent the pressure peak of greatest magnitude.

Comparing the internal pressure transcriptions from an experiment applying a sheet of polyethylene as vent cover to an experiment applying no vent cover, van Wingerden identified a relative steep pressure peak occurring for both configurations. The occurrence of this peak was found to coincide with the flame emerging from the vent opening, and assumed to be associated with ignition of unburnt gas pushed out of the opening prior to the ejected flame.

With regards to the effect of ignition location, van Wingerden [12] concluded that the location of the ignition source had limited influence on the maximum pressure obtained internally. However, analysing the pressure-time development for two configurations he found that the source of pressure generation varied. For centrally ignited explosions in uncongested enclosures, the oscillatory combustion was found to be the most significant source determining the generated overpressure. When ignition was initiated at the rear wall opposite the vent panel, the obtained overpressure was stated to be determined by the external explosion. The external explosion was stated to be of greatest magnitude when ignition was initiated at the rear wall, due to the increase in volume caused by the burnt gas, pushing unburnt gas out

of the vent opening thereby supplying a larger amount of explosive atmosphere. The size of this external explosion was in turn stated to determine the strength of the blast wave.

Based on the experimental results obtained, van Wingerden [12] concluded that the applied variations in vent release pressure, in the range of 0- 10 kPa, were of little or no influence for the further development of the vented explosions. The obtained maximum internal pressure was also observed to be unaffected by the shape of the applied explosion vents. When introducing an obstacle in the centre of the enclosure, van Wingerden found that the vent area was of influence on the maximum obtained internal pressure. In general, the analysis of experiments introducing one internal obstacle and using rear wall ignition, revealed that the maximum internal pressure peak was determined by the turbulent combustion occurring in the wake behind the obstacle. An increased distance between the ignition source and the obstacle resulted in stronger turbulence and consequently a higher peak pressure.

### **2.1.6 Work by Colwell**

The work of Colwell [14] is based on an experimental study investigating the characteristics of vented dust explosions, and the effect these inflict on surrounding structures. Colwell was one of the contributors to the work of Crowhurst et al., described in section 2.1.2 of this thesis. Colwell's work was submitted as part of her Ph.D., and can be regarded as a continued study of the findings described by Crowhurst et al. [9]. The work of Colwell is included as background in this thesis due to the comprehensive experimental data included in here thesis [14] being regarded as a suitable basis for simulations. The full extent of her studies has not been evaluated as her investigations of impact on external structures is not within the scope of this thesis. The findings from Colwell's work will therefore not be discussed, however a brief summary is presented in the following.

The experimental study forming the basis for her work was carried out using a similar experimental setup as the one described in section 2.1.2, for the work of Crowhurst et al. [9]. The enclosure had the dimensions 2.4 m x 2.4 m x 4.8 m, and was of a flexible configuration allowing the utilization of two volumes by the use of a partition wall. Figure 6 in section 2.1.2 provides an illustration of the enclosure used in the experiments. Each enclosure was equipped with a vent of variable size fitted in the upper half of one of the end walls, allowing a vent area of either 1.0 m<sup>2</sup> or 1.4 m<sup>2</sup>. This resulted in a possible vent area of 1.0 m<sup>2</sup> or 1.4 m<sup>2</sup> for the volume of 20 m<sup>3</sup>, and a possible vent area of 2.0 m<sup>2</sup> or 2.8 m<sup>2</sup> for the volume of 40 m<sup>3</sup>. The vent panels used were both conventional pressure relief panels and MDF-panels. The powders used in the experiments were either coal dust with  $K_{St} = 155$  bar m/s or maize starch with  $K_{St} = 129$  bar m/s. External to the vent opening Colwell placed targets of various structures and shapes.

Aiming to identify characteristics associated with variations in the respective experimental configuration, Colwell documented a total number of 300 tests applying various configurations to the enclosure and registering influence of the vented explosion on a variety of targets “*representative of current UK building design*”. The effects of the explosion were registered, measuring internal and external pressure development and pressure displacement on target objects. Measurement of heat flux was also performed on strategic locations. To document the course of events and to measure the extent of the flames emerging from the vent, both high speed and regular video filming was used.

Available numerical methods developed to predict structural response to the effects of vented explosion were evaluated with regards to the experimental work carried out. Colwell found these not to be applicable for the experimental conditions as the methods mainly were developed to assess complex steel structures’ response to internal gas explosions, and evaluation of brick structures exposed to vented gas explosions. Through her studies Colwell found these assessment tools to be insufficient in evaluating the experimental scenarios investigated, however the methods were considered an appropriate basis for continued development of adequate expressions.

## **2.2 Applicability of empirical expressions**

For areas of science where fundamental theoretical relations do not supply a sufficient basis for evaluating a specific physical phenomenon, or where solving the theoretical relations represent an unreasonably comprehensive operation, there have been attempts to develop empirical equations providing a satisfactory estimate of physical properties. The development of such empirical expressions is based on observations and recorded results from experimental studies. An empirical expression describes an observed relationship between properties and parameters, enabling estimation of a variable dependent on these properties. This relationship is found to represent a satisfactory estimate of the variables when compared to the experimental results of the study. However, as the empirical relation is developed based on specific experimental conditions, the applicability of such expressions are limited to the respective experimental conditions they are based upon. An extended applicability could be proven by validating the expressions against a broader span of experimental setups. Regardless, when conditions deviate from those applied for the original experiments the estimates would be of less accuracy.

In an attempt to illustrate the dependency to conditions comparable to those applied to the original experimental study, a comparison of different empirical expressions has been performed. The chosen expressions represent methods for estimating the external pressure generated by vented dust explosions, along the main axis of the vented equipment through the centre of the vent opening. Four expressions have been included in the comparison.

The two first expressions included are those suggested by Wirkner-Bott et al. [5] and the modified version of this suggested by Crowhurst et al. [9]. These expressions have been discussed in section 2.1.1 and 2.1.2, and are referred to as Eq. 2.4 and Eq. 2.7. The relations predict the external pressures based on an estimated maximum external pressure. This maximum external pressure is obtained from another empirical expression suggested by Wirkner-Bott et al. [5], referred to as Eq. 2.1. With regards to limitations in applicability, the expressions by Wirkner-Bott et al. and Crowhurst et al. are stated to be valid only within the conditions described in section 2.1.1 and section 2.1.2. Both expressions have been included in the standards VDI 3673:2002 [6] and EN 14491:2012 [15], supplying guidance on dust explosion venting. The standards recommend the expression by Wirkner-Bott et al. to be applied for venting in a vertical direction, while the expression by Crowhurst et al. is recommended to be applied to venting in a horizontal direction. Such a limitation is not described in the original publications by Wirkner-Bott et al. [5]. Crowhurst et al. [9] did however state that their experimental configuration applied venting in a horizontal direction and suggested this to be a possible reason for the difference when compared to the expression by Wirkner-Bott et al.

Also included in the comparison was an expression described by both van Wingerden [16] and Eckhoff [3], originally suggested by Hattwig. The relation was derived based on a series of vented gas and dust explosions, and estimates the external pressure generated by a vented explosion as a function of distance from the vent opening. As can be seen in Eq. 2.8, this expression is based upon the reduced maximum explosion pressure in the vented enclosure and does not take into consideration the possible effects of an external explosion.

$$P = \frac{P_{red,max} \cdot C_1 \cdot C_2}{r} \quad (2.8)$$

Where:

$P_{red,max}$  = maximum overpressure in vented enclosure [bar]

$\log C_1 = -0.26/A_v + 0.49$

$A_v$  = vent area [ $m^2$ ]

$C_2 = 1$  [m]

$r$  = distance from vent opening [m]

No limitations with regards to applicability have been described by van Wingerden and Eckhoff. The expression is therefore included and assumed to be applicable within the same area as the other expressions.

A similar relation describing the maximum external pressure as a function of the reduced maximum internal pressure is included in EN 14491:2012 [15]. The expression is supplied as an alternative to those suggested by Wirkner-Bott et al. [5] and Crowhurst et al. [9] with regards to prediction of external pressure. It is however stated that the method estimating the largest value is to be used. Harmanny [17]

was the first to suggest that this expression could be used for prediction of external pressure effects caused by vented dust explosions. He referred to it as the Norwegian formula, and stated it to originally be developed by A.T. Skjeltop, A. Jensen and A. Rinnan, describing the blast propagation outside underground ammunition storage. Harmanny argued the suitability of this relation in predicting external blast propagation as it allows for estimation of external pressure in locations deviating from a direct line of sight of the vent opening. Presented in Eq. 2.9 is the empirical relation known as the Norwegian formula.

$$P_{ext,r} = 1.24 \cdot (1.13 \cdot A_v^{0.5} / r)^{1.35} / [1 + (\alpha/56)^2] \cdot p_{red,max} \quad (2.9)$$

Where:

$r$  = distance from the vent [ $m$ ]

$A_v$  = vent area [ $m^2$ ]

$\alpha$  = angle of the direction of the vent,  $0^\circ$  = right in front of the vent

With regards to area of applicability, EN 14491:2012 states this to be the same as for the expression by Wirkner-Bott, while according to Harmanny [17] the Norwegian Formula is valid for the following conditions:

$$\frac{P_{ext,r}}{P_{red,max}}, \text{ from } 10^{-1} - 10^{-4} \text{ (meaning } P_{ext,r} \text{ from 20 mbar to about 1 bar)}$$

$$1.13 \cdot A^{0.5} / r, \text{ from } 10^{-1} - 10^{-4}$$

$$\alpha = 0^\circ - 180^\circ$$

When comparing the two defined areas of validity one finds different parameters determining the applicability of the expression. This is important to note as it serves as a source of confusion and could result in misapplication. In the following the validity specified in EN 14491:2012 has been assumed, in that way obtaining a more unified area of applicability when comparing the predicted values.

## 2.2.1 Comparison of expressions

To demonstrate the variations in predicted values obtained from these expressions, all developed to represent a fair estimate of the external pressure, three fictitious scenarios have been defined. These volumes, along with other necessary conditions are presented in Table 2. As the relation described by Wirkner-Bott et al. suggests an estimate for pressure at distances further from the vent than the estimated distance for maximum external pressure, the expressions have been compared for distances beyond this. Due to the relations by Wirkner-Bott et al. and Crowhurst et al. being based upon the maximum external

pressure estimated using Eq. 2.1, this maximum pressure has been calculated and applied to the further calculations.

Table 2: Volumes and conditions applied to empirical expressions

	Small	Medium	Large
Volume [ $m^3$ ]	1	50	200
$A_v$ [ $m^2$ ]	0.1	2	8
$P_{red,max}$ [ $bar$ ]	0.5	0.5	0,5
Angle of sight [ $^\circ$ ]	0	0	0

Presented in Figure 10 are the pressures predicted applying the smallest volume. At a distance of 10 meters, the predicted values are distributed between three levels of magnitude. The pressures estimated using the *Norwegian Formula* and the expression proposed by Wirkner-Bott.et al. are almost identical, whilst the modified expression suggested by Crowhurst et al. predict the highest pressures for all distances. The expression proposed by Hattwig predict by far the lowest values. It must however be noted that the values obtained using the latter are so low that the assumed applicability to the current scenario can be questioned.

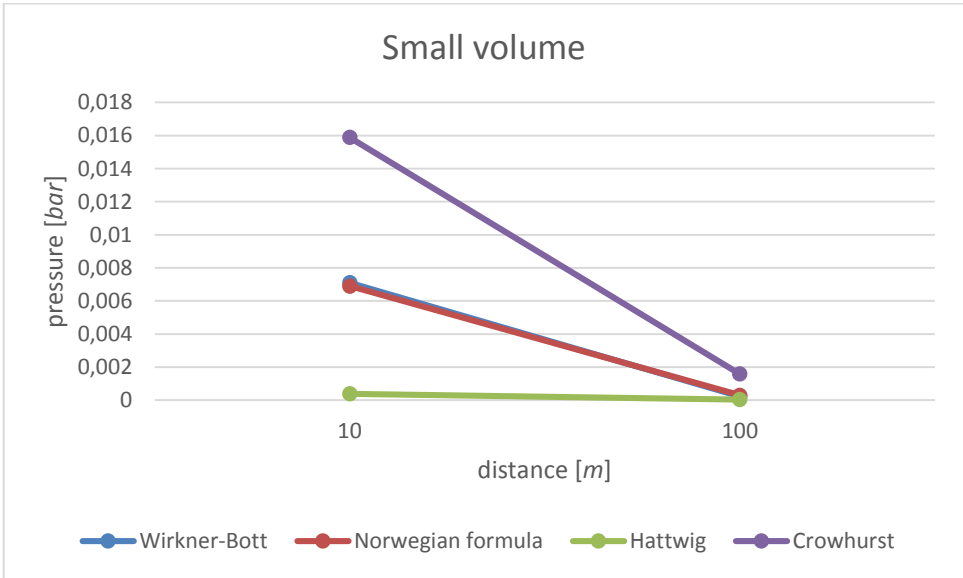


Figure 10: Comparison of predicted values obtained using various empirical expressions for Small scenario (1  $m^3$ )

In Figure 11 the values predicted using the medium volume specified in Table 2 are presented. At a distance of 10 meters the obtained predictions show a difference of one order of magnitude between the expressions providing the largest and the lowest pressures. As for the smallest volume, the highest estimated pressures are obtained using the expression proposed by Crowhurst et al. The pressures obtained using the expressions suggested by Wirkner-Bott et al. and Hattwig are within the same order

of magnitude as predicted using the expression by Crowhurst et al., however estimated pressures are approximately 15-30 % lower. The Norwegian Formula suggests an external pressure of approximately 0.05 bar at a distance of 10 meters, representing one order of magnitude lower than what predicted using the three other expressions.

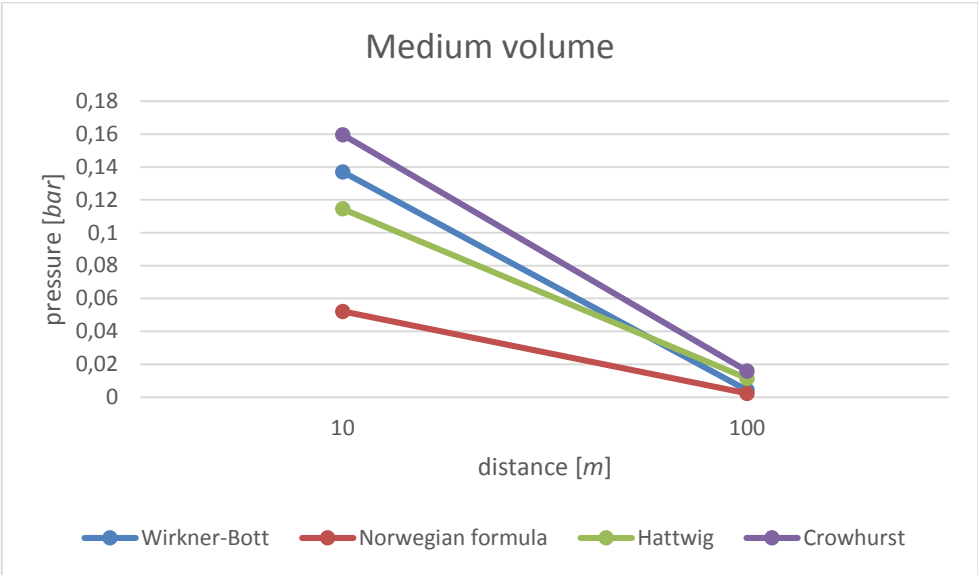


Figure 11: Comparison of predicted values obtained using various empirical expressions for Medium scenario (50 m<sup>3</sup>)

As can be seen in Figure 12, the best correspondence between the four empirical expressions were obtained for predictions applying the largest volume. Using the relation proposed by Wirkner-Bott et al., the distance for the maximum external pressure was estimated to 11.70 m. As explained initially, the prediction of pressure propagation and decay had to be estimated beyond this point. The obtained values for external pressure at a distance of 12 meters were all within the same order of magnitude, however the highest pressure predicted represented almost three times that of the lowest prediction. As for the two previous volumes, the predictions obtained using the equation presented by Crowhurst et al. represent the highest estimated pressures. The estimate obtained using the expression by Wirkner-Bott et al. provide a similar value at a distance of 12 m, however the predicted pressure decay is somewhat steeper. Compared to the expressions by Crowhurst et al. and Wirkner-Bott et al., the predictions using the Norwegian Formula and the expression by Hattwig are significantly lower. The pressure estimated using these expressions are predicted to be approximately one third of the values obtained using expressions by Wirkner-Bott et al. and Crowhurst et al. With exception of estimates obtained using the expression by Crowhurst et al., the predicted pressures seem to converge towards a common value when increasing the distance from the vent.

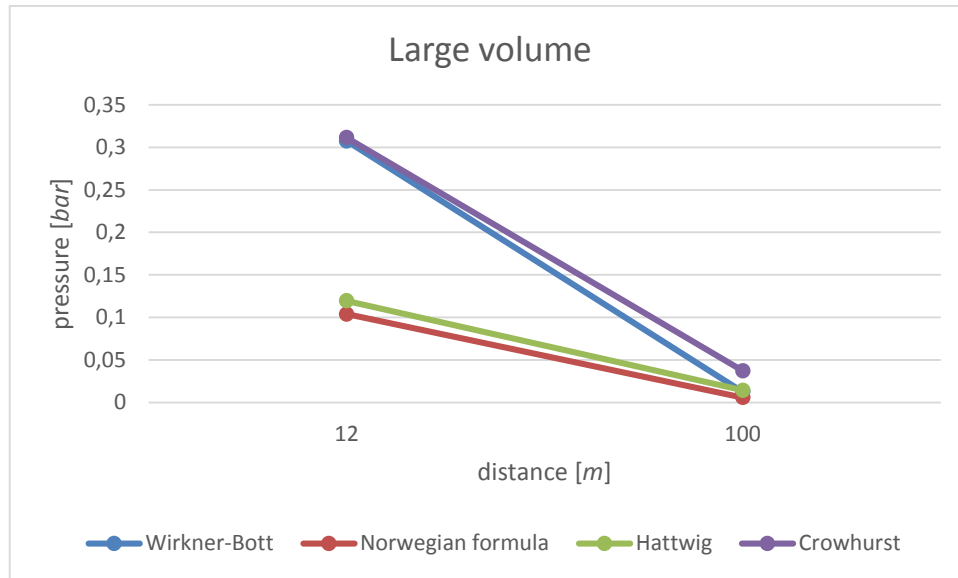


Figure 12: Comparison of predicted values obtained using various empirical expressions for Large scenario (200 m<sup>3</sup>)

As can be seen analysing Figure 10 - Figure 12, there are large differences in the predicted pressures using the various empirical expressions. The most severe deviations between the empirical expressions can be found when applied to small volumes, resulting in predicted pressures with difference of multiple orders of magnitude. For larger volumes, less deviation is observed, however, good agreement amongst the four is not achieved. Comparison of the obtained predictions also revealed the estimated pressure decay with increasing distance to be different for the four expressions. The empirical expression suggested by Crowhurst et al. and Hattwig predict the steepest average pressure decay as a result of distance, followed by the Norwegian formula and the expression by Wirkner-Bott et al. The pressure decay estimated by Crowhurst et al. and Hattwig represents between two and three times the decay predicted by the two other expressions.

Assuming that the predicted pressures estimated using one of the four expressions are to be correct, the use of one of the other expressions would consequently result in an over- or underestimation of the external pressures. If this incorrect estimation is to be applied uncritically in a safety and hazard assessment, the result could be unnecessary high costs when accounting for the overestimated external pressure, or in the worst case lead to critical and dangerous situations due to implementation of insufficient safety measures as a result of an underestimation obtained using an inaccurate empirical expression.

Attempting to explain the differences in predictions it is necessary to break down each of the empirical relations. The four expressions, to some extent, use the same parameters as input for calculating the external pressure. The differences in predicted values are therefore mainly dependent on the described relation between the parameters included in the equation. These relations are derived to express the



correlation found between the parameters measured during the respective experimental studies. Looking at the four expressions included in this comparison, it can be found that they directly or indirectly use the maximum reduced explosion pressure,  $P_{red,max}$ , to estimate the magnitude of the external explosion. The Norwegian Formula and the expression by Hattwig use this parameter directly, while Wirkner-Bott et al. and Crowhurst et al. use it to estimate an external maximum pressure, which subsequently is used to calculate the decay of pressure. Also considered in the expressions are the vent area ( $A_v$ ) and the distance from the vent opening ( $r$ ). None of the expressions account for the reactivity of the fuel used, and the turbulence conditions present upon ignition. This is believed to be an insufficiency in describing the external pressures as these factors along with the fuel concentration strongly effect the ignitability, rate of combustion, ability to propagate an explosion, and consequently the pressure build-up. In the case of a rich mixtures, the explosive mixture vented to the outside of the enclosure would be less effected by dilution, thus able to propagate a more severe external explosion compared to lean mixtures. The reactivity of the fuel would also be of influence in this context as a more reactive fuel type would be able to ignite more easily, and to give a more violent external combustion. Also excluded from the expressions are turbulence conditions, which are known to influence the combustion rate. This is of special relevance in the case of dust as the dispersion of dust would cause some presence of turbulence upon ignition. Obtained experimental results would be influenced by such initial turbulence, which in turn would be reflected in the empirical correlations developed based on these results.

The main intent of this comparison is to not to undermine the specific empirical equations included, but to underline the strong dependency to the experimental conditions in which they are based upon. The large deviations illustrated in Figure 10 - Figure 12, and discussed above, clearly illustrate an inadequacy in a wide applicability of empirical relations. When using empirical expressions, it is therefore important to keep in mind this dependency, especially when applied to conditions deviating from those investigated during the original experimental study. A preferable and ideal approach would be to base predictions and estimates on methods developed to be independent of experimental results, in turn requiring specific conditions for validity.

A potential approach offering such independency could be the use of Computational Fluid Dynamics. CFD is based on, and offer, numerical methods for approximating a solution of the continuity, momentum and energy equations – the governing equations of fluid flow, often referred to as the complete Navier-Stokes equations. These equations are based on the fundamental principles of physics, assuming conservation of mass and energy and Newton's second law,  $F = m \cdot a$ . Basing calculations on these fundamentals should in theory allow for a wide range of validity, contrary to empirical expressions which applicability is limited to those conditions represented in the initial experiments. The use of approximations in obtaining numerical solutions for the governing equations does however result in the need for validation of the CFD software.

# 3 Software & simulation setup

In an attempt to identify a suitable method for obtaining accurate predictions of explosion characteristics without being constrained by a limited area of validity, it has been regarded as appropriate to evaluate the applicability of CFD software. Included as part of this thesis is a series of simulations, set up to investigate the ability to reproduce experimentally recorded values obtained from multiple experimental studies of vented gas and dust explosions. The CFD software chosen for these simulations is FLACS, or FLAME ACcelerator Simulator.

## 3.1 FLACS

FLACS, is a CFD program developed as a tool to aid in the assessment of safety and damage potential of explosions and fires. The software facilitates simulation of dispersion of gases, leaks of fluids, ignition and explosions of clouds of gas, dusts, vapours and mists, blast and shock wave propagation and jet and pool fires.

The FLACS Manual [18] describes FLACS as “ [...] a 3-dimensional (3D) CFD code that solves Favre-averaged transport equations for mass, momentum, enthalpy ( $h$ ), turbulent kinetic energy ( $k$ ), rate of dissipation of turbulent kinetic energy ( $\varepsilon$ ), mass-fraction of fuel ( $Y_F$ ) and mixture-fraction ( $\xi$ ) on a structured Cartesian grid using a finite volume method. The RANS equations are closed by invoking the ideal gas equation of state and the standard  $k - \varepsilon$  model for turbulence (Launder & Spalding, 1974). FLACS solves for the velocity components on a staggered grid, and for scalar variables, such as density, pressure and temperature, on a cell-centred grid. The accuracy of the Flacs solver is second order in space and first/second order in time.”

A realistic method for representation of the geometry and the congestion it causes is of great importance, especially in the prediction of flame propagation and explosion. Introduction of obstacles in a fluid flow will increase turbulence, resulting in a larger flame surface causing an increase in the combustion rate, in turn causing the flame propagation to accelerate. One of the main factors separating FLACS from other conventional CFD software [18], is the porosity concept applied in the simulations. The porosity concept represents geometric objects not coinciding with the grid, by assigning porosities to the relevant cell. The use of such porous cells in representation of smaller geometric elements, permits the use of simplified representation of the geometry. Instead of representing a congested area of for example an oil refinery by applying a detailed and accurate geometry, a percentage porosity can be assigned to the area. This porosity is taken into account by the subgrid-models applied in FLACS. The subgrid-models [18] are developed to represent a simplified but adequate measure for turbulence, restriction of flow and flame folding caused by the objects represented by the porosity assigned to the congested area.

Application of a porosity model as this allows for simulations of scenarios in large geometries applying a coarse grid, as the subgrid-models aim to secure a sufficient representation of smaller objects.

## **3.2 Background for using FLACS**

The simulations performed as part of this thesis have been carried out running FLACS v10.4. There are multiple reasons for choosing the FLACS software for the simulation of experimental work. FLACS has been in continuous development since the early 1980's [18], supported by, and in close cooperation with the oil and gas industry. This collaboration with the industry is regarded as an advantage as this calls for a greater applicability in using the software as an engineering tool, and not only in assessment of physical phenomena. Also regarded as a major advantage is that the developer, Gexcon AS, has its own laboratory and test department performing a wide variety of experimental tests concerning gas and dust explosions. This in-house availability to experimental data has allowed for an extensive validation of the software. The fact that FLACS enables assessment of dispersion, propagation of flame and blast waves, and that the software has undergone an extensive validation has led to FLACS being a widely used CFD software in safety and risk evaluation within process industries. This is regarded as beneficial as the extensive and continued use of the software results in further testing and validation. Last but not least, a reason for choosing FLACS is that this software is one of few CFD software supporting simulation of dust explosions through the extension DustEx (formerly known as DESC – Dust Explosion Simulation Code).

Also contributing to the choice of using FLACS is the opportunity to carry out this thesis in collaboration with Gexcon AS in Bergen – the developer of the software. The collaboration with Gexcon was desirable due to their recognized expertise within the field of gas and dust explosion, the closeness to the research community and that the continued development of the software causes validation to not be entirely completed, meaning that the outcome of this thesis hopefully would serve as a valuable input to this work.

## **3.3 Procedures for FLACS-simulations**

Setting up a simulation in FLACS is typically divided into three main parts: pre-processing, simulation and post-processing - pre-processing being the most important configurational wise. In this part the basic input settings are being defined, both with regard to the physical and to the computational aspect of the simulation. Pre-processing can in turn be divided into four main categories: designing geometry, grid, scenario and computational setup, all carried out in the Computer Aided Scenario Design (CASD) module in FLACS. CASD is the Graphical User Interphase (GUI) implemented in FLACS, allowing the user to define desired settings for the simulations.

### 3.3.1 Pre-processing

#### Geometry and grid

Defining the geometry in FLACS can be done either by building the geometry in the pre-processor CASD, or by importing a geometry from a technical drawing of a supported CAD file format. When building the geometry one also need to keep in mind the guidelines for grid design, especially with regard to recommendations for sizing and distribution of grid cells. In the FLACS User Manual [18] several guidelines and recommendations are given on how one should arrange the grid with regard to both current geometry and the applied scenario. In areas of interest, a *core grid* consisting of cubical grid cells should be applied. Walls, and other larger parts of the geometry should align with the lines of the grid [18]. In other words, the major parts of the geometry should coincide with grid lines in x, y and z-direction. The manual also includes recommendations for the number of grid cells one should apply across different types of clouds, when confined, semi-confined, no confinement, etc., as well as recommendations for the different scenario-types (dispersion, explosion, dust, etc.). With regards to the extent of the *total domain*, or entire grid, recommendations are somewhat looser. The extent of the total grid must be of sufficient size to ensure no undesired influences from the boundaries on the predicted fluid flow [18].

#### Scenario

The second step in setting up a simulation in FLACS is to define the scenario or basic settings for the simulations. Input for both the physical scenario and for the computation of the simulation are made at this step. Possible input parameters are dependent of the type of scenario chosen; gas or dust explosion, dispersion, fire, etc. When choosing the applicable scenario, FLACS assigns a default setup applying typical simulation settings for that respective scenario. In the following bullet points the relevant main options for definition of simulation input and output in FLACS will be presented in short. The described options are mainly limited to those utilized in the simulations performed as part of this thesis. However, some additional functionality is still described as this is regarded to be of importance. Please refer to the FLACS Manual [18] for more detailed descriptions or elaboration on applicability.

- **Monitor points:** Monitor point enables the user to define specific locations within the Cartesian grid where certain specified variables are registered and logged, allowing analyzation of the predicted development of the variable. A vast variety of variables are available. Typical variables of interest are pressure (P), dynamic pressure (DRAG), velocities (UVW), mass fraction (FUEL). The relevance of these variables are however dependent on the physical phenomenon of interest in the simulation scenario.

- **Pressure relief panels:** A pressure relief panel can be used in the simulations either to represent a conventional mitigation measure, or to define an area of interest where specified variables are monitored. Definition of panel properties such as size, location, release pressure, area weight and panel type is possible.
- **Single Field 3D output:** Allows the user to define variables to be monitored in the entire simulation domain. The selected variables are saved automatically allowing the user to present simulation data in various diagrams or to visualize the results in up to 3-dimensional presentations.
- **Simulation and output control:** Specification of frequency, or intervals, in which FLACS is specified to perform calculations and log results. Influences sensitivity and extent of the obtained data set. The possibility to alter the simulation termination criterion for the simulation is also possible.
- **Boundary Condition:** The ability to assign different boundary conditions to the outer boundaries of the simulation domain. Available boundary conditions are EULER, WIND, NOZZLE, PLANE\_WAVE, SYMMETRY, and BERNOULLI. The appropriateness of the boundary condition is dependent on the respective scenario and geometry, e.g. WIND is applicable in representing an external wind field typically used in dispersion simulations.
- **Initial Conditions:** Enable representation of relevant conditions at the beginning of the simulation. Conditions such as temperature, pressure and turbulence can be specified at this step.
- **Gas composition and volume:** Offers the possibility to define a cloud, and to define relevant properties of the cloud. When applying a gas explosion scenario one can specify gas type(-s), stoichiometry, etc. of the cloud. In the case of dust explosion, specification of concentration and of appropriate fuel file is possible. This fuel file contains relevant properties for the respective dust. Further description of the use of fuel file is provided in section 5.1.
- **Multiple or custom gas clouds:** Offers the possibility to set multiple clouds, or clouds of other shapes than rectangular.
- **Leaks:** Allows for application of leakages in the simulated geometry. Application of a leak provides both combustible cloud and associated momentum (turbulence conditions). Leaks can amongst others be represented as point leaks, area leaks and suction, however area leaks are not supported in DustEx.

- **Ignition:** Specification of position, size and effect of ignition point. If relevant, it is also possible to define delayed ignition.

In addition to the options described above, various functionality is available allowing the user to customize the simulation, ensuring an adequate representation of the desired scenario and the ability to extract predictions of relevant variables.

### 3.3.2 Running of simulation

When the desired grid, geometry and scenario have been defined the porosities for the simulations need to be calculated. This is due to FLACS being based on a porosity concept. After calculating the porosities, the simulation is ready to run. Running of the simulation can be administrated either in *FLACS Run Manager*, the included application for administration of running simulations, or by using basic commands in *Linux Terminal* or equivalent. The run time of a simulation depends largely on the complexity of the scenario of the simulation, the number and size of grid cells and the interval at which FLACS is specified to perform calculations.

### 3.3.3 Post-processing

After the simulation has been run the data calculated can be analysed in a post-processor called *Flowvis*. This post-processor allows the user to prepare the acquired data in graphs, diagrams and 2D and 3D visualizations. The number of parameters available in the post-processor depends on the specifications made by the user during pre-processing and definition of scenario. Naturally only default parameters or parameters specified during pre-processing are available for processing after ended simulation.

# 4 Gas explosions

To serve as basis for evaluating the applicability of CFD software in accurately predicting the external effects associated with vented gas explosions, a series of simulations have been performed. The simulations discussed in this chapter are all based on experimental data of vented gas explosions. Relevant data sets have been identified and gathered from available scientific publications.

## 4.1 Setup gas simulations

Definitions of simulation setup have been performed in *CASD*, using *Gas Explosion* as applied scenario type. The default settings for such a simulations scenario has been used as basis for the setup of the experimental tests described in the following. Details with regards to experimental setup have been obtained from referred literature, and the simulations setup has been adjusted accordingly to represent equal conditions. However, should information of importance for the combustion process, and consequently the simulation results, be omitted from the available descriptions of the experiments, the settings applied to the simulation scenarios have been based on justified assumptions.

If other settings are not specified for the respective simulations, the default settings in *FLACS* have been applied. Settings not directly influencing the simulation output have not been described.

### 4.1.1 Setup of experiments by Harrison and Eyre

The first simulated series was based on the experimental work of Harrison and Eyre [1]. As already mentioned in section 2.1.4 of this thesis, Harrison and Eyre conducted tests with vented gas explosions in an enclosure with a volume of 30 m<sup>3</sup>. In the tests either “North Sea Equivalent Gas” or propane were used as fuel, and parameters such as stoichiometry of the gas, ignition point and vent area were varied to be able to evaluate the influence of these parameters. The reason for choosing these experimental tests as basis for the first simulations were the comprehensive set of experimental data offered in the article by Harrison and Eyre [1]. From the article one can obtain initial conditions for each test, recorded peak pressures, along with pressure/time profiles for three of the tests.

Being the first simulations performed, the experiments by Harrison and Eyre became a more comprehensive simulation series. Setting up simulations of these experiments served as an “educational trial run”, with the aim to develop a suitable approach also applicable for the following simulations of similar experimental scenarios.

## Preliminary test

Prior to the tests referred to below, a series of trial simulations were performed to identify the importance of alterations in the geometric dimensions, and the impact of such in combination with deviations from guidelines in the FLACS Manual [18].

A sketch of the experimental setup used by Harrison and Eyre [1] is provided in Figure 8 of this thesis. The explosion chamber used was an enclosure of rectangular shape with the internal dimensions 5.92 m x 2.38 m x 2.16 m. No CAD-drawing/-file of the enclosure was available and the enclosure therefore had to be built in FLACS.

For simulations of gas explosions within a confined vessel, and subsequent modelling of flame acceleration, the FLACS Manual [18] recommends to resolve the internal volume of the vessel by at least 5-6 grid cells in the smallest direction. The entire gas cloud is recommended to be resolved by at least 15 cells. For unconfined or partly confined gas clouds it is recommended to use “*a minimum of 13 grid cells across the cloud in directions where both sides are unconfined, and a minimum of 10 grid cells in directions where the cloud meets confinement*”. For openings of importance, i.e. vent openings, the recommendation is to resolve the opening by at least 6-8 cells. These guidelines are however made for regions of high-congestion. After conducting some tests with this fairly simple geometry, it could easily be seen that the guidelines for dissolving of geometry while applying a uniform cubical grid would not combine with the recommendations for this type of scenario, total number of grid cells, maximum percentage difference and maximum aspect ratio for the cells. The only way that allows for the grid and geometry to comply with the recommendations [18], is by using a very large number of grid cells. This is not desirable due to the long computational time required to run simulations with large numbers of grid cells. To agree with guidelines given in the FLACS Manual [18] regarding geometry and grid, some minor alterations to the original dimensions were necessary.

Experimenting with the original dimensions, and to comply with the recommendations for the lines of the geometry to coincide with the grid lines, additional grid lines were added at strategic coordinates thereby aligning with the enclosure. The added grid lines complying with the boundaries of the geometry did in some cases result in larger differences between adjacent cells than what recommended in the FLACS Manual [18]. To compensate for this, multiple grid lines were added to smoothen the transition zone, thereby complying with recommendations regarding sizing of adjacent cells [18]. The use of original dimensions in combination with added grid lines did however result in deviations from guidelines for application of a cubic core grid. Considering this, and that no prominent trend could be found when applying this methodology, no further investigation of this approach was performed.



During the initial planning of the simulation, various tweaks to the original geometry were performed with the intent to find the optimum compromise between combination of guidelines, and maintaining original geometric dimensions. After conducting a comprehensive test series, it seems as if the optimal compromise is one that allows the geometry to completely align on the grid without larger adjustments to the original proportions, while simultaneously allowing the geometry to resolve in a wide number of cell sizes, thus allowing the performance of grid sensitivity test.

After discussing findings from the preliminary tests with more experienced FLACS users [19, 20], a prioritized list for the importance of the guidelines was established. The following prioritized order was applied to the simulations:

1. Applying a cubic core grid
2. Allowing the geometry to align on the grid, both enclosure and vent opening
3. Maintaining original dimensions
  - a. Maintaining volume
  - b. Maintaining a proportional vent area

It must be noted that in the paper by Harrison and Eyre [1] a mismatch between the fraction of the vent area to that of the wall, and the stated vent area was discovered. When taking into consideration that the total geometry has been subject to multiple adjustments, the vent fraction is considered to be the most accurate source for scaling of the vents in the simulations. This may cause the vent to be slightly smaller than those used in the experiments, possibly causing the simulations to predict slightly higher internal pressures.

## **Applied geometry and grid**

To investigate the influence of different tweaks to the geometry, the simulations of the tests by Harrison and Eyre were performed with two different geometries of similar size and dimensions, both thought to be an appropriate adaption of the original geometry.

In the first geometry, hereby referred to as *Geometry 1*, the dimensions of the enclosure were altered to 6.00 m x 2.30 m x 2.20 m (x-, y- and z-direction), giving a total volume of 30.36 m<sup>3</sup>. These dimensions were chosen as they give approximately the same volume as the original enclosure, while at the same time allowing the geometry to resolve without requiring a grid of very high resolution. Grid sensitivity test for this geometry revealed that the cell size corresponding to the best predictions was that of 0.05 m (this to be discussed more extensively in section 4.2.1).

The second geometry, *Geometry 2*, used in the simulations had a dimension of 5.90 m x 2.40 m x 2.15 m (x-, y- and z-direction), resulting in a volume of 30.44 m<sup>3</sup>. These dimensions were applied after the observation of 0.05 m being the grid size giving the most corresponding simulations. Prior to this a main approach had been to allow geometry to resolve in a core grid of 0.10 m. The dimensions of the entire grid are described in detail in Table 3.

*Table 3: Dimensions of grid applied to simulations using a 30 m<sup>3</sup> enclosure from the experiments by Harrison and Eyre [1]*

	<b>X [m]</b>	<b>Y [m]</b>	<b>Z [m]</b>
Core, start	-0.10	-2.00	0.00
Core, end	14.50	4.30	5.00
Core, cell size	0.05	0.05	0.05
Total, start	-1.00	-5.00	0.00
Total, end	40.00	7.30	10.00
Size	Stretched	Stretched	Stretched

Monitor points were defined to correspond to the location of pressure transducer used in the experiments. The monitor points were defined on the ground at distances of 0 m, 5 m, 10 m, 15 m and 20 m, in the centre line of the vent opening.

## Scenario

Presented in Table 4 are the test setups used in the experimental series by Harrison and Eyre [1]. The tests highlighted are those where pressure-time-graphs are available, thus the ones chosen for simulation.

Table 4: Experimental data set, modification of original table by Harrison and Eyre [1]

Test	Fuel	Vent	Ignition location	Fuel concentration [%v/v]	Stoichiometry, [ $\lambda$ ]	Peak overpressure at rear of chamber, [mbar]	Peak overpressure recorded externally, [mbar]	Location of external pressure, [m]
B1	C <sub>3</sub> H <sub>8</sub>	1/2	C	4,45	11,1	170	108	0
B2	C <sub>3</sub> H <sub>8</sub>	1/2	F	4,42	1,1	10	3	---
B3	C <sub>3</sub> H <sub>8</sub>	1/2	R	4,41	1,1	286	227	5
B4	N.G.	1/2	C	10	1,07	52	26	0
B5	N.G.	1/2	R	10,2	1,1	215	145	0
B6	N.G.	1/4	C	10,1	1,08	205	112	0
B7	N.G.	1/4	R	10,3	1,11	542	324	5-10
B8	N.G.	1/4	F	10	1,07	---	---	---
B9	C <sub>3</sub> H <sub>8</sub>	1/4	C	4,51	1,13	195	104	0
B10	C <sub>3</sub> H <sub>8</sub>	1/4	R	4,47	1,2	892	682	5
B11	C <sub>3</sub> H <sub>8</sub>	1/4	R	4,44	1,11	1100	445	5
B12	N.G.	1/4	R	12,2	1,35	36	46	5
B13	N.G.	1/4	R	7,6	0,8	330	98	5-10
B14	N.G.	1/8	R	10,1	1,08	---	---	---
B15	N.G.	1/8	C	10,1	1,08	403	145	5
B16	N.G.	1/8	R	10	1,08	1067	345	---
B17	C <sub>3</sub> H <sub>8</sub>	1/8	C	4,45	1,11	425	221	5
B18	C <sub>3</sub> H <sub>8</sub>	1/8	R	4,39	1,1	1340	418	5

\* R = ignition initiated at rear wall, C = ignition initiated at centre of vessel

All the three test scenarios described in the following were applied to both *Geometry 1* and *Geometry 2*. All scenario settings were adjusted to account for difference between the two geometries.

### Description of B3

The first experimental test setup was the one referred to as test *B3* in Table 4. As for all the tests by Harrison and Eyre, this experiment was performed in the 30 m<sup>3</sup> enclosure described earlier in this section. The enclosure was equipped with a vent of area equalling half the area of the end wall. The vent was given the dimensions 1.6 m x 1.6 m and sought located at the centre of the end wall, venting in x-direction. However, to allow for the vent opening to be resolved on a grid of 0.10 m an exact centration was not possible. It was therefore necessary to place the vent slightly off centre in horizontal direction. The vent was in the experiments covered with a thin polythene sheeting. When analysing the internal pressure recordings Harrison and Eyre [1] assigned the small amplitude of 10-20 mbar, present shortly

after ignition, to the release of the vent. Based on this an assumed vent release pressure ( $P_{\text{stat}}$ ) of the vent was set to 0.010 bar. The weight of the sheeting was assumed to be 0.1 kg/m<sup>2</sup>.

The ignition for test *B3* was initiated at the centre of the end wall opposite to the vent opening. Gas concentration specified for the simulations were set according to the experiments. The gas was specified to be a homogenous cloud of propane (C<sub>3</sub>H<sub>8</sub>) and air, mixed to a stoichiometric equivalence ratio of 1.10, and set to cover the entire internal volume of the enclosure. The purity of the propane was 99.5%.

#### Description of B5

Like for test *B3* the experimental setup for test *B5* included the use of the 30 m<sup>3</sup> enclosure fitted with a vent of half the area of the end wall, equalling to a vent area of 2.56 m<sup>2</sup>. Also the same location, release pressure and weight was used for this simulation.

In test *B5* the point of ignition was also specified to be at the centre of the rear wall, opposite to the vent opening. However, the type of gas used in this test was North Sea Equivalent Gas, consisting of 96% methane and 4% ethane. The gas concentration was of a stoichiometric equivalence ratio of 1.10. As for test *B3* the cloud was specified to be a homogenous cloud covering the internal volume of the enclosure.

#### Description of B6

The physical setup used in test *B6* differ from that of test *B3* and *B5*. In this test the vent area was specified to one fourth of the area of the end wall. This vent was given the dimensions 1.15 m x 1.10 m, resulting in a vent area of 1.265 m<sup>2</sup>. As for the two previously described simulation setups, the vent was sought placed at the centre of the end wall. However, the need for resolving the vent opening on the grid resulted in a location slightly off centre. Other settings applied to the vent panel were similar as for the two previously described setups. The ignition point in this test was specified to be in the geometric centre of the enclosure, corresponding to the ignition point used in the experiment.

### **4.1.2 Setup of experiments by van Wingerden**

The second case subject to simulations was based on the work of Kees van Wingerden [12, 13] and W.P.M. Mercx, C.J.M. van Wingerden and H.J Pasman [21]. The experimental work was initially performed by van Wingerden, however, the experimental data has also formed the basis for the publication by Mercx et al. [21]. The experimental work is a study of vented gas explosions conducted in a concrete bunker of 4.0 m x 3.7 m x 2.6 m, equalling to a volume of 38.5 m<sup>3</sup>. A graphical image of the applied geometry is provided in Figure 13. In the experimental series, parameters such as size and position of vent areas, and position of ignition point was varied to investigate the influence of these. The data presented in the mentioned papers include pressure-time-curves for two of the tests, covering

ignition at the centre and at the rear of the enclosure while applying a vent area of 4.1 m<sup>2</sup>. Due to the available pressure development curves, these experiments were considered a suitable basis for simulations.



*Figure 13: Graphical image of enclosure of 38,5 m<sup>3</sup> used in FLACS for simulations of experiments van Wingerden [12].*

## **Geometry and grid**

The geometry used in the simulations of the work of Van Wingerden [12, 13] was implemented in CASD. To best represent the actual geometry used by van Wingerden, it was necessary to gather information from all of the above mentioned references. For some of the dimensions of the geometry, differences between data presented in the articles were observed. In these cases, the work of Ir. M. Dragosavic [22] was also examined as this work is based on experiments using the same concrete bunker. In the case of any continued inconsistencies, the dimensions used by van Wingerden were applied. The main dimensions of the room, being 4.0 m x 3.7 m x 2.6 m (x-, y- and z-direction), allowed for the use of both 0.05 m and 0.10 m grid and was therefore maintained for the applied geometry. In the experiments of interest, the vent opening was specified to be 4.1 m<sup>2</sup>, and located in the centre of the end wall. As described in section 2.1.5, the system allowing application of various vent areas was based on attaching sheets of plywood to a framework constructed of steel beams. This method caused the steel beams to cross the vent opening when configured for the specific experiments. To account for the

turbulence these beams might represent, three rectangular shaped boxes were arranged in an H-shape and placed at the assumed location of the beams. An exact location of the beams and vent opening were not available. The opening is therefore assumed to have a size of 3.4 m x 1.4 m, venting in the x-direction. These are considered reasonable dimensions given the defined area of the vent and the remaining sizes of the enclosure. Presented in Figure 14 are sketches of the geometric setup applied in the simulations. The entire geometry, including vent opening and beams align completely on the grid applied for the simulation.

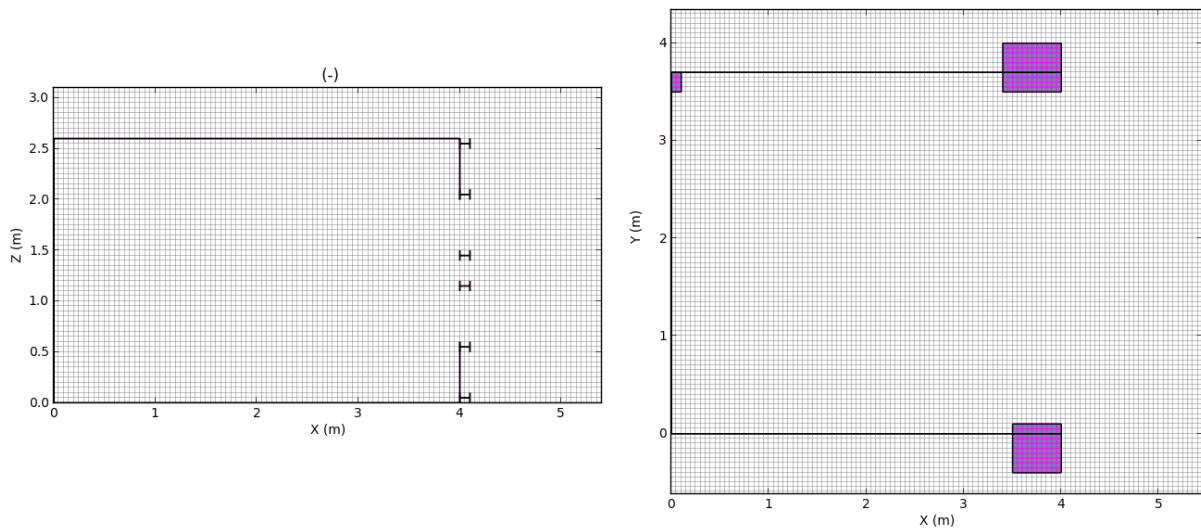


Figure 14: Geometry cross-section aligned on the grid applied to the simulations of experiments by van Wingerden [12].

When setting up the geometry and grid for the simulations, experiences gained when simulating experiments by Harrison and Eyre formed the basis for sizing of the grid. Comparing results from experiments and simulations showed that a core cell size of 0.05 m represented the best simulation results for the geometry used by Harrison and Eyre. Due to the geometry used by van Wingerden being approximately of the same size, a similar cell size was applied to the core grid for this geometry. The boundaries of the total grid domain were placed sufficiently far from the area of interest to avoid reflections or other influence from these boundaries. The dimensions of the entire grid are presented in Table 5.

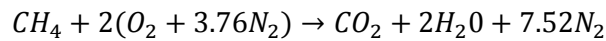
Table 5: Dimensions of grid applied to simulations using a 38,5 m<sup>3</sup> enclosure, van Wingerden [12]

	X [m]	Y [m]	Z [m]
Core, start	0.00	-2.50	0.00
Core, end	14.50	6.20	7
Core, cell size	0.05	0.05	0.05
Total, start	0.00	-10.00	0.00
Total, end	30.00	13.70	12.60
Size	Stretched	Stretched	Stretched

## Scenario

The experimental scenarios referred to by van Wingerden [12] and Mercx et al. [21] are vented gas explosions with ignition initiated either at the geometric centre or at the rear wall. The enclosure was filled with a methane gas of purity 99.5%, up to a concentration equalling 10% v/v, a slightly rich mixture as the stoichiometric concentration for methane is 9.5% v/v. This expression for fuel concentration had to be converted to equivalence ratio ( $\lambda$ ) as the latter is the format handled by FLACS.

Stoichiometric concentration



This corresponds to a stoichiometric fuel concentration of:

$$\begin{aligned} n &= \text{number of mol} \\ \frac{n}{2}CH_4 + n \cdot 4.76(N_2 + O_2) \\ &\rightarrow \frac{1}{1 + 2 \cdot 4.76} = 9.5\% \end{aligned}$$

Fuel concentration of 10% v/v leads to:

$$\begin{aligned} CH_4 &= 0.10 \\ O_2 + N_2 &= 0.90 \end{aligned}$$

Oxygen being the substance reacting with the methane, thus the substance of interest:

$$\begin{aligned} n_{O_2} \cdot 4.76 &= 0.90 \\ \rightarrow n_{O_2} &= \frac{0.90}{4.76} = 0.189 \end{aligned}$$

Giving an equivalence ratio of

$$E_r = \lambda = \frac{\frac{n_{Fuel}}{n_{O_2}}}{\left(\frac{n_{Fuel}}{n_{O_2}}\right)_{Stoich}} = \frac{0.10}{\frac{0.189}{2}} = 1.058$$

An equivalence ratio of 1.058 is therefore used in the simulations. The gas cloud is assumed to cover the entire volume of the enclosure, and to be homogenous.

In the experiments, five layers of polyethylene film was placed in front of the vent opening to retain the gas cloud prior to ignition. As stated in the paper by van Wingerden [12] the influence of such had little or no apparent impact on the overpressures generated. Vent relief pressure is nonetheless set to 0.010 bar to represent the presence of the polyethylene sheets. A weight of 0.1 kg/m<sup>2</sup> is assumed for the material of the vent panel.

Monitor point were placed at locations equal to the ones used for placing of pressure transducers in the experiments. The external transducers are assumed to be located on, or near the ground and are therefore given such positions in the simulations. To comply with guidance provided in the FLACS Manual [18], the locations for the monitor points were picked to not coincide with grid lines.

### **4.1.3 Setup for varying test volume**

After conducting several simulations based on experimental data for vented gas explosions, some additional simulations were performed to further investigate the findings from these initial simulations. The supplementary simulations were not based on experimental work, but are purely simulation sensitivity scenarios. The first attempt was to investigate the effects of variations in volume of enclosures with similar geometric shape. The geometries in these simulations were based on the enclosure used by Harrison and Eyre [1], described in section 2.1.4 and 4.1.1. The two sizes chosen for simulations were one of approximately half the volume, and one of almost twice the volume of the original.

#### **Geometry and grid – Vol.1, smaller volume**

The geometry used for the simulations with a smaller enclosure was designed to be of similar geometric shape, but with approximately half the volume of the one used by Harrison and Eyre [1]. The geometry was scaled to correspond to a volume of approximately 15 m<sup>3</sup>, with a vent area equalling to one half of the end wall. The dimension chosen for the enclosure was 4.80 m x 1.85 m x 1.75 m (x-, y- and z-direction), giving a volume of 15.54 m<sup>3</sup>. A vent of dimensions 1.30 m x 1.30 m, equalling to an area of 1.69 m<sup>2</sup>, was fitted at the end wall, venting in x-direction. These dimensions were chosen as they comprise to the desired volume, and at the same time allow the geometry to resolve in a grid of cell size 0.025 m and 0.05 m. Applying such cell sizes is assumed reasonable as the best fitting grid for a geometry of twice the size was a core grid consisting of 0.05 m cells. Due to the reduced size of the enclosure, the boundaries of the core grid, as well as the total grid, were adjusted accordingly. The dimensions of the entire grid are presented in Table 6.



Table 6: Dimensions of grid applied to simulations using a 15 m<sup>3</sup> enclosure, Vol.1

	X [m]	Y [m]	Z [m]
Core, start	-0.10	-1.60	0.00
Core, end	11.60	3.45	4.00
Core, cell size	0.05	0.05	0.05
Total, start	-0.10	-4.00	0.00
Total, end	32.00	5.85	8.00
Size	Stretched	Stretched	Stretched

### Scenario – Vol.1, smaller volume

The scenario applied to the simulation is identical to the one applied for the simulation of test B3, but with adjustments according to the scale of the current geometry. The monitor points applied for this simulation were of distance according to the reduced scale, resulting in an interval of 4 m. Minor adjustments were also made to the monitor points, to avoid placement on grid lines.

### Geometry and grid – Vol.2, smaller volume

After analysing the results of the simulation including the enclosure described above as Vol.1, the need for a similar simulation with a smaller enclosure of *identical* proportions as Geometry 1 was identified. The smaller enclosure, Vol.1, had some minor deviations from the exact geometric proportions due to adaption to a grid with core cell size of 0.05 m. It was desirable to compare these to the results from simulations including an enclosure of identical proportions and aspect ratio as those applied for Geometry 1.

For the new enclosure the dimensions of Geometry 1 were multiplied by a factor of 0.8, giving dimensions of 4.80 m x 1.84 m x 1.76 m, and a volume of 15.54 m<sup>3</sup>. These dimensions do not differ a lot from those applied for Vol.1, however the dimensions allow for the geometry to resolve in a cubic core grid of cell size 0.04 m. This cell size was also obtained by multiplying by a factor of 0.8. The remaining parameters of the grid were also corrected by a factor of 0.8. The enclosure was equipped with a vent of size 1.28 m x 1.28 m, giving a vent area of 1.638 m<sup>2</sup>, venting in the x-direction.

The exact scaling of both geometry and grid resulted in an identical number and distribution of grid cells, both in the core and the total extent of the grid. The factor of 0.8 was not a random choice, but a result of FLACS CASD allowing specification of up to two decimals for cell size of the core grid. To obtain an enclosure volume of approximately half the volume the factor of 0.8 was the best fit, both volume and grid wise. The dimensions of the entire grid are presented in Table 7.

Table 7: Dimensions of grid applied to simulations using a 15 m<sup>3</sup> enclosure, Vol.2

	<b>X [m]</b>	<b>Y [m]</b>	<b>Z [m]</b>
Core, start	-0.04	-1.60	0.00
Core, end	11.60	3.44	4.00
Core, cell size	0.04	0.04	0.04
Total, start	-0.04	-4.00	0.00
Total, end	32.00	5.84	8.00
Size	Stretched	Stretched	Stretched

### Scenario – Vol.2, smaller volume

Compared to the previously described simulation setup, no other changes were made than minor adjustments to the dimensions of the geometry. The dimensions of the gas cloud, ignition point and vent panel were adjusted accordingly to replicate an identical scenario to the one described for Vol.1.

### Geometry and grid – Vol.3, larger volume

The larger geometry was designed with dimensions corresponding to a volume of almost twice the size, while maintaining a similar geometric shape as the original geometry used by Harrison & Eyre [1]. The size of the enclosure was set to 7.20 m x 2.80 m x 2.60 m, giving a volume of approximately 52.42 m<sup>3</sup>, with a vent opening of dimensions 1.90m x 1.90 m equalling to an area of 3.61 m<sup>2</sup>.

As for the simulation of a smaller volume, the grid used for simulation with an enclosure of larger volume was adjusted accordingly. The core grid consisted of cubical cells with a size of 0.10 m. Both the extent of the core grid and the total grid were enlarged to fit simulations of explosion in a larger enclosure. The dimensions of the entire grid are presented in Table 8.

Table 8: Dimensions of grid applied to simulations using a 52 m<sup>3</sup> enclosure, Vol.3

	<b>X [m]</b>	<b>Y [m]</b>	<b>Z [m]</b>
Core, start	-0.10	-2.40	0.00
Core, end	17.40	5.20	6.00
Core, cell size	0.10	0.10	0.10
Total, start	-0.10	-6.00	0.00
Total, end	48.00	8.80	12.00
Size	Stretched	Stretched	Stretched

### Scenario – Vol.3, larger volume

The simulation scenario applied is identical to the one defined for the simulation of test *B3*, but with adjustment to account for the increased dimensions. The gas cloud was extended to account for the larger geometry. Ignition point and monitor points were altered to represent the same locations, but for a larger geometry. Additional monitor points were added in x-direction. Small adjustments were made to the location of monitor points, ensuring a placement not coinciding with the grid lines.

### Geometry and grid – Vol.4, larger volume

As for the smaller volume, analysing the simulations including Vol.3 called for an additional simulation of a larger enclosure with *identical* proportions and aspect ratio as Geometry 1. While the geometry described as Vol.3 was adapted to allow for resolving in a grid of cell size 0.10 m, a scaled version with identical aspect ratio was designed by applying a multiplication factor of 1.2 to the dimensions of Geometry 1. This resulted in dimensions of 7.20 m x 2.76 m x 2.64 m, giving a volume of 52.46 m<sup>3</sup>, and a vent of size 1.92 m x 1.92 m, equalling to an area of 3.686 m<sup>2</sup>.

The grid for the simulation of the scaled geometry was also defined using a multiplication factor of 1.2. The core grid consisted of cubical cells with a size of 0.06 m. Compared to the grid applied to the simulations of the 30 m<sup>3</sup> enclosure, the range of the core grid and total grid were adjusted by a factor of 1.2. As for the choice of a factor of 0.8 when designing the smaller enclosure, the factor of 1.2 was not random. The factor of 1.2 corresponds to almost twice the volume of the original enclosure, while simultaneously allowing the grid to be scaled in a cell size only including two decimals. The dimensions of the entire grid are presented in Table 9.

Table 9 Dimensions of grid applied to simulations using a 52 m<sup>3</sup> enclosure, Vol.4

	X [m]	Y [m]	Z [m]
Core, start	-0.06	-2.40	0.00
Core, end	17.40	5.16	6.00
Core, cell size	0.06	0.06	0.06
Total, start	-0.12	-6.00	0.00
Total, end	48.00	8.76	12.00
Size	Stretched	Stretched	Stretched

### Scenario – Vol.4, larger volume

The scenario for this simulation did not differ from the preceding in other ways than some adjustments to the size of the geometry. The dimensions of the gas cloud, vent panel and ignition point were adjusted accordingly to replicate an identical scenario as the one applied for earlier simulations of test *B3* in the 30 m<sup>3</sup> enclosure.

#### 4.1.4 Setup of tests varying vent sizes

As for the simulations investigating the effect of change in volume for similar shaped geometries, an additional simulation series aiming to examine the effect of variation in vent area was carried out. Again the experiments by Harrison and Eyre [1] were used as a base for the simulations.

##### Geometry and grid

The geometry used for these investigative simulations were based on Geometry 1 used in earlier simulations. The vent area was however changed to one fourth and one eighth of the area of the end wall. The chosen dimensions for the vent area of one fourth were 1.15 m x 1.10 m, giving an area of 1.265 m<sup>2</sup>. For the vent of one eighth, the applied dimensions were 0.80 m x 0.80 m, corresponding to an area of 0.64 m<sup>2</sup>.

An identical grid as that described in section 4.1.1 was applied. The core grid was made up of cubical cells of size 0.05 m, and defined to cover the entire geometry. The core grid was also extended beyond the opening of the vent to include external monitor points of interest. The boundaries of the total grid were set sufficiently far from the area of combustion, ensuring no undesired influence affecting the combustion and explosion process.

##### Scenario

With exception of adjustment of vent area, an exactly identical scenario as for the simulation of *B3* was applied to the simulations with various vent areas. A homogenous cloud of air and propane, mixed to an equivalence ratio of 1.10 was set to cover the entire internal volume of the enclosure. Ignition was initiated at the centre of the rear wall of the enclosure. The vents used in the two different simulations were set to have a  $P_{\text{stat}}$  of 0.010 bar.

## 4.2 Results and discussion

### 4.2.1 Results simulations of experiments by Harrison & Eyre

The initial simulations of tests by Harrison and Eyre [1] were performed as an extensive simulation series with the aim to establish a common approach to the setup of simulations of vented explosions in uncongested geometries. As FLACS is a software designed to simulate and predict fluid flow, combustion and explosion in large geometries with many obstacles, the guidelines suggested in the FLACS Manual [18] may not always be directly applicable to an enclosed geometry of low congestion.

## Preliminary tests

The guidelines for setting up simulations included in the FLACS Manual [18] are developed on the basis of the extensive validation work performed to document the accuracy of the software, and to document the best approach when simulating various scenarios and geometries. Due to the guidelines being based on simulations reproducing similar values to those obtained experimentally, the validation has naturally not been conducted for every scenario possible. When applied to some combinations of scenario and geometry one may experience contradicting guidelines. As a consequence, the initial tests served as a trial series with the aim of developing an approach resulting in the most accurate simulations.

Before running the simulation setup described as “Applied geometry” in section 4.1.1, an alternative simulation series was performed applying small variations in size of enclosure, size of vent, placement of vent opening and in the size of grid cells. The main goal was to identify the parameters of importance when defining a geometry and scenario similar to the experimental setup used by Harrison and Eyre [1].

### Geometry

With regards to variations to the geometric setup used in the initial simulations, the significance of such was most visible when looking at dimensions of the geometry in combinations with settings for the applied grid. Unsurprisingly, variations to the geometry applied to the same grid resolution resulted in variations with regard flame propagation and pressure build-up.

When a geometry with the original dimensions was applied to a uniform cubic grid, the walls and openings of the enclosure did not coincide with the lines of the grid, consequently the geometry did not align on the grid. To be able to represent the parts of the geometry not coinciding with the grid, FLACS assigns various degrees of porosity to the cells only partially filled by the geometry. In Figure 15, the outer dimensions of the geometries are allowed to be aligned on the grid, however the original dimensions of the vent opening are maintained for the geometry on the right. Consequently, the boundaries of this vent opening do not align with the applied grid and the transition from the solid walls of the enclosure to the orifice of the vent is therefore represented by porous cells. When analysing results of the initial simulations this could be the reason for some of the deviating results between simulations with different levels of resolved geometry. The porous cells associated with the partly resolved geometry, i.e. vent opening, contributes to increased levels of turbulence [18]. This increased level of turbulence is assumed to increase the combustion rate. Fluid flow across the edges of the vent opening are obvious sources of turbulence. Assigning porous properties to the grid cells, however, results in a larger surface area, thus generating more turbulence than what is realistic in physical situations. It is also assumed to be unfortunate that similar parts and sizes of the structure are represented in different

ways in the simulation. Inconsistency in definition of similar objects could lead to comparable parts of the geometry influencing the fluid flow in different ways.

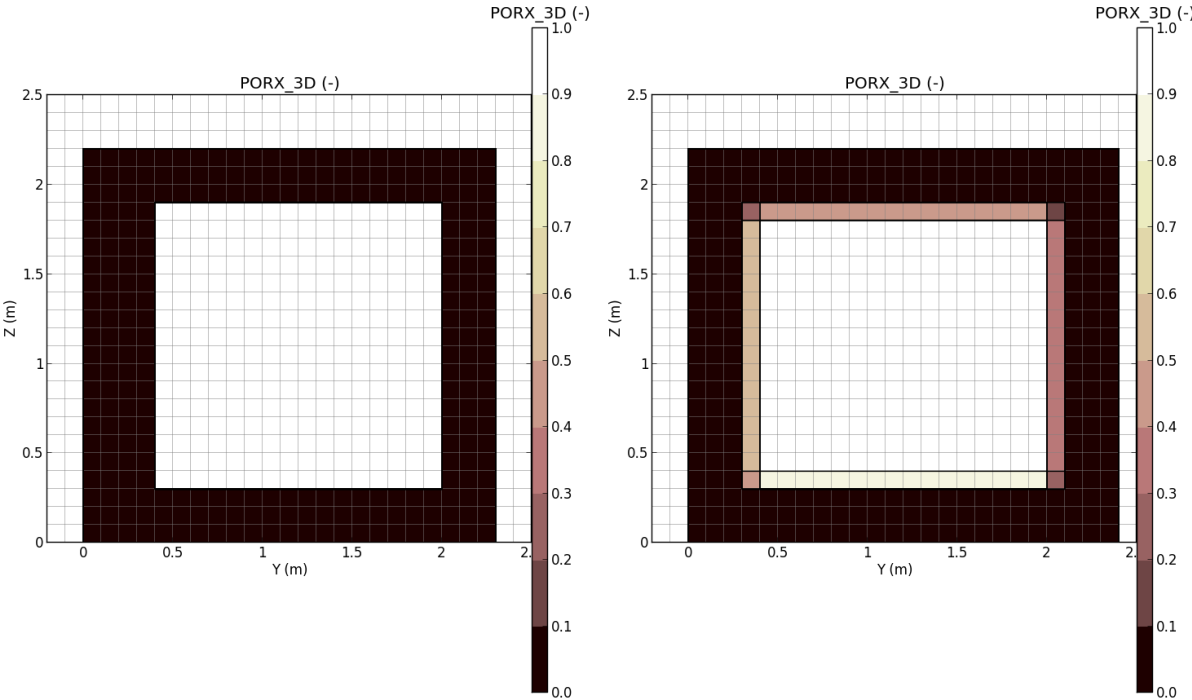


Figure 15: Resolving of alternative geometries with application of identical grid

Grid

The core grid was defined to include the entire volume of the enclosure. As the external phenomena occurring outside the vent being of interest, the core grid was extended to also include an area outside of the vent. This allowed the external combustion propagation to be included in the fine mesh of the core grid. The lack of obstacles outside the enclosure led to some uncertainties regarding the importance of a fine grid on the accuracy of the predictions of variables. To establish the importance of the extent of the core grid, an initial simulation series was performed. This series included seven simulations where the limits of the core grid were varied systematically to investigate the influence on the values obtained. The cell size applied to the core of these simulations was 0.10 m. The maximum dimensions of the total grid were maintained during the tests.

Table 10 list the parameters of the core grid, applied to the various simulations. As can be seen, the only dimension changed in these simulations is the extent in x-direction, which also coincides with the direction of the venting. The purpose of this exercise was to investigate how far beyond the vent opening it is necessary to extend the core grid to obtain accurate values for the predicted variables.

Table 10: Settings for core grid in the investigation of importance of extending core grid externally

Simulation No.	X, start [m]	X, end [m]	Y, start [m]	Y, end [m]	Z, start [m]	Z, end [m]	Cell size [m]
300001	-0.10	6.50	2.00	4.30	0.00	5.00	0.10
300002	-0.10	8.50	2.00	4.30	0.00	5.00	0.10
300003	-0.10	10.50	2.00	4.30	0.00	5.00	0.10
300004	-0.10	12.50	2.00	4.30	0.00	5.00	0.10
300005	-0.10	14.50	2.00	4.30	0.00	5.00	0.10
300006	-0.10	16.50	2.00	4.30	0.00	5.00	0.10
300007	-0.10	18.50	2.00	4.30	0.00	5.00	0.10

When analysing the results of the simulations utilizing different extensions of the core grid, it immediately became clear that the extent of the core grid affects the predicted values. Figure 16 shows the predicted pressures at an internal monitor point for all seven simulations. At this point the simulations calculate the specified variables over the same number and sizes of grid cells. It can be seen that the pressure development for the different simulations are almost the same. However, looking at Figure 17 it can be seen that the predicted development of pressures for the external monitor point 5 m from the vent opening varies between the simulations. Extending the grid further from the vent opening causes the external phenomena to be resolved over a larger number of grid cells, and as can be seen this causes prediction of higher pressures. When comparing these predictions to the experimental recordings by Harrison and Eyre, the simulations where the core grid included the external monitor point were found to give the best prediction for that respective monitor point.

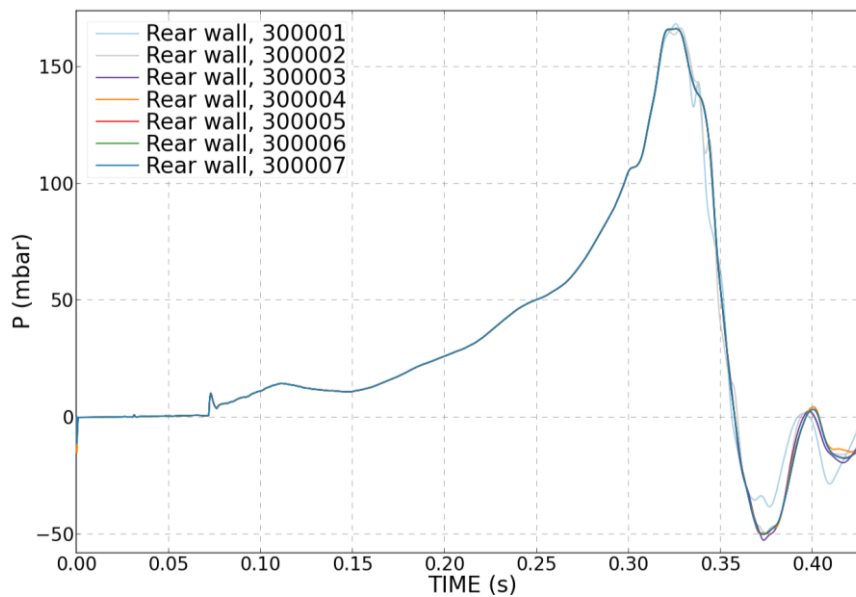


Figure 16: Internal pressures at rear wall of enclosure for the seven simulations investigating effects of extended core grid

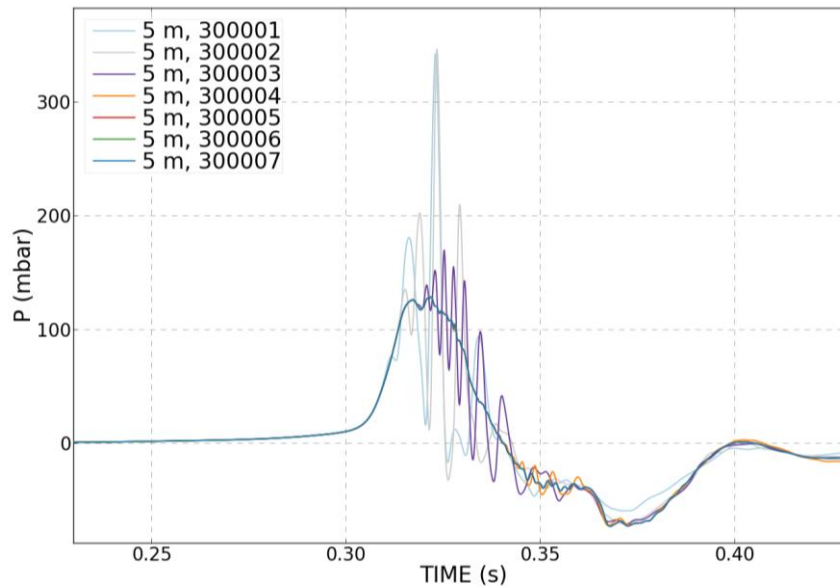


Figure 17: External pressures, 5 m from vent opening for the seven simulations investigating effects of extended core grid

### Grid sensitivity

Multiple grid sensitivity tests were performed in an attempt to further refine the grid, thereby obtaining improved predictions and gain better understanding of grid dependency on simulation results. A grid is believed to be well suited for the simulation when the predicted variables lead towards the same values even with changes in cell sizes. The results of the simulations with an enclosure as described in section 4.1.1 did however show a strong grid dependency for the simulation of external explosions in uncongested geometries. Figure 18 presents the pressure-time development at the same monitor point for three similar simulations where the only difference between the three is the cell size applied to the core grid. The extent of the grid, along with the geometry and scenario used are the same for the simulations.



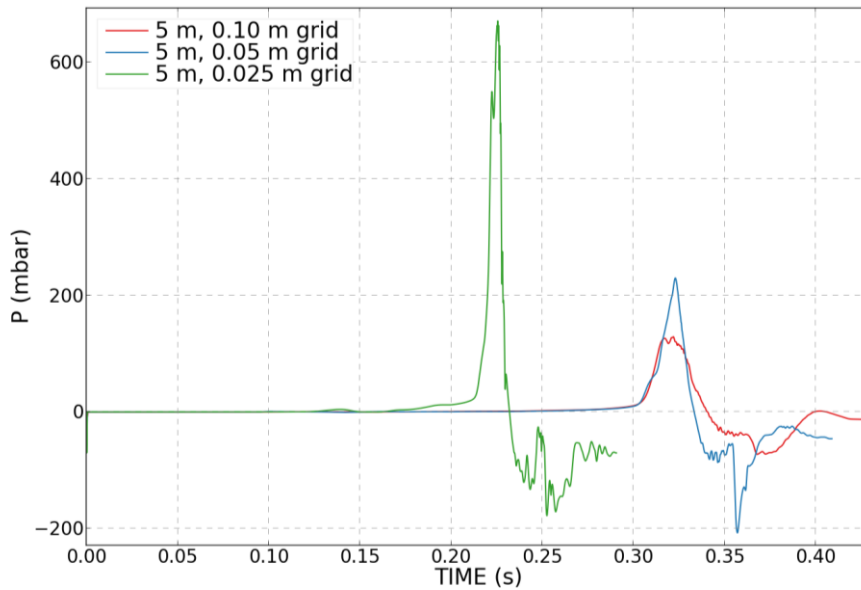


Figure 18: Simulated external pressure development at distance of 5.00 m from vent, applying grid of 0.10 m, 0.05 m and 0.025 m

As can be seen in Figure 18 the graphs show a major difference in the magnitude of the peak pressures, but also for the point in time in which the peak occurs. The simulations using 0.10 m and 0.05 m grid show a quite similar development, however the predicted pressure peak using a finer grid is almost double to that of the coarser grid. Looking at the simulation using a 0.025 m grid an even larger difference can be seen for the predicted pressure peak. Using this cell size also result in the occurrence of the pressure peak being predicted at an earlier point in time. This suggest a strong grid dependency for the type of scenario simulated. Comparing the three simulations to experimental results recorded by Harrison and Eyre [1] show that simulations using a 0.05 m grid represent the best predictions of current pressure values. Applying such a cell size to simulations involving geometries of the sizes as those investigated in this thesis is not unproblematic. The computation time required for the simulations described above was in the range from approximately 5 hours, up to almost two months when applying a 0.025 m cell size. A rule of thumb with regards to computational time is that half the cell size requires 16 times the computation time. A multiplication by two for halving in each direction (x, y and z), and a multiplication of two for a halved time step. The long computational time is inconvenient, however not necessarily regarded as a problem as long as the obtained results are of satisfactory accuracy.

### Test B3

As mentioned several times, the initial simulations of experiments by Harrison and Eyre became an extensive series of simulations leading to a common approach to the simulation setup. The test simulations with regard to the effect of grid showed 0.05 m to be the appropriate cell size. This opened

up for adjustments to the enclosure dimensions allowing even better compliance to those of the original enclosure. For this reason, the simulations of tests by Harrison and Eyre were performed simulating the same test setups for two geometries, aiming to determine the significance of the geometric differences.

The first simulations subject to comparison with experimental results were those representing the test configuration referred to as test B3. As can be seen in Figure 19, the pressure-time-curve providing values recorded in the experiments presents the data in a three dimensional diagram. This makes a direct comparison of pressure development somewhat difficult, however the trends recorded are apparent and combined with the peak pressures obtained from Table 4 a comparison is still possible. In Table 4 we find both the internal and external pressure peak as well as the location of these. The largest external pressure peak is recorded at the pressure transducer located at a distance of 5 meters from the vent opening. The peak internal pressure is recorded at the rear of the chamber. In Figure 20 the predicted pressure-time-curves for the corresponding monitor points are presented. The predicted pressures for both Geometry 1 and Geometry 2 are presented in the figure. Studying the pressure curves for both geometries, it can be seen that the pressure developments at the monitor points follow each other closely. The same trends are found for the rise of pressure and the predications are within the same area of magnitude, however some differences in the peak values are registered.

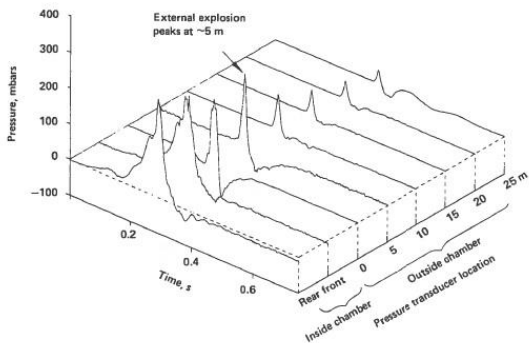


FIGURE 3 Pressure signals recorded inside and outside chamber during a vented explosion. Test B3, propane, rear ignition and 1 area vent.

Figure 19: Experimental pressures, test B3, Harrison and Eyre[1]

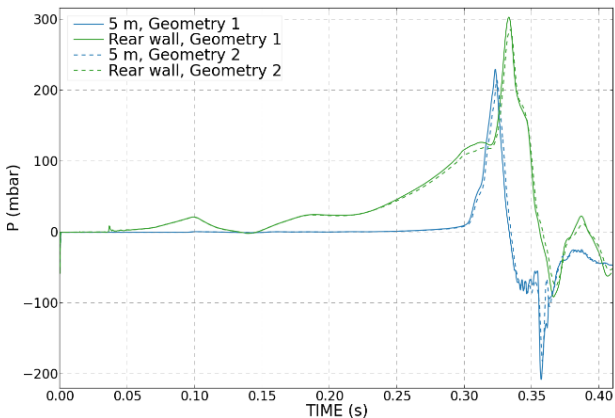


Figure 20: Simulated pressures applying Geometry 1 and Geometry 2, test B3

Looking at the simulations with Geometry 1, the value for internal peak and external peak pressures are predicted to 303 mbar and 254 mbar respectively. When applying Geometry 2, the same values are predicted to 286 mbar for the internal peak, and 237 mbar for the external peak pressure. Comparing these results to the pressures recorded experimentally show quite good accuracy of the simulations. As presented in Table 11, the internal pressures are over predicted by 0-5.94 %, and the external pressures are over predicted by 4.41-11.89 %. It must be noted that the maximum external peak values, both using Geometry 1 and Geometry 2, were predicted at the monitor point directly outside the vent, at a distance

of 0 m. Also included in Table 11 are the predicted values at the monitor point corresponding to the distance where the external peak pressure was recorded in the experiments. The predicted pressures at the corresponding distance are also in good agreement to the experimental values. The deviation in location of predicted peak pressure may be due to several reasons. An immediate assumption is that this might be caused by modifications to dimensions and location of the vent opening, necessary to allow for the vent to be resolved on the applied grid.

*Table 11: Comparison of recorded pressure peaks and pressures peaks obtained by simulations, for test B3*

Test	Origin	Internal peak		External peak		
		Pressure [mbar]	Percentage deviation	Pressure [mbar]	Percentage deviation	Location [m]
B3	Experimental	286	0 %	227	0 %	5
	Simulation - <i>Geometry 1</i>	303	5.94 %	254 (230)	11.89 % (1.32 %)	0 (5)
	Simulation - <i>Geometry 2</i>	286	0 %	237 (215)	4,41 % (-5.29 %)	0 (5)

## Test B5

The second test setup subject to simulations were those referred to as test *B5*, described in section 4.1.1. Available pressure-time-curves for this test, presented in Figure 21, serve as a much better base for comparison than the one available for the previous test. The simulated pressure development for the monitor points corresponding to the location of the recorded pressure peaks are presented in Figure 22. Contrary to what observed for the experiments of test *B3*, the largest external pressure peak recorded in test *B5* was located immediately outside the vent opening at a distance of 0 m. When analysing pressure curves obtained as output from the simulations, the locations of the predicted external pressure peak was found to coincide with the location observed in the experiments. As for test *B3* the values obtained from simulations with both geometries are presented in the figure. The axes of the simulations are identical to those of the experimental recordings, however it is easily noticeable that the simulated pressure development has not been continued further than approximately 0.47 s. The reason for this is that beyond this point the recorded pressures stabilize and show no significant changes in the pressure development.

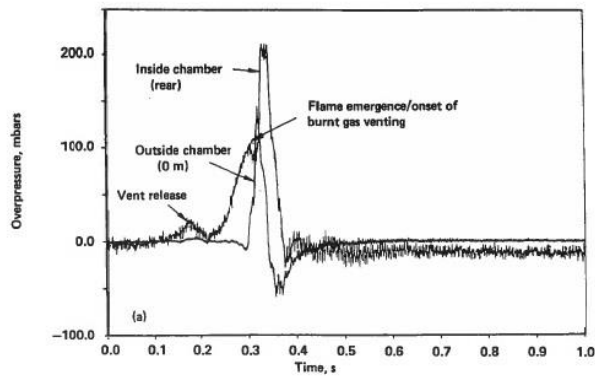


Figure 21: Experimental pressure, test B5, Harrison and Eyre [1]

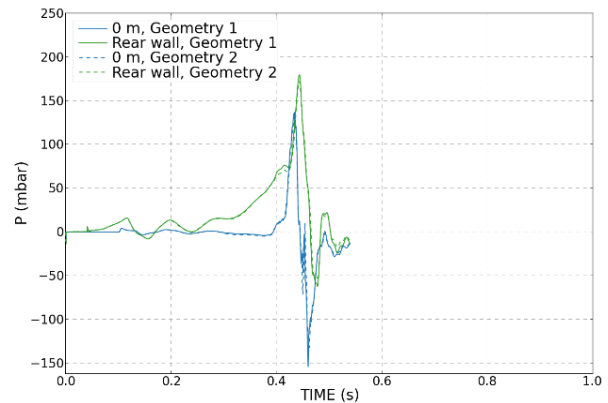


Figure 22: Simulated pressures applying Geometry 1 and Geometry 2, test B5

When comparing the pressure-time-curves, the characteristics of the pressure development in the experiments are easily recognizable in the plots extracted from the simulations. The pressure peak identified in the experiments as the release of the vent, along with the peak associated with the flame emerging out through the orifice of the vent are both identifiable in the plots of the simulated pressure development. A correct prediction of the origin of these peaks were also confirmed by analysing the time for vent opening and the visualization of flame propagation obtained from the simulations. Both of these clearly displaying the physical phenomena coinciding with the timing of the pressure peaks. Also visible in Figure 22 is the occurrence of the external pressure peak immediately prior to the largest internal peak pressure. In physical situations this phenomenon is associated with the ignition of ejected combustible gas, resulting in an external explosion. The external explosion gives rise to a new internal pressure peak, either due to the fact that the external explosion temporarily choking ventilation of internal excess pressure, or as the blast wave from the external explosion propagates in through the vent opening [10]. The ability to reproduce these trends in the simulated pressures is a strong indication that the external explosion is represented in the simulations.

Comparing the peak pressure values predicted in the simulations to the experimental values obtained from Table 4, we find slightly larger deviations than seen for test B3. Presented in Table 12 are the predicted peak pressures obtained from the simulations. For the two geometries applied, the values for the internal pressure varies from an over prediction of 2.79% to an under prediction of 7.44%. For the external pressures the predictions are of less accuracy. These pressures are over predicted by 19.31% and 11.03% for the two geometries. Despite the increased deviations compared to experimental values, the simulations are still regarded as fairly accurate, especially with regards to replication of tendencies in pressure development. It is however important to be aware of the limitations in accuracy when evaluating the output from the simulations.

Table 12: Comparison of recorded pressure peaks and pressures peaks obtained by simulations, for test B5

Test	Origin	Internal peak		External peak		
		Pressure [mbar]	Percentage deviation	Pressure [mbar]	Percentage deviation	Location [m]
B5	Experimental	215	0 %	145	0 %	0
	Simulation - Geometry 1	221	2.79 %	173	19.31 %	0
	Simulation - Geometry 2	199	-7.44 %	161	11.03 %	0

## Test B6

The approach for evaluating the accuracy of the simulations of test B6 was similar to those of the preceding. Figure 23 shows the recorded pressure-time-curves for the transducer at the rear of the enclosure and for the one located on the ground immediately outside the vent opening. Combined with Table 4 these serve as a good basis of comparison when evaluating the simulations.

As for test B5, the external peak pressure for test B6 was recorded directly outside the vent opening while peak internal pressure was recorded at the rear of the enclosure. The output pressures obtained from the simulations, presented in Figure 24, present the predicted internal and external peaks at the corresponding monitor points.

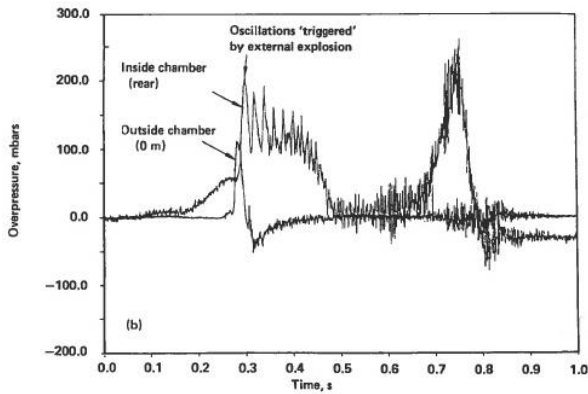


Figure 23: Experimental pressure, test B6, Harrison and Eyre [1]

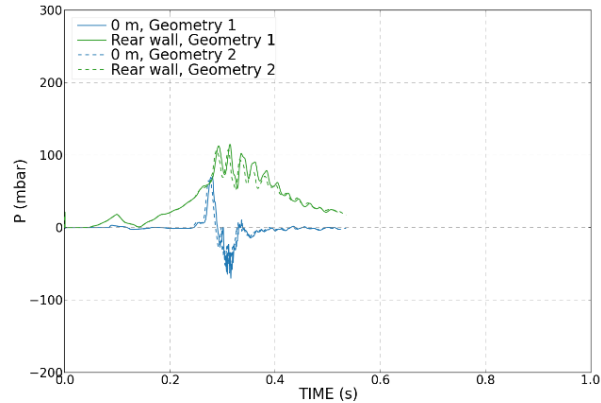


Figure 24: Simulated pressures applying Geometry 1 and Geometry 2, test B6

When comparing the pressure development in Figure 23 and Figure 24, it can be seen that the initial tendencies of the pressure rise are similar for both experimental and simulated values. Pressure build-up after vent release is recognizable in the predicted pressure curve, and an internal pressure peak likely caused by the external explosion choking the ventilation of internal volume production is also recognizable. It is observed that the predicted internal pressure does not capture the magnitude of the oscillations triggered by the external explosion. A reason for this might be that the grid resolution

applied to the simulation is not sufficient to completely capture these oscillations. The experimental recording also shows continued oscillating behaviour for the internal pressure, building up to a second pressure peak. This second pressure peak is not represented in the pressure predictions obtained from the simulations. The second peak is however believed to be associated with an acoustic wave onset by the external explosion [1], propagating in through the vent opening, reflecting at the rear of the enclosure giving rise to large and narrow pressure peaks. The occurrence of such a peak is explained by Cooper et al. [10] to be caused by pressure waves induced by the combustion process coupling with acoustic waves, resulting in an oscillating peak of high frequency. The grid resolution necessary to reproduce such oscillatory pressure peaks is one of great refinement. FLACS [18] does however not support a grid resolution enabling prediction of these acoustically enhanced oscillations, thus explaining the lack of ability to predict the second pressure peak recorded during the experiments.

Keeping in mind the insufficiencies in predictions of pressures described above, the deviations in peak values are fully understandable. As presented in Table 13 the peak pressures predicted using FLACS are considerably lower than those recorded in the experiments. Values obtained applying Geometry 1 and Geometry 2 to the simulations show an under prediction between 35-40 % for internal pressures, and an under prediction of about 24-30% for external pressures.

*Table 13: Comparison of recorded pressure peaks and pressures peaks obtained by simulations, for test B6*

Test	Origin	Internal peak		External peak		
		Pressure [mbar]	Percentage deviation	Pressure [mbar]	Percentage deviation	Location [m]
B5	Experimental	205	0 %	112	0 %	0
	Simulation - <i>Geometry 1</i>	133	-35.12 %	85	-24.11 %	0
	Simulation - <i>Geometry 2</i>	123	-40.00 %	78	-30.36 %	0

## 4.2.2 Results simulations of experiments by van Wingerden

For simulations of experiments by van Wingerden, data for two experimental setups were obtained from his publications [12, 13]. As described in section 4.1.2, the scenarios investigated were identical in setup with regards to volume of enclosure, vent area and gas mixture, but with variations in location of ignition point. Ignition was initiated at the centre, and at the rear of the enclosure. Recordings of external pressures at a distance of 7 m from the vent opening, as well as internal pressures were presented in the graphs enclosed below.

## External pressures

When comparing experimental results to those extracted from the simulations it can be seen that the compliance for predicted external pressures are rather poor. Figure 26 presents the predicted external pressures when igniting in the geometric centre of the enclosure. As can be seen, a marginal pressure peak of 0.5 kPa is predicted at the monitor point corresponding to a distance of 7 m from the vent. This difference represents one order of magnitude lower than the registered experimental peak of approximately 3.1 kPa, shown in Figure 25. The second, and largest, experimental pressure peak is by van Wingerden [12], however stated to be related to an internally generated acoustic wave. This wave cannot be represented in the simulations as FLACS is unable to predict acoustic waves [18], and consequently fail to predict the blast wave caused by acoustically enhanced oscillatory combustion. The predicted peak pressure therefore correspond to the first registered experimental pressure peak of 1.5 kPa, caused by the external explosion [12]. Comparing the two, reveal that the predicted peak represents one third of the experimental value, still regarded as a large deviation. The pressure predicted with ignition at the rear of the enclosure, displayed in Figure 28, is more apparent. However, when compared to the experimental recordings presented in Figure 27, it is evident that the predicted peak value of 2.8 kPa is considerably lower than the recorded experimental peak of approximately 7.0 kPa.

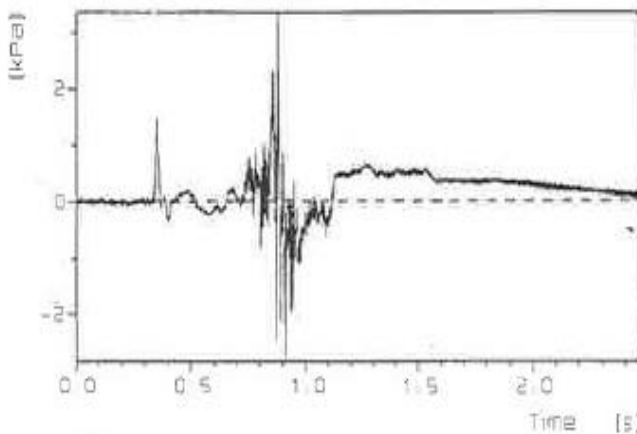


Figure 25: Experimental external pressure at 7 m, central ignition [12]

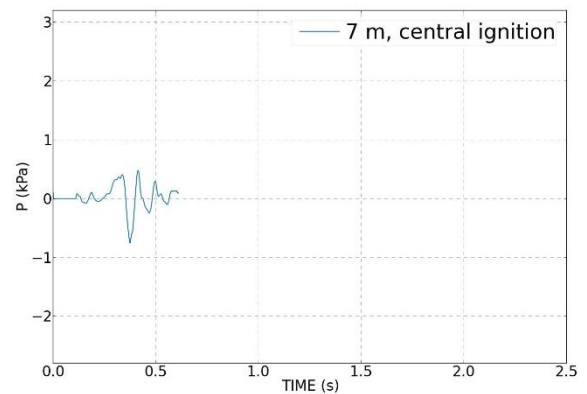


Figure 26: Simulated external pressure at 7 m, central ignition

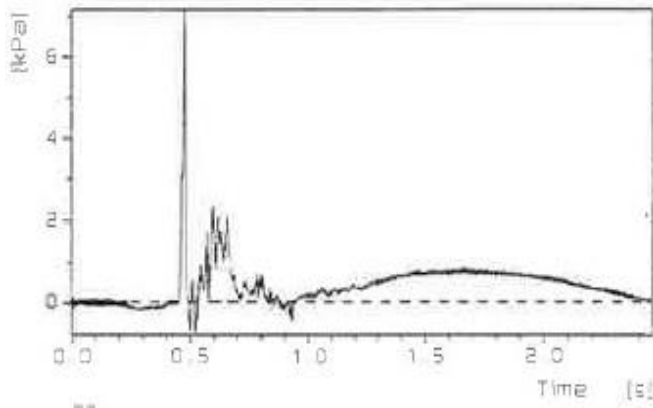


Figure 27: Experimental external pressure at 7 m, rear wall ignition [12]

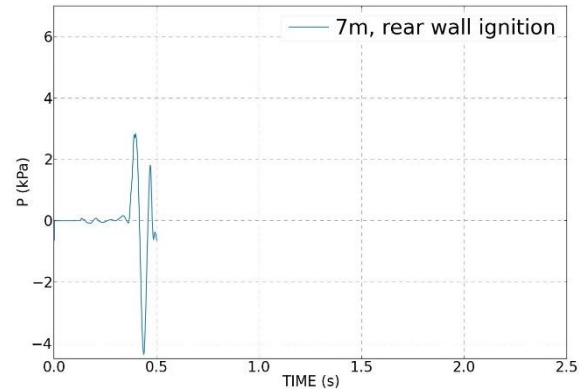


Figure 28: Simulated external pressure at 7 m, rear wall ignition

The most severe deviation observed when analysing the external pressure predictions was assumed caused by the failure to predict effects of acoustic waves. However, a weak agreement is also evident for the comparable pressure peaks. In an attempt to explain this weak agreement between pressures predicted in the simulations and the experimental recording, it would be appropriate to evaluate the resolution applied to the core grid. As the grid sensitivity tests described in section 4.2.1 revealed a strong grid dependency, it would be beneficial to perform similar investigations for the simulations of experiments by van Wingerden [12]. Even though the enclosures are of similar volumes, the geometrical shapes are not alike. The applied cell size could consequently be of influence on the predictions of variables. The simulations described earlier in this section were carried out applying a cell size of 0.05 m. The next, smaller cell size, allowing the geometry to resolve would be 0.025 m. Running a simulation applying this cell size was however not considered convenient, as the comparable simulation applying a cell size of 0.025 m to the simulations of experiments by Harrison and Eyre [1] had a run time of approximately 2 months. Also contributing to this decision was the fact that cell sizes moving towards 0.02 m can cause considerable over predictions, due to the subgrid models in FLACS not being applicable for so small cell sizes [18].

## Internal pressures

Internal pressure recordings and predictions for ignition initiated at the centre of the enclosure are presented in Figure 29 and Figure 30. Comparing the two reveals that the predicted internal pressure peak of 1.7 kPa deviates significantly from the peak experimental values of approximately 26 kPa. According to van Wingerden [12], the maximum internal pressure obtained with central ignition was due to pressure increase caused by oscillatory combustion, in turn enhanced by an acoustic wave produced during the combustion. The impact of oscillatory combustion on the development of maximum internal pressure was also described by Cooper et al. [10]. Examining the pressure transcriptions in Figure 29 and comparing it to the pressure predictions in Figure 30, it is clearly visible that the predicted



pressure development obtained from the simulations fail to reproduce the oscillatory combustion. As mentioned in section 4.2.1, the grid resolution required to represent acoustic peaks is not supported in FLACS [18], thus explaining this inability to reproduce these oscillatory peaks. In light of this, the first registered experimental peak of 6 kPa is assumed to be the peak corresponding to the predicted peak value. Comparing this peak to the predicted pressure peak do however still show a significant deviation, representing an under prediction of 65-75 %. A possible explanation for the poor agreement between the first internal pressure peaks is the assumed vent release pressure applied to the simulations. This release pressure is of direct influence on the initial pressure build-up [10], and a possible deviation between experimental  $P_{stat}$ , and that applied in the simulations can consequently cause the predicted pressure to differ from the experimental. This possible explanation will also be applicable for ignition initiated at the rear of the chamber.

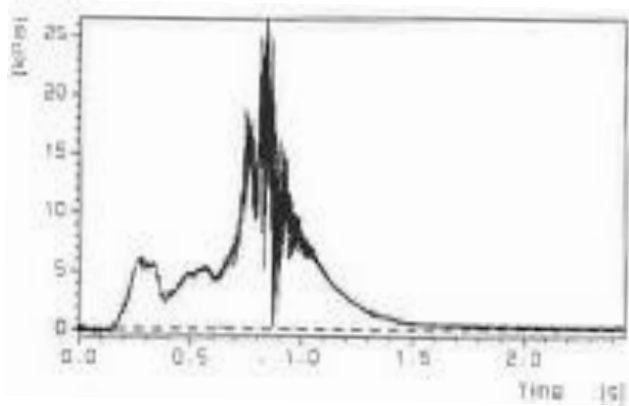


Figure 29: Experimental internal pressure, central ignition [12]

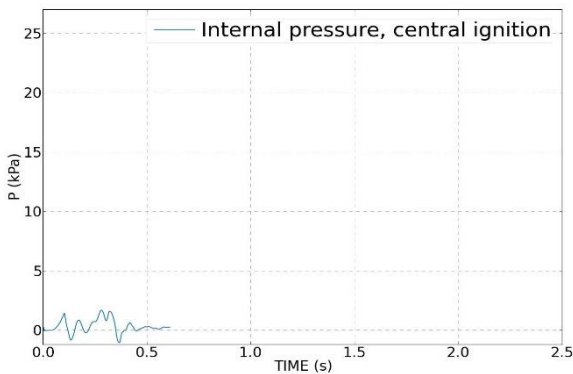


Figure 30: Simulated internal pressure, central ignition

Studying Figure 31 and Figure 32, a significant deviation can also be found for ignition initiated at the rear end of the enclosure. The predicted internal pressure of 7 kPa represents almost half of the experimental value of 13.5 kPa. Both in the case of central and rear ignition the pressures-time-curves show multiple, and more distinct peaks than those predicted for the external pressures. If one disregards the apparent deviations in magnitude of the peaks, similarities can be found for the trends in pressure development. A resemblance can be distinguished with regards to number of peaks, and time of occurrence in the initial parts of the pressure build-up. This is especially evident for the curve representing internal pressure when igniting at the rear end of the enclosure.

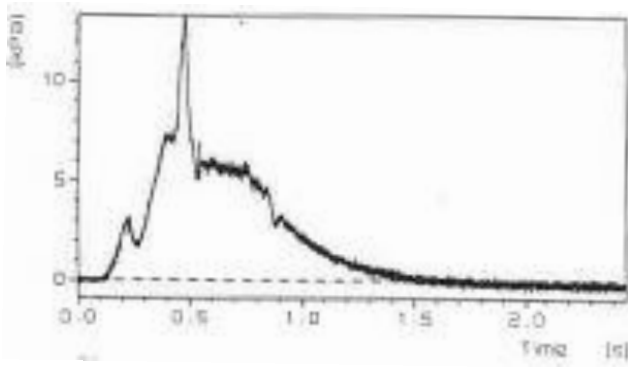


Figure 31: Experimental internal pressure, rear wall ignition [12]

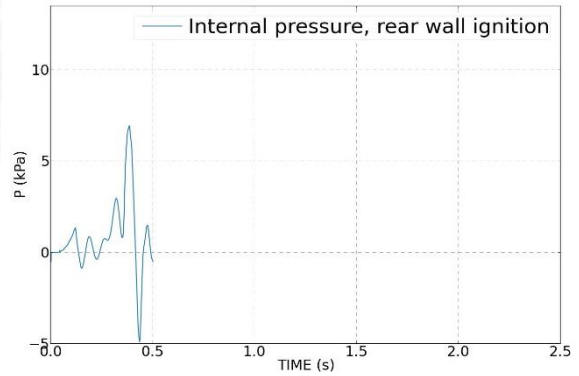


Figure 32: Simulated internal pressure, rear wall ignition

In an attempt to explain the differences between experimental results and those obtained from the simulations, it can be beneficial to revisit the work of Cooper et al. [10]. The trends of the internal pressure predictions are quite similar to the initial phase of the typical pressure development (Figure 7) described by Cooper et al. [10]. As can be seen in Figure 33, comparing the first part of the pressure profile suggested by Cooper et al. to the predicted internal pressure for rear ignition reveal a striking resemblance between the two. Note that the axis in the diagram displaying internal predictions have been adjusted. It is likely to assume that the first predicted pressure peak can be assigned to the release of the vent, and that the larger distinct peak can be assigned to pressure build-up as a result of the rate of volume production exceeding that of reduction caused by venting. After this second peak the simulation reaches the default termination criteria and no further pressure development is simulated.

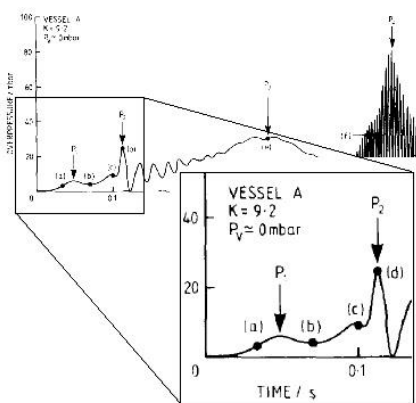
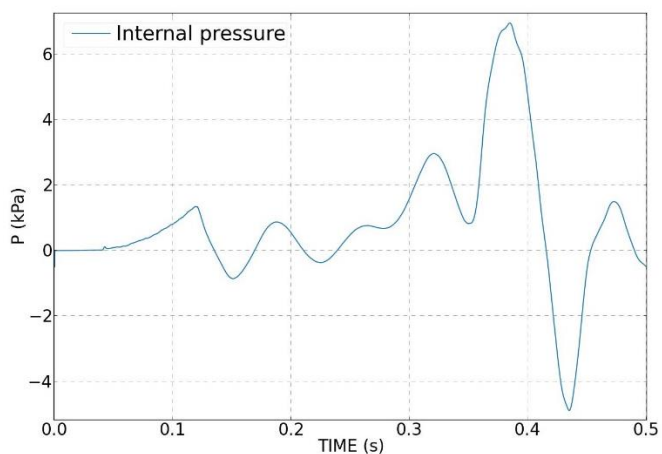


Figure 33: Comparison of initial pressure development (Cooper et al. [10]) and simulated pressure development with rear wall ignition



Combining these tendencies with the poor prediction of the external pressure leads to the assumption that the internal pressure prediction with rear wall ignition actually represents a plausible pressure development and that the lack of impact from an external explosion causes the further increase in pressure to cease. This assumption is substantiated by the findings of van Wingerden [12], concluding that for rear wall ignition, the internal pressure was determined by the influence and magnitude of the external explosion.

### 4.2.3 Results simulations of tests volume

To investigate the importance of vessel volume on external phenomena associated with the vented explosions, a series solely based on simulations with no comparable experimental work was carried out. As described in the section 4.1.3 the volumes used in this simulation series were based on the enclosure used by Harrison and Eyre [1], but adjusted to half or double the original volume. The scenarios simulated were identical for all simulation runs, with adjustments to account for the respective volume used in the simulation.

#### Volume of 15 m<sup>3</sup>

Initial simulations using a volume adjusted to half the size of that used by Harrison and Eyre showed significant differences in predicted pressure, both internally and externally. The internal pressure predicted for the volume of 15 m<sup>3</sup> peaks at 176 mbar, while the external pressure peaks at 158 mbar. The location of the largest external peak was registered immediately outside the vent, representing the same proportional distance as the experimentally recorded external peak for the vessel of 30 m<sup>3</sup>. Comparing the pressure predicted in this simulation, to those obtained for test *B3* by Harrison and Eyre, it was found that both internal and external pressure predictions were between 25-50% lower for the simulations applying a smaller volume. Some differences in pressures are expected given the changed volume and consequently a smaller amount of combustible gas. The values of the obtained pressure predictions were however very similar to those obtained for the simulations of the 30 m<sup>3</sup> using a coarser grid than that of 0.05 m.

Discovering these similarities, a comparable simulation applying a geometry not only similar in shape, but with identical proportions to the one corresponding to a volume of 30 m<sup>3</sup> was performed. This corrected geometry is referred to as Vol.2 in section 4.1.3. Changes made to the geometry were minor, and the main difference between the two simulations were an application of a core cell size of 0.05 m in the first simulations, contrary to a cell size of 0.04 m for the simulation of scaled proportions (Vol.2). The simulation based on this new geometry with volume 15 m<sup>3</sup> represented an identical scaling of the simulations of test *B3*, both with regards to geometry and applied grid. Consequently, the geometry was

resolved over the identical number of cells in all three directions, and the extent of the core and total grid was proportionally equal to those applied for B3.

When analysing the results of the simulation using the latter geometry, a significant change in predicted pressures becomes apparent. A distinct increase in all pressures is evident, putting them in the same range as the simulation corresponding best to the values recorded experimentally for test B3. Displayed in Figure 34 and Figure 35 are the pressure predictions obtained from the two simulations applying the geometries of similar and identical shape. Using a geometry of identical proportions with an applied core grid of 0.04 m gives an internal pressure peak of 309 mbar, contrary to an internal peak of 176 mbar using a geometry of similar proportions and a cell size of 0.05 m. External values when comparing the same simulations were 246 mbar for identical proportions, to 158 mbar for that of similar proportions. As can be seen, the predicted pressures are within the same order of magnitude, however a percentage difference approximately between 55-76 % and indicates a strong grid dependency.

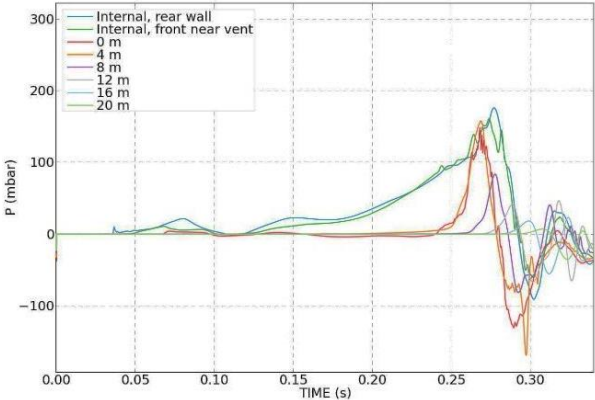


Figure 34: Enclosure of 15 m<sup>3</sup> of similar shape (Vol.1), applying a grid of 0.05 m

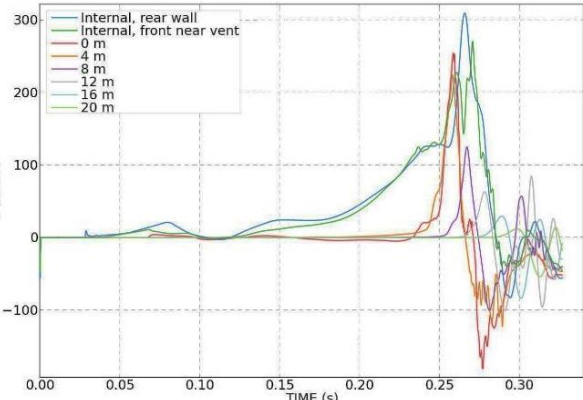


Figure 35: Enclosure of 15 m<sup>3</sup> of identical shape (Vol.2), applying a grid of 0.04 m

**Volume of 52 m<sup>3</sup>**

Continuing to analyse the results of comparable simulations of larger volumes show similar trends as the ones observed for smaller volumes. The first simulation including larger geometries is described in section 4.1.3. This simulation applied a geometry of similar shape as the enclosure of 30 m<sup>3</sup>, but with a volume of almost twice the size. Considering the dimensions of the enclosure, combined with experiences from simulations of experiments by Harrison and Eyre, a cell size of 0.10 m was applied to the core grid. These settings combined with other settings for Vol.3, described in section 4.1.3, gives the pressure transcripts presented in Figure 36.

Evaluating the result of the predicted pressures one can identify a small peak at approximately 0.1 s. This peak corresponds to the opening of the vent panel. After this the pressure drops, before it starts to

increase again as a result of what is assumed to be the volume production by combustion exceeding the volume reduction by ventilation. The external explosion occurs immediately prior to the peak in internal pressures, however the pressure curve for the internal pressure shows no change in rate of increase. It is therefore assumed that the impact from external phenomena on the internal pressure development is negligible, if present at all.

In an attempt to further investigate the grid dependency looking at volumes of 15 m<sup>3</sup>, a similar exercise was performed for larger volumes. A comparable simulation was set up using a geometry of identical proportions, and applying a scaled grid. This simulation is described in detail, and referred to as Vol.4, in section 4.1.3 of this thesis. As for the simulation of Vol.2, this simulation represents an identical scaling of the simulation of test B3, both with regards to geometry, grid and cell size. Predicted pressures obtained using this identically proportioned geometry is displayed in Figure 37. The pressures predicted internally peaks at 328 mbar, compared to 165 mbar for the simulation using a similar geometry with a coarser grid. For external pressure peaks the values using Vol.4 are predicted to 280 mbar, contrary to 148 mbar using Vol.3. As for the comparison of volumes of 15 m<sup>3</sup> the adjustments to the geometry are assumed to be of minor importance.

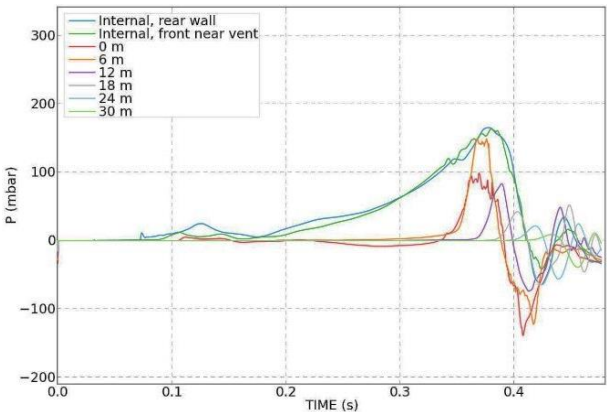


Figure 36: Enclosure of 52 m<sup>3</sup> of similar shape (Vol.3), applying a grid of 0.10 m

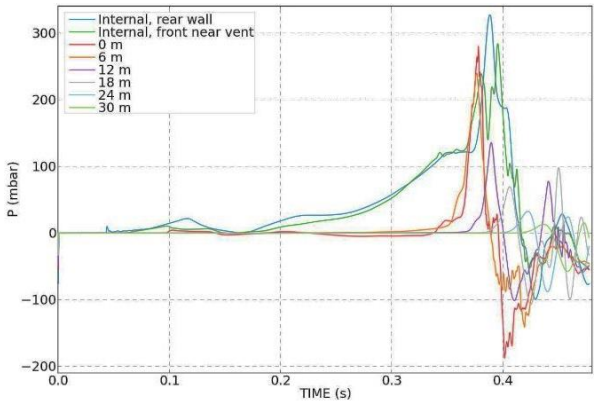


Figure 37: Enclosure of 52 m<sup>3</sup> of identical shape (Vol.4), applying a grid of 0.06 m

**Joint analysis for all the three volumes:**

In an attempt to summarize the findings from simulations with different volumes, it could be beneficial to compare the simulations of all the three volume variations. Presented in Figure 38 are pressure-time-curves using both coarser and finer grids for simulations with 15 m<sup>3</sup>, 30 m<sup>3</sup> and 52 m<sup>3</sup> enclosures.

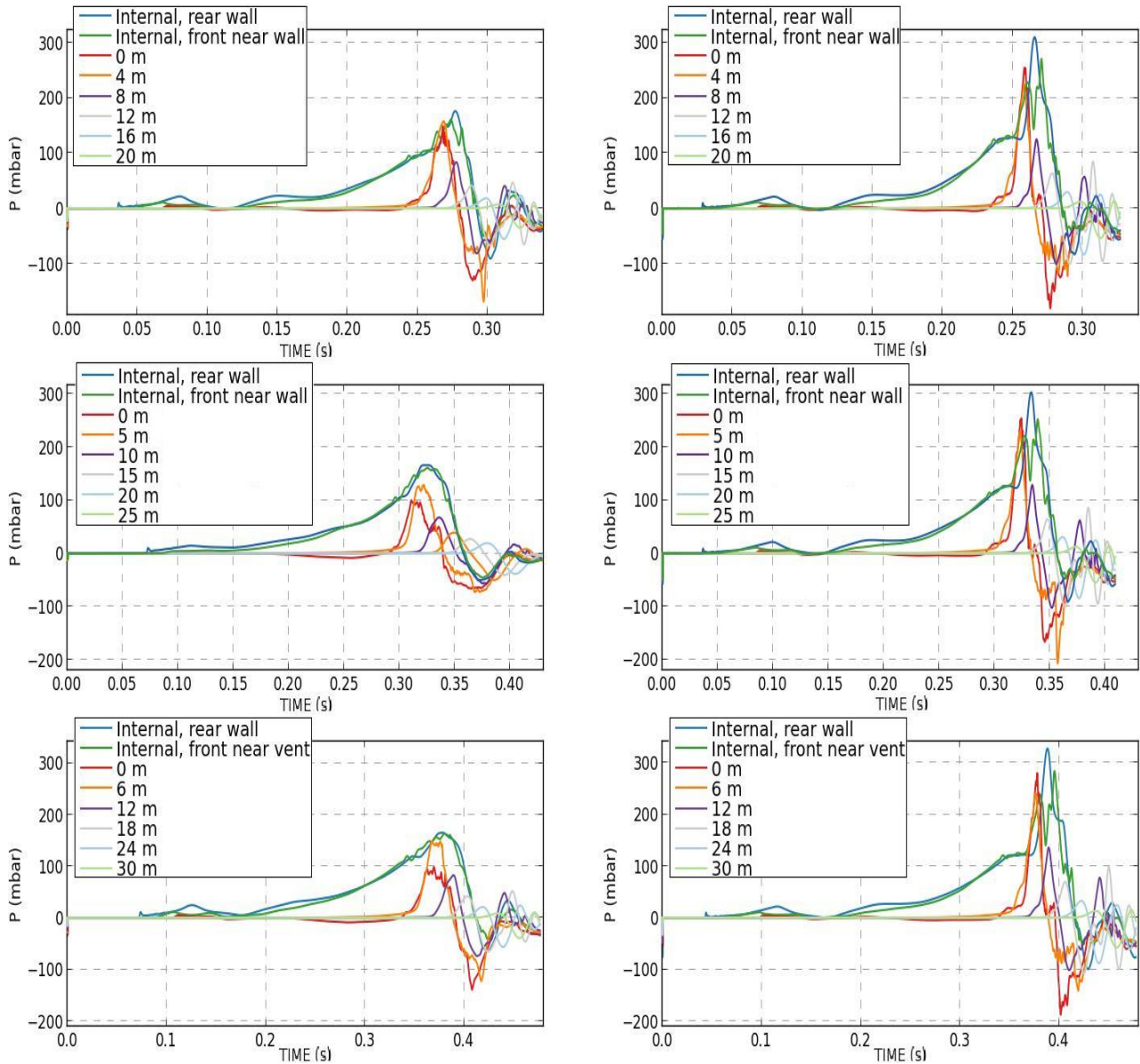


Figure 38: Effect of grid size on pressure development for simulations in volumes of  $15 \text{ m}^3$  (top),  $30 \text{ m}^3$  (middle) and  $52 \text{ m}^3$  (bottom). Left hand side - simulations of similar geometries, using a grid of 0.05 m, 0.10 m and 0.10 m. Right hand side - simulations applying identical shapes, using scaled grids of 0.04 m, 0.05 m, and 0.06 m.

As can be seen in the Figure 38, the trend when moving from a coarser to a finer grid is striking, and can be found for all the three volumes. Studying the comparable graphs, it is apparent that the simulations running a finer grid displays sharper pressure peaks of greater magnitude, and that the occurrence of the external pressure peaks falls prior to the internal peaks. As described earlier, this is associated with the interaction between the external explosion and the internal pressure generation, underlining the importance of correct grid refinement for prediction of external explosions. In the case of simulation with a volume of  $30 \text{ m}^3$  it must be noted that the geometry applied in these simulations are identical, and the difference between the two is limited to the cell size applied in the core grid. Looking

at the volume of 30 m<sup>3</sup> presented in the two middle pressure graphs in Figure 38, it can be seen that the trends in pressure development when moving to a finer grid is similar to those observed for volumes of 15 m<sup>3</sup> and 52 m<sup>3</sup>. This leads to the assumption that the distinct difference in predicted pressures is caused by the variations in cell size, and that influence due to the minor adjustments in dimensions of the enclosure is insignificant. To substantiate this, it can be appropriate to refer to the work of Vagesh D. Narasimhamurthy [23], investigating the effects of grid size on modelling of turbulence using FLACS. Among many combinations of geometry and grid settings, the investigation included an analysis of completely resolved geometries with variations of cell size in the applied grids. The latter combination is of specific interest due to the comparability to the simulations performed for enclosures of 15 m<sup>3</sup>, 30 m<sup>3</sup> and 52 m<sup>3</sup>. In his examination, Narasimhamurthy [23] found the turbulence to develop in a similar manner in the initial phase of the fluid flow. However, as the flow was allowed to evolve further with time, different predictions of turbulence were observed between the simulations applying grids of different cell size. The development of turbulence when applying a finer grid was of considerably higher intensity as time passed. It must be noted that the investigations by Narasimhamurthy [23] were performed on fluid flows without combustion. His findings are however believed to be applicable to the simulations discussed in this thesis. Looking at the physical scenario simulated in this thesis, similar conditions to those investigated by Narasimhamurthy [23] can be found in front of the propagating flame front. In this region the increasing volume of the combustion products shoves the flame front forward, pushing the unburnt gases forward, thereby representing a fluid flow. Considering the known increased effect of turbulence on the rate of combustion [2], and consequently pressure development, the increased turbulence associated with a finer grid is assumed to play an important role also in the simulations carried out in this thesis.

Another factor, possibly contributing to the differences in pressures observed with changes in cell size, is that of changed effective time resolution. The effect of this was briefly discussed in the work of Jonathan Puttock, Debapriya Chakraborty and Walter Farmayan [24] concerning gas explosion modelling using PDRFoam, a CFD-model based on the open-source package OPENFOAM®. Included in their publication was a comparison of simulations utilizing grids of different cell sizes, stating that smaller cell sizes leading to shorter time steps represents a better resolution for sharp pressure peaks. Examining the graphs in Figure 38 one finds that the pressure predictions applying a finer grid display significantly sharper pressure peaks than those using a coarser grid. In turn indicating that a better resolving of the phenomena, over a finer time step, can be a contributing factor in explaining the large differences when applying various cell sizes, even of small differences.

## 4.2.4 Results simulations of tests vent size

Like for the simulations utilizing enclosures of different volumes, but of similar shapes, a series of simulations investigating the impact of variations of vent area has been carried out. As described in section 4.1.4, these simulations were based on the well refined simulations of experiments by Harrison and Eyre [1]. The original intent of these simulations was not to verify the software FLACS with regards to agreement to experimental results, but to evaluate how the predicted explosion process is affected by variations of the vent area, assuming that the simulation setups represent correct predictions of the development. With an exception of variations in vent area, the simulations were carried out using an identical setup as for simulation of test *B3* applying Geometry 1. Similar tests were also carried out by Harrison and Eyre, however basing the simulations on the scenario of test *B3* resulted in some minor differences in fuel concentration for the gas cloud.

Running the same simulation scenario for gas explosion applying various vent sizes to an otherwise identical geometry, resulted as expected in different pressure predictions both with regard to internal and external values. The peak characteristics obtained from the simulations are compared in Table 14. A clear dependency of vent area is traceable for the build-up of internal pressure. As the vent area is reduced, the predicted internal pressure increases noticeably. This trend in the development of internal pressure is as expected and in fact a good example of the basic principle of explosion venting. An opening in the enclosure reduces the internal pressure by venting the excess volume generated by the internal combustion. A smaller vent area will cause a decrease in the rate of volume reduction by venting, consequently resulting in development of a larger internal peak pressures. This relation is described in more detail by Crowhurst et al. [9].

*Table 14: Simulated peak pressures applying various vent area*

Vent		Internal peak pressure [mbar]	External peak pressure [mbar]	Distance, external peak [m]
Fraction [-]	Area [m <sup>2</sup> ]			
1/2	2.56	303	254	5
1/4	1.265	469	419	15
1/8	0.64	1081	371	5

Comparing the external pressure peaks, one finds the largest prediction to be associated with the use of a vent area of 1.265 m<sup>2</sup>, or 1/4 of the area of the end wall. In an attempt to explain this, it can be beneficial to look at the effect the vent area has on the venting process. When considering vented gas explosions ignited at the end opposite the vent, the larger volume of the burned gas will push the flame front towards the vent opening faster than the reactions of the combustion, in turn pushing unburnt gas out of the vent. A vent of larger area will pose less restriction to the outflow of unburnt gas, resulting in ejection of a



larger amount of gas compared to a vent of smaller area. The restricted outflow caused by a smaller vent will result in an increase in the internal pressure, causing the gas to be expelled through the vent with a greater force. This will in turn lead to increased levels of turbulence, both in the shear layer between the unburned gas and the quiescent external air, and within the expelled gas itself. A possible explanation of the largest external pressure being predicted when using a vent of 1/4 of the area of the wall, is that this vent area results in the optimal combination of amount of expelled gas and level of turbulence, causing the most violent external explosion. This assumption can be substantiated by the work of Harrison and Eyre [1] describing a vent of “*intermediate size*” to cause the most severe external blast wave. Harrison and Eyre assumed flow velocity and amount of expelled gas to be of significant influence with respect to the formation of external blast waves, however stated that their experimental data was insufficient to form basis for a general conclusion.

Analysing the external flame development when utilizing the three different vent areas, the two types of explosions described by Crowhurst [9] et al. are clearly visible. Looking at Figure 39, a distinct difference in the shape of the external explosion or flame is visible. The external explosion displayed with the use of a vent of 1/2 is of a near spherical shape with a centre not far from the vent opening, thus representing a clear example of the *Type 1* explosion. On the other hand, the external explosion observed when using a vent of 1/8 is a clear example of a *Type 2* explosion, displaying a flame stretching far from the vent opening, but with little propagation in directions normal to the flow and no clear centre. The characteristics of the flame observed when simulating explosions using an area of 1/4 of the end wall is not a clear example of any of the two types of explosions. The extent of the external flame is almost as far as that observed using a vent of 1/8 area, however a spherical flame propagation can be observed originating from a point at a distance of approximately 10-15 m away from the vent. The nature of the external flame shows characteristics associated with both categories of explosions, thus substantiating the assumption that the external explosion using a vent of area 1/4 could result in a combination of physical phenomena causing the most severe external explosion.

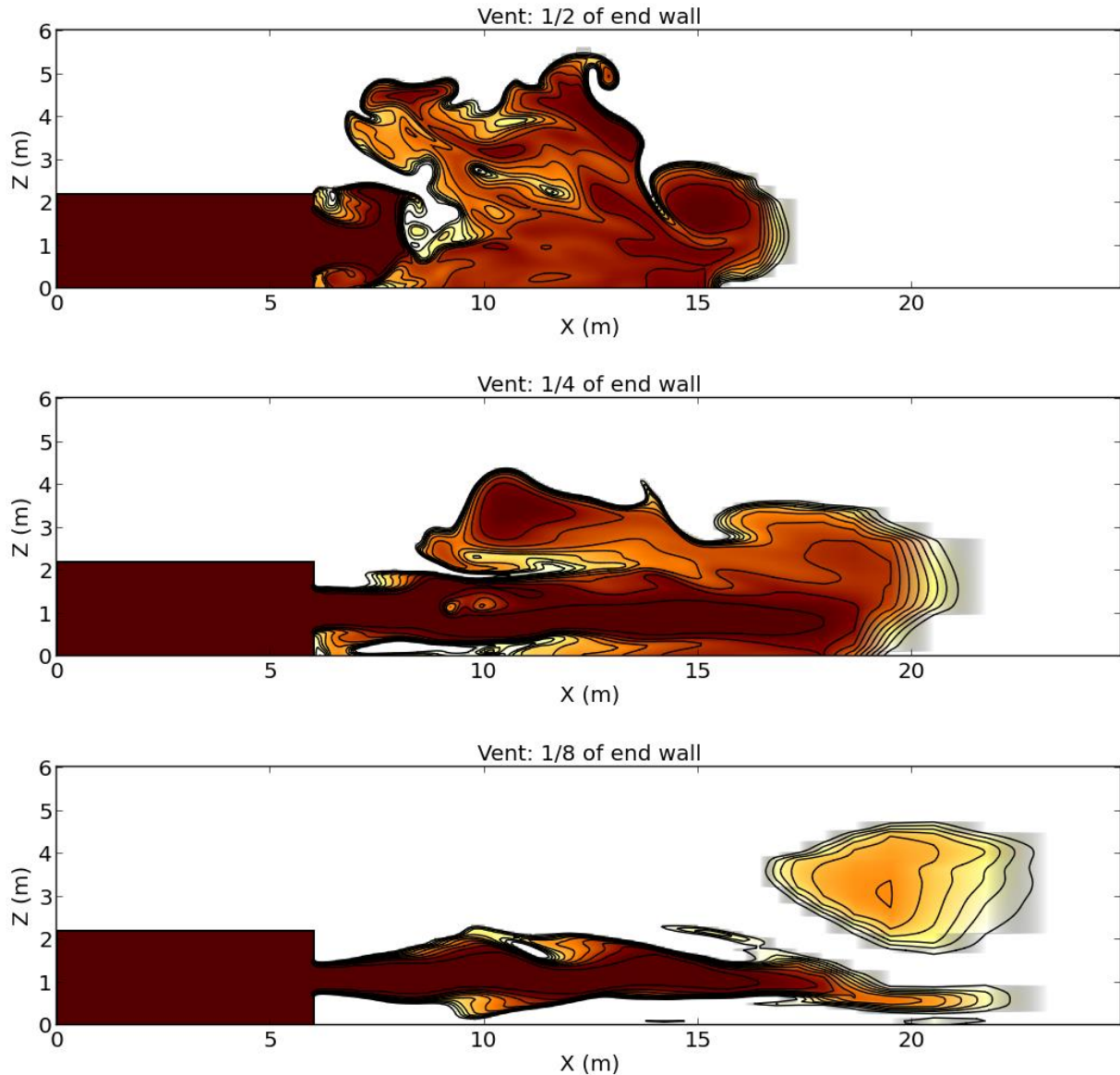


Figure 39: Extent of external flame using vents of 1/2 (top), 1/4 (middle) and 1/8 (bottom) of the area of the end wall

As already mentioned, similar experiments applying vents of different sizes were carried out by Harrison and Eyre [1]. Even though there are some differences with regards to the fuel concentration applied, the experimental results are regarded as an appropriate comparison in evaluation of the simulations. Comparing the values obtained from the simulations show acceptable agreement for the predicted values for most of the parameters. However, as can be seen in Table 15, the internal pressure predicted with the use of a vent area of 1/4 deviates considerably from the experimental value.

Table 15: Comparison of simulation and experimental results applying different vent openings

Vent		Origin	Fuel concentration /stoichiometry [%v/v]/[λ]	Internal peak pressure [mbar]	External peak pressure [mbar]	Distance, external peak [m]
Fraction [-]	Area [m <sup>2</sup> ]					
1/2	2.56	Simulation	4.41/1.10	303	254	5
		Experimental	4.41/1.10	286	227	5
1/4	1.265	Simulation	4.41/1.10	469	419	10
		Experimental	4.44/1.11	1100	445	5
1/8	0.64	Simulation	4.41/1.10	1081	371	5
		Experimental	4.39/1.10	1380	418	5

In an attempt to explain the large deviation in predicted internal pressure for this configuration it can be beneficial to look to the pressure transcript from the respective simulation. Displayed in Figure 40 is the pressure-time curve extracted from the simulation of the vented gas explosion applying a vent of 1/4. As can be seen in this figure, the graph showing pressure development at the internal monitor point displays oscillations at the peak of the curve. If this oscillating nature is accurate, a possible source for the deviating pressure can be insufficient grid resolution. As discussed in section 4.2.3, the prediction of sharp peaks is strongly dependent on the cell size applied to the simulation. Another possible explanation, also related to the oscillations, is a lack of ability to predict the coupling of various instabilities. This coupling was described by Cooper et al. [10]. As described in section 4.2.1 the current edition of FLACS is not able to predict acoustically enhanced oscillations [18], possibly explaining the predicted internal pressure being only 40% of that recorded experimentally. Acoustically enhanced pressure peaks are not observed for all vented explosions in empty geometries, however when present, these peaks usually represent the peaks of largest magnitude in the experimental recordings [10]. Consequently, the lack of ability to reproduce acoustically enhanced peaks must be regarded as an insufficiency when using the software as a tool in the assessment of explosion risk, magnitude and consequence.

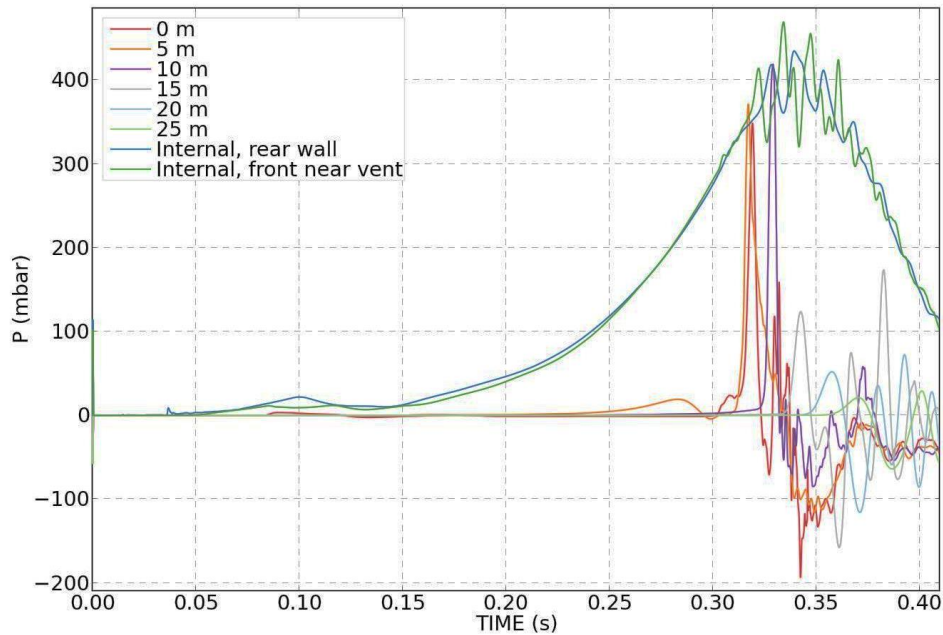


Figure 40: Simulated pressure development for an enclosure of  $30 \text{ m}^3$ , applying a vent area of  $1/4$  of the end wall

#### 4.2.5 Key findings – gas explosions

Comparing the analysis of the simulations of vented gas explosions one can see some similarities in the results. With regards to geometry it can be established that the most realistic representation of a simulation scenario is built around a geometry completely resolved on the grid. The two different geometries applied for the simulations of experiments by Harrison and Eyre [10] clearly showed differences in the predicted pressures when running the same scenario. The simulations were in favour of Geometry 2 in tests *B3* and *B5*, and in favour of Geometry 1 in test *B6*. As the deviations in predictions for the geometries were of similar magnitude, no clear recommendation of the two is possible. These simulations, as those investigating effect of difference in volume, revealed a much greater dependency on the applied grid than to minor adjustments to the dimensions of the geometry.

To be able to capture the external phenomena it was found necessary to extend the core grid far beyond the vent opening of the enclosure, including the areas affected by the flow out of the vent. With regards to the cell size of the core grid, it was found that the accuracy of the predictions depends strongly on application of a very fine core grid. Especially with regards to capturing the external phenomena, the sizing of the grid cells was found to be of great importance. The ratio of size of grid cells to the dimensions of the geometry has shown to be of major significance, even when the core grid is within the guidelines in the FLACS manual. The strong grid dependency displayed is regarded as unfortunate. For the experimental work simulated in this thesis, the available experimental recordings enabled continued refinement of the grid until agreeing predictions were obtained. In the application of FLACS

as an assessment tool, such experimental recordings are usually not available, and in fact the desire to perform simulations may be exactly to compensate for a lack of experimental data. The unavailability of experimental results to serve as reference, cause the need for clear guidelines leading to satisfactory predictions, or preferably a continued development of the software reducing the sensitivity to grid size. Based on the strong grid sensitivity observed it is recommended to apply a geometry which allow resolving in a grid of multiple core cell sizes without the need to reconfigure the geometry.

For the simulations where an appropriate grid was applied, the predicted pressures revealed agreement to experimental values not only with regard to peak values, but also with regard to the characteristics of pressure development. The prediction of minor peaks identifiable in the experimental pressure recordings were found to be in agreement. These peaks were also possible to identify as those described in the theories of Cooper et al. [10]. Comparing internal and external pressure predictions also suggests that the interaction of internal and external explosions described by both Cooper [10] and Harrison and Eyre [1] can be predicted correctly, thus underlining yet again the importance of accurate prediction of external phenomena. As seen in, and assumed for, the simulations of experiments by van Wingerden [12], failing to predict the external explosion consequently influences the pressure build-up internally. Also observed to effect prediction of internal pressure development is the inability to predict acoustically enhanced oscillatory combustion. Consequently, for simulations of experiments where such pressure peaks have been registered, the obtained pressure peaks are greatly under predicted.

The best pressure predictions obtained from the simulations of experiments by Harrison and Eyre, were achieved using a core cell size of 1/120 of the length of the geometry in the direction of the flow. Application of such a size ratio is not unproblematic. Implementing this ratio can introduce undesirable constraints to the scaling of the geometry, in turn leading to difficulties performing grid sensitivity analysis. Compliance to one specific cell size of strict size ratio may cause the dimensions of the geometry not to completely resolve if applying a different cell size, thus causing the need to reconfigure the entire geometry if a grid sensitivity test is to be required. Application of such a size ratio can also introduce challenges when applied to both larger or smaller geometries. If used for larger geometries where the main extent of the geometry differs from the direction of the flow, the application of a cell size ratio of 1/120 in the direction of the flow, while simultaneously including the entire geometry and area outside the vent, can result in generation of an undesirably large amount of grid cells. This can in turn cause a significant increase in computational time, and requirement for digital storage, which is regarded as impractical especially if there should be a need to perform multiple simulations. Applying this ratio to smaller geometries can introduce problems if the ratio leads cell size towards 0.02 m or less, as the subgrid models implemented in FLACS are not compatible with cells of so little size [18].

# 5 Dust explosions

Included in this chapter are multiple simulations based on experiments investigating the external effects of vented dust explosions. Relevant data sets have been identified and gathered from available scientific publications. The simulations have been performed, and included to serve as a basis for evaluation of the applicability of CFD software in accurately predicting the external effects associated with vented dust explosions.

## 5.1 Setup dust simulations

Defining a simulation scenario of vented dust explosions is quite similar as for gas explosion, using the graphical user interface CASD for specifications of relevant parameters. For dusts, however, *Dust Explosion* has to be specified as applied scenario type. As FLACS-DustEx handles the dust cloud by representing it as a very thick and heavy gas with high viscosity, most of the simulation setup is similar for both scenario types. However, as the combustion model applied for dust simulations differ from what used for gases [18], some significant differences are evident. Where the fuel properties for *Gas Explosion* scenarios are specified directly in the pre-processor CASD, the fuel properties when utilizing a Dust Explosion scenario is extracted from a separate fuel file required specified in CASD. The physical properties of the dust, collected from this fuel file are compiled based on a series of experiments giving different characteristic values such as pressure and laminar burning velocity, over a wide range of concentrations. To represent a realistic simulation setup, such fuel files should be prepared based on physical tests performed in a 20-litre sphere [25], classifying the specific dust evaluated.

If other settings are not specified for the respective simulations, the default settings in FLACS have been applied. Settings not directly influencing the simulation output have not been described.

### 5.1.1 Setup of experiments by Wirkner-Bott

As described in section 2.1.1, the work of by Wirkner-Bott et al. [5] was based on an experimental test series of vented dust explosions in vessels of various sizes. The tests were performed using dust/air mixtures corresponding to two different  $K_{St}$ -values. Parameters such as vent area and vent release pressure were varied to be able to evaluate the influence of such. As for previous experimental work chosen for simulation, the work of Wirkner-Bott et al. [5] was considered appropriate for simulations due to the availability of recorded pressure development from the conducted tests.

## Geometry and grid - 1 m<sup>3</sup> vessel

In the publication by Wirkner-Bott et al. [5] the vessel of 1 m<sup>3</sup> was described to be of cylindrical shape with a length to diameter ratio of 1. Illustrations supplied in the paper by Wirkner-Bott [5] show that the vessel is slightly rounded in the end opposite to the vent opening.

Due to FLACS being based on a Cartesian grid, it is not possible to adapt a cubic grid to geometries of curved or leaning shapes. The recommended approach [18] for represent such shapes is by designing the curved and inclining geometries as stepped walls. In the case of even more complex geometries such as spheres, the shape can be represented by using a combination of stepped walls and assigning different porosities to the grid cells in the area of transition from solid object to empty cells. However, the latter approach is recommended to be applied with caution due to the risk of leaks associated with the use of porous walls [18].

As with the former experiments chosen for simulations, no CAD-drawing of the enclosure was available. The geometry therefore had to be built in FLACS' geometry module, CASD. To represent the geometry used in the experiments a stepwise approach was chosen. The geometry was built using a box of rectangular shape which in turn was "hollowed out" using cylinders of various sizes. A cross-section of the implemented geometric shape can be seen in Figure 41.

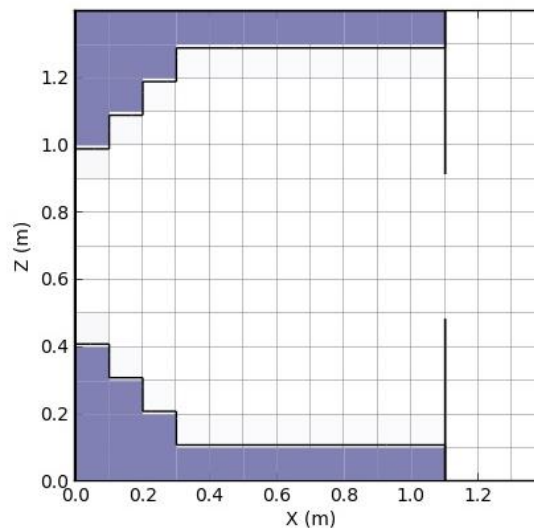


Figure 41: Cross-section of the implemented 1 m<sup>3</sup> vessel used by Wirkner-Bott et al. [5].

By applying a box slightly larger than the cylinders representing the internal volume, leaks through the stepped walls of the cylinders were avoided. A cylinder with centre in the middle of the box represented the pressure relief vent. The vent had a diameter of 0.45 m equalling to an area of 0.15 m<sup>2</sup>, venting in x-direction. In CASD a vent relief panel was defined to cover the area of the orifice. To correspond to what applied in the experiments, the panel was set to open at a pressure difference of 250 mbar.

To comply with the placement of transducers in the original experiment, monitor points were defined at the centre line of the vent opening, at distances of 2.00 m, 4.00 m, 6.00 m, 8.00 m, 10.00 m and 12.00 m. Internal monitor points were defined at the end wall opposite the vent opening, and at the middle of the vessel.

For this simulation, the core grid was defined as a uniform cubic grid with cell size 0.10 m in all dimensions. The core grid was extended to include the entire geometry, as well as the external area where combustion and/or explosion may occur. The total grid domain was extended sufficiently to avoid possible influences from boundaries. The dimensions of the entire grid are presented in Table 16.

*Table 16: : Dimensions of grid applied to simulations using a 1 m<sup>3</sup> vessel, Wirkner-Bott et al. [5]*

	X [m]	Y [m]	Z [m]
Core, start	0.00	-2.00	0.00
Core, end	16.00	3.00	4
Core, cell size	0.10	0.10	0.10
Total, start	0.00	-5.00	0.00
Total, end	25.00	6.00	7.00
Size	Stretched	Stretched	Stretched

## Scenario - 1 m<sup>3</sup> vessel

The setup of the simulation scenario in FLACS is defined to represent similar experimental conditions as those described by Wirkner-Bott et al. [5]. The fuel was set to be a maize dust with reactivity equal to a  $K_{St}$ -value of 100 bar m/s or 200 bar m/s. A homogeneous dust cloud was defined to cover the entire internal area of the vessel. In the paper by Wirkner-Bott et al. [5] no descriptions were given of dust concentrations applied in the tests. Common practice during tests with ignition of flammable dust/air mixture is to aim for the most reactive concentration of the current dust. Studies and classifications of maize starch has documented the most reactive concentration to be in the range of 450-550 g/ m<sup>3</sup> [3]. The concentration used in the simulations of tests by Wirkner-Bott et al. [5] was therefore set to 500 g/ m<sup>3</sup>. This can of course represent a significant source of error and must be taken into account when evaluating the results of the simulations.

The dust used by Wirkner-Bott et al. [5] was specified to be of one type, however the ignition delay and thus the turbulence level of the dust cloud was varied to create conditions resembling the two different  $K_{St}$ -values. As describe in the introduction of section 5.1, different dust characteristics are represented by a specified fuel file. As the work of Wirkner-Bott et al. [5] was performed decades ago, and prior to the development of FLACS-DustEx, naturally no such fuel file was obtainable. Due to the unavailability of values for the specific dusts used in the experiments, the only way to represent values needed by FLACS-DustEx is by modifying known alternatives. This of course represents a possible source of error,



however experience from simulations performed at Gexcon AS indicates that obtained predictions represent a fair agreement to experimental findings. The data and fuel files used in these simulations were based on tests with a maize dust with  $K_{St}$ -value measured to be 150 bar m/s, conducted in a standard 20-litre vessel. To obtain the desired characteristic properties of a dust with a  $K_{St}$  deviating from this, it is necessary to manipulate the laminar burning velocity in the fuel file describing the properties of the dust with  $K_{St}$  of 150 bar m/s. By manipulating these, the reactivity of the dust represented in the fuel file is changed. The modified files are used in simulations of dust clouds of various concentration, in a model of a standard 1 m<sup>3</sup> vessel. This vessel is chosen as the maximum rate of pressure rise in this volume is numerically identical to the  $K_{St}$ -value. Results from the simulations are in turn analysed to find maximum rate of pressure rise,  $dP/dt_{max}$ , for the modified dust at the desired concentration. An adequate scaling is achieved when simulations in the 1 m<sup>3</sup> vessel, using the adjusted fuel file, show that the maximum  $dP/dt$  at the desired concentration corresponds to the  $K_{St}$ -value specified for the dust used in the experiments. By doing this it is possible to represent the characteristics of the dust used in the actual experiments without being in possession of test results for that specific dust.

To obtain adequate representation of dusts with characteristics as those used in the experiments, the original fuel file was adjusted with a factor of 0.90 and 1.75, thus giving similar characteristics at the applied dust concentration. As can be seen in Figure 42 and Figure 43 the dust adjusted by a factor of 0.90 corresponds to a  $dP/dt_{max}$  of approximately 100 bar/s and the dust adjusted by a factor of 1.75 to approximately 200 bar/s when the concentration of 500 g/m<sup>3</sup> is applied. The dust represented by these modified fuel files are therefore regarded as satisfactory representations of the respective dusts.

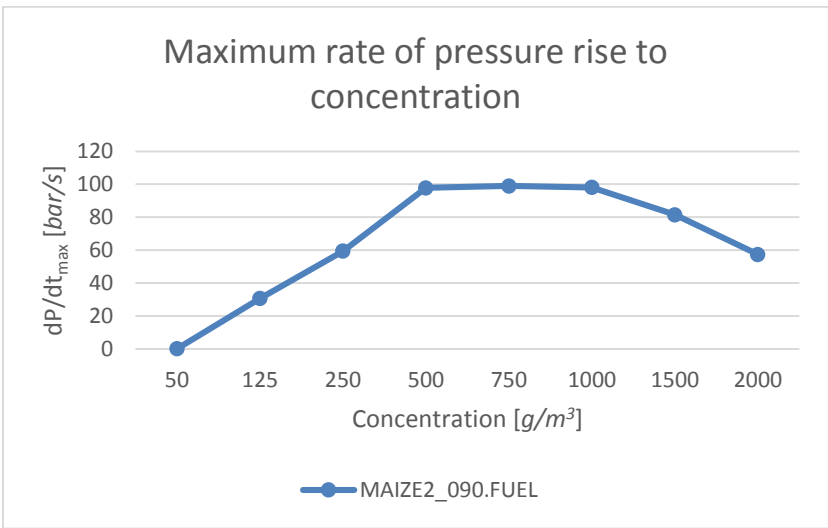


Figure 42: Maximum rate of pressure rise at different concentrations using adjusted  $K_{St}$ -value equalling 100 bar m/s. Applied to represent a dust used in the experiments by Wirkner-Bott et al. [5]

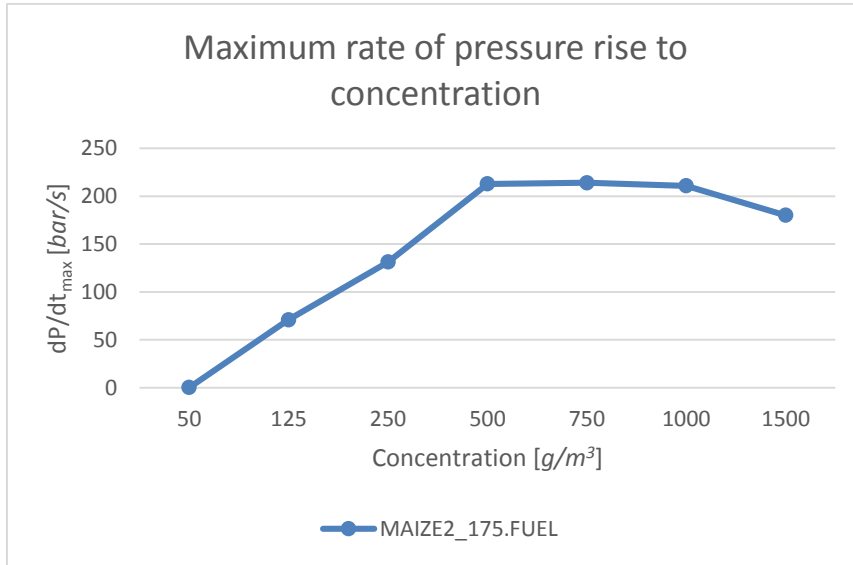


Figure 43: Maximum rate of pressure rise at different concentrations using adjusted  $K_{St}$ -value equalling 200 bar m/s. Applied to represent a dust used in the experiments by Wirkner-Bott et al. [5]

Position for ignition was set at the centre of the end wall opposite the vent opening, with an energy set to 10 kJ. As the generation of a dust cloud is reliant on the dispersion of dust in air, and gravity causes such cloud to settle with time, the fundamental nature of a dust cloud must to some extent be turbulent upon ignition. The initial turbulence settings applied in the simulations was therefore set different from zero. As the experimental data did not include such information, the applied values were chosen based on recommendations made by one of the supervisors [19]. Turbulence levels were initially set to a characteristic velocity ( $U$ ) of 1 m/s, relative turbulence intensity ( $RTI$ ) of 3.5 and a turbulence length scale ( $l_s$ ) of 0.05 m. These values were chosen as they have shown to give a fair prediction for dust simulations in different vessels and enclosures.

### Geometry and grid - 60 m<sup>3</sup> vessel

The 60 m<sup>3</sup> vessel was described to be of cylindrical shape, with rounded walls in both ends. An orifice of circular shape, with an area of approximately 2.00 m<sup>2</sup> was located in one of the end walls, venting the excess pressures in a vertical direction (z-direction).

A similar approach to that applied when designing the vessel of 1 m<sup>3</sup> was used when defining the 60 m<sup>3</sup> vessel. A rectangular box hollowed out by cylinders of various sizes represented the shape and volume of the original vessel used in the experiments. Contrary to the vessel of 1 m<sup>3</sup>, the vessel of 60 m<sup>3</sup> had both internal end walls slightly rounded. This was solved by a slight stepwise narrowing of the cylinder radiuses in both ends of the vessel. Figure 44 show a cross sectional view of the middle of the vessel.

The sizes of the cylinders used were made on the basis of keeping the geometry simple, while simultaneously maintaining a corresponding geometric shape and volume.

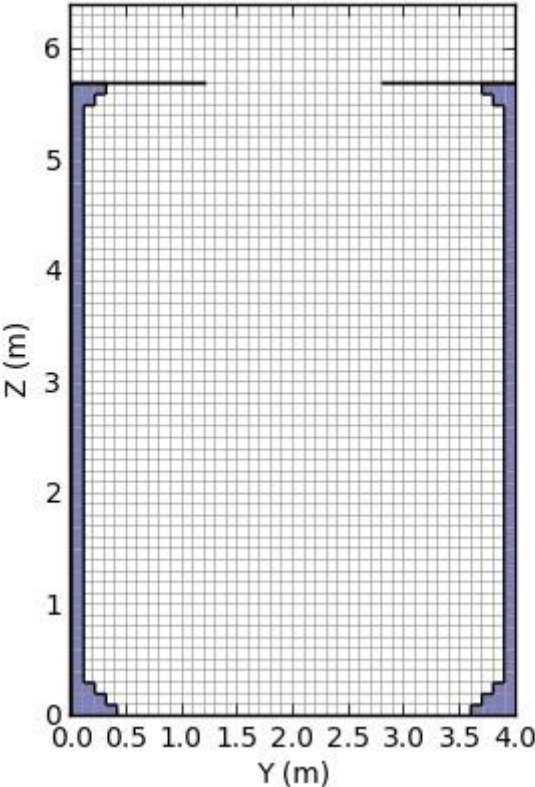


Figure 44: Cross-section of the implemented 60 m<sup>3</sup> vessel used by Wirkner-Bott et al. [5]

Monitor points were added to comply with the location of pressure transducers in the experimental series. Inside the vessel two monitor points were defined, one at the centre of the bottom wall, and one close to the side wall in the middle of the vessel (vertically). The external monitor points were mounted on a pole, locating them in the centre line of the vent. External monitor points were located at a distance of 2.00 m, 4.00 m, 6.00 m, 8.00 m, 10.00 m and 12.00 m outside the vent opening.

As for the earlier simulations, the size of the grid applied to the simulations in the 60 m<sup>3</sup> vessel was also determined based on a combination of experiences from the previous simulations and on the guidelines for grid sizing found in the FLACS Manual [18].

The core grid was defined as a uniform cubic grid with cell size 0.10 m in all dimensions. The core grid was extended to include the entire geometry, as well as the external area where combustion and/or explosion may occur. The total grid domain was extended sufficiently to avoid possible influences from boundaries. The dimensions of the entire grid are presented in Table 17.

Table 17: Dimensions of grid applied to simulations using a 60 m<sup>3</sup> vessel, Wirkner-Bott et al. [5]

	X [m]	Y [m]	Z [m]
Core, start	-2.50	-2.50	0.00
Core, end	6.50	6.50	18.00
Core, cell size	0.10	0.10	0.10
Total, start	-7.50	-7.50	0.00
Total, end	10.00	10.00	30.00
Size	Stretched	Stretched	Stretched

## Scenario - 60 m<sup>3</sup> vessel

The simulation scenario was defined, replicating the experiments described by Wirkner-Bott et al. [5]. Simulations in the 60 m<sup>3</sup> vessel were set up defining a homogenous dust cloud with concentration of 500 g/m<sup>3</sup>, specified to cover the internal volume of the vessel. The dusts used were specified to have a  $K_{St}$ -value equal to 100 bar m/s and 200 bar m/s. The ignition point was set at the bottom, in the centreline of the vessel, opposite to the vent opening. Effect of ignition was set to be 10 kJ. The explosion vent panel was defined to have a static release pressure of 100 mbar. Initial turbulence parameters were, as initial simulations for 1 m<sup>3</sup> vessel, set to characteristic velocity 1 m/s, Relative Turbulence Intensity 3.5 and Turbulence length scale 0.05 m. Turbulence settings were made after recommendations by one of the supervisors [19].

### 5.1.2 Setup of experiments by Colwell

During the experimental studies forming the basis for her Ph.D., Sarah Colwell [14] conducted experiments with vented dust explosions. The experiments were conducted in an enclosure with a flexible arrangement allowing the use of volumes of either 20 m<sup>3</sup> or 40 m<sup>3</sup>, in combination with multiple vent openings of various areas and shapes. Data presented in the thesis include internal and external pressure-time-curves for two of the test carried out, along with a detailed descriptions of the experiments. These experimental data were therefore regarded as a suitable basis for simulations.

### Geometry and grid

The enclosure was constructed of an arrangement of stands and beams serving as a structural framework, with steel plates bolted onto the framework giving the desired geometrical shape. The dimensions for the 40 m<sup>3</sup> enclosure were 2.4 m x 4.8 m x 3.6 m, (height x width x depth), while the 20 m<sup>3</sup> enclosure were of dimensions 2.4 m x 2.4 m x 3.6 m. Figure 45 illustrates the possible configuration of the enclosure.

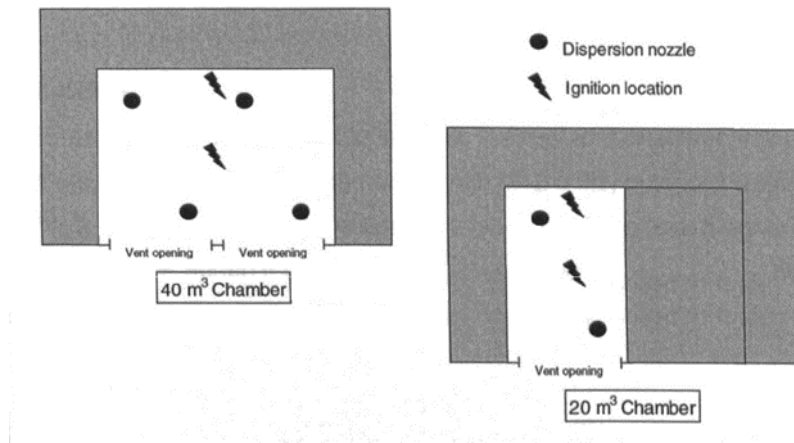


Figure 45: Illustration of enclosure, seen from above, Sarah Colwell [14]

As can be seen in Figure 45, the two different volumes are obtained by using a partition wall mounted in the middle of the 40 m<sup>3</sup> enclosure, giving a volume of half the size. The enclosure of 40 m<sup>3</sup> was equipped with two vent panels located on the upper half of one of the walls, leaving only one vent when separated into a volume of 20 m<sup>3</sup>. The vent area for the enclosure of volume 20 m<sup>3</sup> was set to be 1 m<sup>2</sup> and for the enclosure of volume 40 m<sup>3</sup> to be 2.8 m<sup>2</sup>, divided between two vents. Figure 46 displays the enclosure configured for a volume of 20 m<sup>3</sup>.

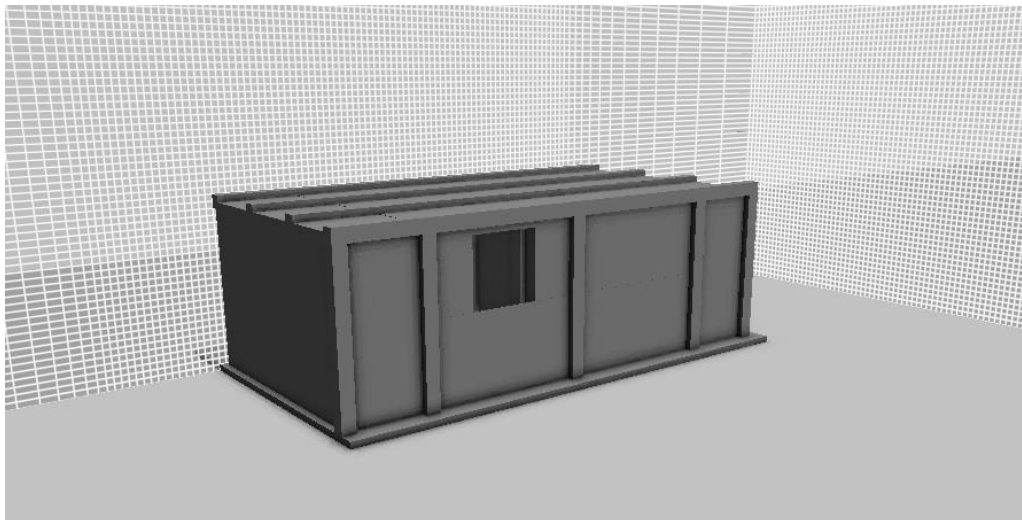


Figure 46: Graphical image of enclosure of 20 m<sup>3</sup> used in FLACS for simulations of experiments by Colwell [14]

When designed in FLACS the original dimensions of the geometry were maintained, however no further description than “upper half of wall” were available for location and dimensions for the vents. The locations of these are therefore assumed to be at the centre of the upper half of the end wall. Dimensions assigned to the vent opening are chosen with the aim of maintaining the vent area stated by Colwell, and

to allow the vent opening to completely resolve on the grid. In the simulations, the 20 m<sup>3</sup> enclosure was given a vent of size 1.0 m x 1.0 m, while the 40 m<sup>3</sup> enclosure was equipped with two vents of size 1.4 m x 1.0 m.

The enclosures were designed with dimensions allowing the entire geometry, including vent openings, to resolve in a grid of cell size 0.05 m and 0.10 m. These sizes were chosen keeping in mind experiences regarding suitable cell sizes for simulations of experiments by Harrison and Eyre [1]. The core grid was made up of uniform cubic cells, covering the entire volume of the dust cloud and extended to also include all relevant parts of the geometry, along with external areas of interest. To avoid influence or undesirable effects from the outer boundaries of the grid, these were placed sufficiently far from the area where combustion and explosion takes place. To avoid unnecessary computational time, the grids applied to the simulations of 20 m<sup>3</sup> and 40 m<sup>3</sup> enclosure were not given the same dimensions. Presented in Table 18 are the dimensions of both the core, and the total grid used for simulations in the 20 m<sup>3</sup> enclosure. Table 19 presents the corresponding values for simulation in the 40 m<sup>3</sup>.

*Table 18: Dimensions of grid applied to simulations using an enclosure of 20 m<sup>3</sup> enclosure, Colwell [14]*

	X [m]	Y [m]	Z [m]
Core, start	-0.10	-2.80	-0.10
Core, end	12.00	5.20	5.50
Core, cell size	0.10	0.10	0.10
Total, start	-0.10	-5.20	-0.20
Total, end	30.00	10.40	11.00
Size	Stretched	Stretched	Stretched

*Table 19: Dimensions of grid applied to simulations using an enclosure of 40 m<sup>3</sup>. Colwell [14]*

	X [m]	Y [m]	Z [m]
Core, start	-0.10	-2.80	-0.10
Core, end	12.00	7.60	5.50
Core, cell size	0.10	0.10	0.10
Total, start	-0.10	-5.20	-0.10
Total, end	30.00	10.20	10.00
Size	Stretched	Stretched	Stretched

## Scenario

The two experiments by Colwell, simulated as a part of this thesis, do not only differ in volume and vent area. The two experiments also differ with regards to properties of the dust cloud, and ignition point. In the following the two setups will be presented.

The test conducted in the 20 m<sup>3</sup> enclosure was carried out using maize starch with K<sub>St</sub> of 129 bar m/s, with variation between batches stated to be +/- 12%. The concentration of dust in air was measured to 500 g/m<sup>3</sup>. The vent area used was of 1.00 m<sup>2</sup> with a static release pressure of 7.5 kPa, i.e. 0.075 bar. Ignition of the dust cloud was initiated at the centre of the enclosure.

For the test performed in the 40 m<sup>3</sup> enclosure the same type of dust was used, however, in this test the concentration of the dust cloud was specified to be 750 g/ m<sup>3</sup>. The 40 m<sup>3</sup> vessel was equipped with two vent panels, each of size 1.4 m<sup>2</sup>, giving a total area of 2.8 m<sup>2</sup>. The static release pressure for these vents were 10.6 kPa and 9.60 kPa, corresponding to 0.106 bar and 0.096 bar respectively. The ignition point in the test was specified to be at the centre of the rear wall of the chamber. Note that this does not represent the same ignition point as applied in the smaller enclosure.

The dust used by Colwell [14] in her work was specified to have a K<sub>St</sub> of 129 bar m/s. As for the simulations described in section 5.1.1, no fuel files for the specific dust used in the experiments were available. Consequently, the characteristics of the dust used by Colwell [14] had to be represented by adjusting a known alternative. For the concentrations of 500 g/m<sup>3</sup> and 750 g/m<sup>3</sup> used in the current experiments, the best scaling of the fuel file, was by a factor of 1.12. By multiplying with this factor the simulations in the 1 m<sup>3</sup> vessel show a good correspondence to the specified K<sub>St</sub> at the desired concentrations. As can be seen in Figure 47 the dP/dt<sub>max</sub> when applying the adjusted fuel at a concentration of 500 g/m<sup>3</sup> and 750 g/m<sup>3</sup> corresponds to approximately 129 bar/s.

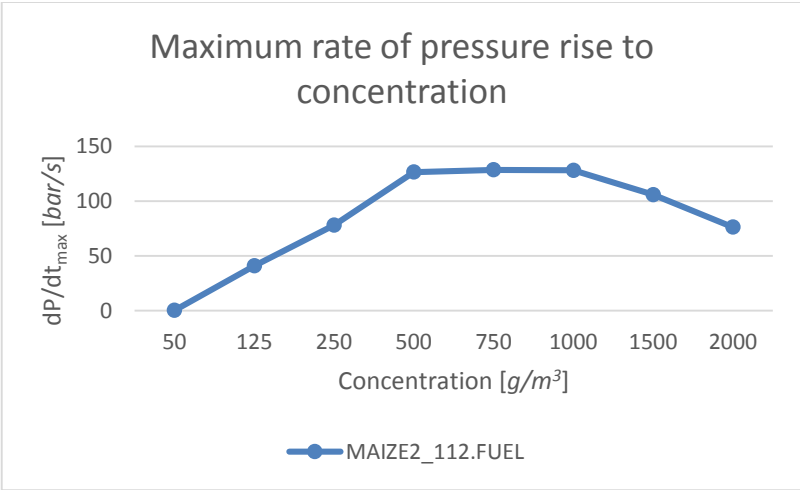


Figure 47: Maximum rate of pressure rise at different concentrations using adjusted K<sub>St</sub>-value equalling 129 bar m/s. Applied to represent a dust used in the experiments by Colwell [14]

Monitor points were placed according to locations used in the experimental setup. Internally, the 20 m<sup>3</sup> enclosure was equipped with one transducer in the ceiling, one in the side wall and one located in the wall below the vent opening. The 40 m<sup>3</sup> enclosure utilized the same locations of the transducers,

however these were also mirrored around the centre line (partition wall) of the vessel giving a total of six pressure transducers. External transducers were located in the ground in the centre line of the 40 m<sup>3</sup> enclosure, resulting in a slight angle to the centre line of the vents. These were located at distances 0.50 m, 2.50 m, 3.75 m, 5.00 m, 7.50 m 10.00 m, 15.00 m and 20.00 m.

Initial turbulence parameters were set based on recommendations by one of the supervisors [19] and on the same basis as described in section 5.1.1. Values set to characteristic velocity 1 m/s, Relative Turbulence Intensity 3.5 and Turbulence length scale 0.05 m.

## 5.2 Results and discussion

### 5.2.1 Results simulations of experiments by Wirkner-Bott

From the work of Wirkner-Bott et al. [5] it has been attempted to simulate four different experiments: two tests in a 1 m<sup>3</sup> vessel, and two tests in a 60 m<sup>3</sup> vessel. For each vessel two tests were performed using the same type of maize starch dust. The time of ignition was however delayed for one of the tests with the intent to simulate dusts of different reactivity ( $K_{St}$ -value). By adjusting the ignition delay Wirkner-Bott et al. [5] claimed to obtain two different atmospheres inside the enclosure, comprising of a dust/air mixture with a turbulence level corresponding to two dusts with characteristics equalling to a  $K_{St}$ -value of 100 and a  $K_{St}$ -value of 200.

Due to the article not supplying any data for initial turbulence, the first setup for these simulations were run with initial turbulence conditions based on experiences from previous simulations. These values have shown to be appropriate for multiple simulations leading to fair predictions when compared to other experimental work [19].

#### Initial simulation results – 1 m<sup>3</sup>

The pressure predictions presented in Figure 49 are obtained from the initial simulation of explosion in the 1 m<sup>3</sup> using a dust with reactivity stated to equal to a  $K_{St}$  of 100 bar m/s. Presented in Figure 48 and Figure 49 are the experimental pressures and the predicted pressure obtained from the simulations. The peak internal pressure predicted in the simulation was found to be 261 mbar, contrary to the peak experimental value lying in the range of 300-350 mbar. This represent an under estimation between 50-100 mbar for the internal pressure. Looking at the external values a deviation of 60-65 mbar can be observed between the recorded value of 75-80 mbar and the value of 14 mbar predicted in the simulations. This equals a percentage deviation of 15-25% for the internal explosion and a deviation of over 80% for the external explosions. There were also deviations between the recorded and the predicted



location of the external peak. The experimental peak was registered at a distance of approximately 5 meters from the vent opening, whereas the external peak in the simulation was obtained at a distance of 2 m.

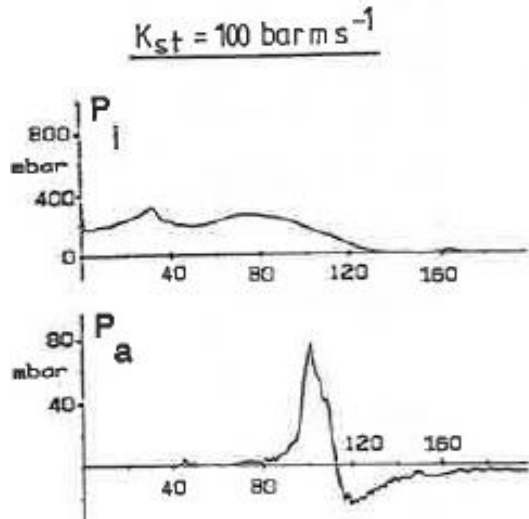


Figure 48: Experimental internal and external pressure,  $1 \text{ m}^3$  vessel,  $K_{St} = 100 \text{ bar m/s}$ , Wirkner-Bott et al. [5]

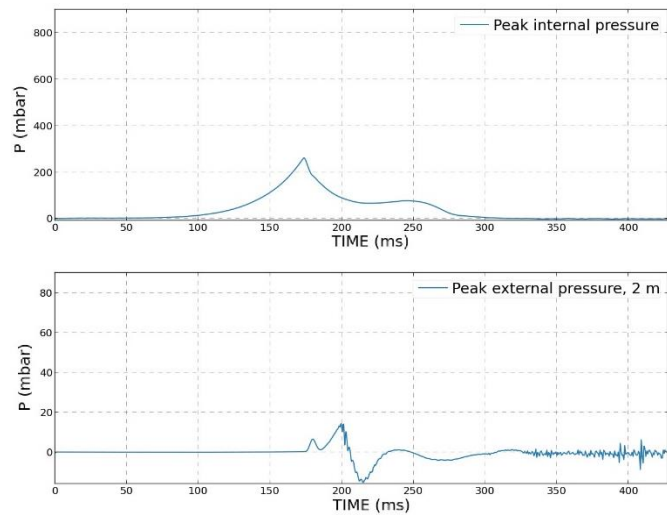


Figure 49: Simulated internal and external pressure,  $1 \text{ m}^3$  vessel,  $K_{St} = 100 \text{ bar m/s}$

Evaluating the results of initial simulations of explosion in the  $1 \text{ m}^3$  using a dust assumed to equal to a  $K_{St}$  of  $200 \text{ bar m/s}$ , also showed deviations between experimental records and values obtained by the use of simulations. The pressure development recorded during the experiments is presented in Figure 50, while values obtained by simulations are presented in Figure 51. The peak internal pressures recorded experimentally was in the area of  $700\text{-}750 \text{ mbar}$ , while  $450 \text{ mbar}$  was the predicted internal pressure peak. The degree of compliance for external pressures were somewhat in the same region, recorded to approximately  $100 \text{ mbar}$  in the experiments, compared to  $48 \text{ mbar}$  predicted in the simulations. The percentage deviations for internal and external pressures are in the range of  $50\text{-}65\%$ . With regard to the location of the maximum external pressure, there was good agreement between the experiments and simulations, both defining the peak at a distance of approximately  $2 \text{ m}$ .

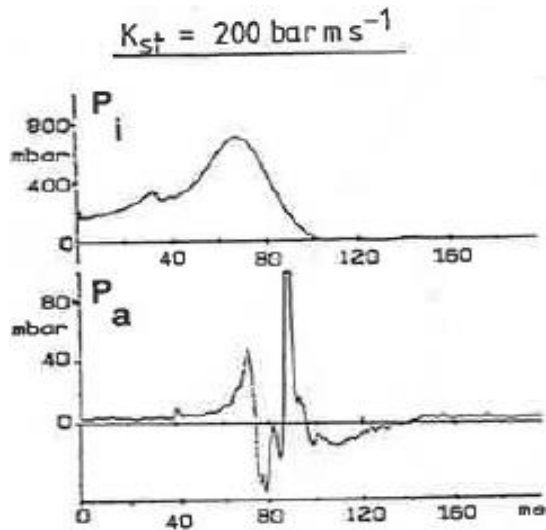


Figure 50: Experimental internal and external pressure, 1 m<sup>3</sup> vessel,  $K_{St} = 200 \text{ bar m/s}$ , Wirkner-Bott et al. [5]

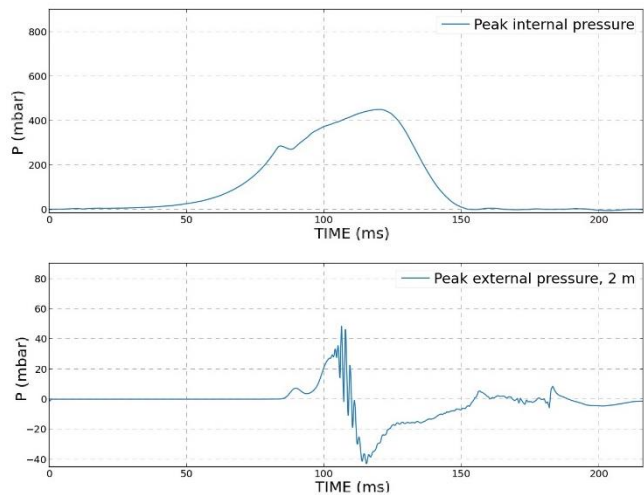


Figure 51: Simulated internal and external pressure, 1 m<sup>3</sup> vessel,  $K_{St} = 200 \text{ bar m/s}$

The results from the initial simulations, both using dust reactivity equalling to  $K_{St}$  of 100 bar m/s and of 200 bar m/s, show significant deviations in predicted pressure peaks. The predictions are however within the same size of magnitude as the peak values recorded in the experiments.

Comparing the internal pressure recording to the predictions reveal some similarities in the pressure development. The recorded pressure transcription, for both dust reactivities, display a distinct peak in the initial parts of the curve. These initial peaks, also visible in the predicted pressures, are believed to be connected to the release or rupture of the vent panel. Similar to the experimental pressures, the continued pressure predictions show tendencies to a build-up of a second peak, however the predictions do not capture the magnitude of the increase in pressure. Consequently, the predicted peaks are both of lower values and of a more moderate rate of pressure rise. The predictions of external pressure development show similar trends to those observed for the experiments. However, the level of magnitude does not correspond to those registered in the experiments.

### Initial simulation results - 60 m<sup>3</sup>

When analysing the results of the Wirkner-Bott et al. [5] simulations using the setup described in section 5.1.1, it is clearly visible that the internal pressures are greatly over predicted compared to the experimental results. Simulations using a dust with reactivity equalling to  $K_{St}$  of 100 bar m/s gave a peak internal pressure of 948 mbar compared to a corresponding pressure of 300-350 mbar recorded in the experiments. For a dust with reactivity equalling to  $K_{St}$  of 200 bar m/s, the predicted internal peak pressure of 2307 mbar represents a significant over prediction, compared to a recorded peak pressure of 700-750 mbar for the corresponding experimental test. Both of these predictions are approximately three

times higher than the experimental values. The same similarity cannot be found when comparing external pressure peaks. Simulations using the less reactive dust, predicts the external pressure peak to be 53 mbar, representing an under prediction of 150 mbar compared to the experimental peak recorded to be around 200 mbar. The same under prediction is not detectable when analysing the pressure transcription for the more reactive dust. Comparing external pressures from the experiments to the simulations, using a dust with reactivity equalling to  $K_{St}$  of 200 bar m/s, reveal quite good compliance between the two. The external pressure peak is predicted to 185 mbar, while the corresponding experimental peak is logged to be 180-200 mbar. For both dust reactivities, the locations of external peak pressures were recorded at distances in the range of 6-8 meters above the vent opening. This location corresponds well with those obtained in the simulations, however for the simulation using the more reactive dust mixture a comparable external pressure peak was also observed at a distance of 2 m from the vent.

Comparing the pressure recordings in Figure 52 and Figure 54, to the pressure predictions in Figure 53 and Figure 55, one can find similar trends in the pressure development obtained from both the experiments and the simulations. Both the number and order of pressure peaks are comparable, however the predicted internal pressure peaks are greater than those recorded experimentally. This can be considered an indication of the simulations representing a more reactive dust mixture, either due to incorrect representation of the dust, or by the simulation settings not replicating the experimental conditions, e.g. turbulence.

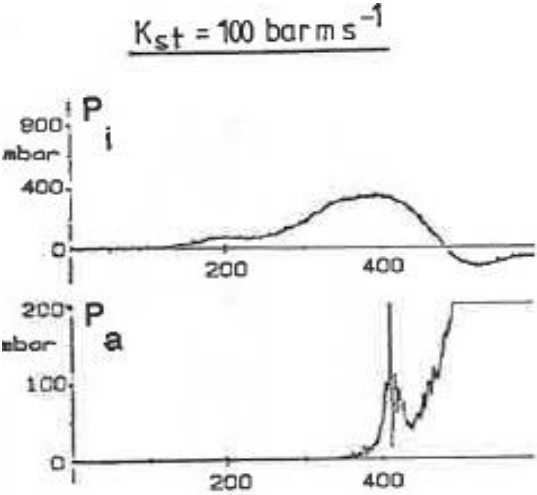


Figure 52: Experimental internal and external pressure: 60 m<sup>3</sup> vessel,  $K_{St} = 100 \text{ bar m/s}$ , Wirkner-Bott et al. [5]

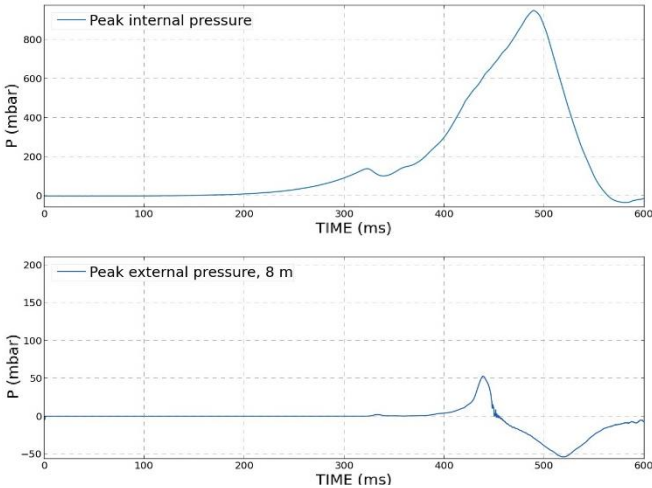


Figure 53: Simulated internal and external pressure, 60 m<sup>3</sup> vessel,  $K_{St} = 100 \text{ bar m/s}$

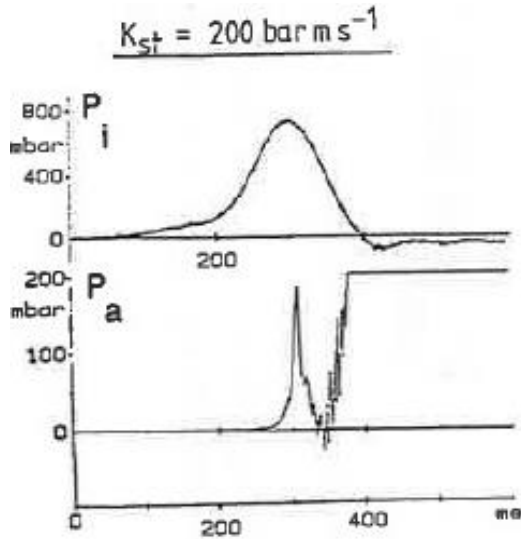


Figure 54: Experimental internal and external pressure: 60 m<sup>3</sup> vessel, K<sub>St</sub> = 200 bar m/s, Wirkner-Bott et al. [5]

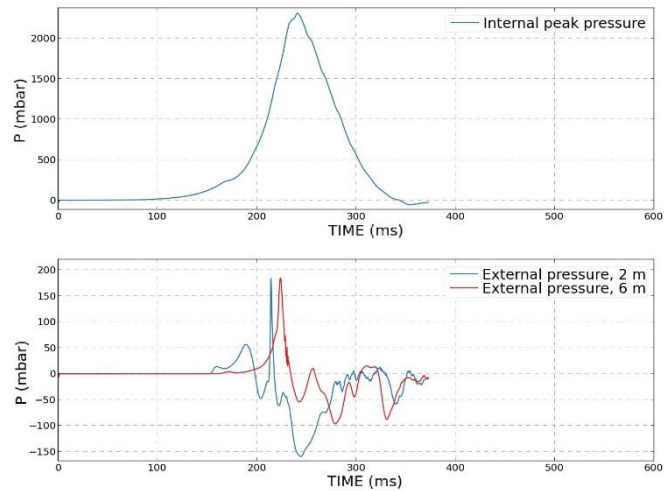


Figure 55: Simulated internal and external pressure, 60 m<sup>3</sup> vessel, K<sub>St</sub> = 200 bar m/s

## Improvement/refinement of specified scenario conditions

Evaluating the initial simulations of experiments by Wirkner-Bott revealed no apparent trend in the predictions of pressures. Comparing to gas simulations, no recognizable cause for such deviations was detectable. A possible source for the discrepancies was however identified recalling the method used by Wirkner-Bott for representation of different dust characteristics. The use of delayed ignition, hence the decay of turbulence after dispersion, to resemble the different dusts suggests that the representation of initial turbulence in the simulations is not comparable to that in the experiments. An initial assumption was therefore that the reason for the deviations could be due to different and/or wrong representation of initial turbulence in the simulations.

In an attempt to find initial turbulence levels corresponding to the values recorded for internal pressure, a “reverse methodology” was applied. As can be seen in Eq.1.1, the K<sub>St</sub>-value is a parameter based on the maximum rate of pressure rise registered when igniting a dust cloud in a closed vessel. Rearranging Eq.1.1 for the dust of K<sub>St</sub> = 200 bar m/s, considering explosions in the vessel of 60 m<sup>3</sup>, gives the following corresponding maximum pressure rise:

$$(dP/dt)_{max} = \frac{K_{St}}{V^{1/3}} = \frac{200 \text{ bar m/s}}{(60m^3)^{1/3}} = 51.087 \text{ bar/s}$$

By performing multiple simulations with a closed vent opening, and systematically adjusting the initial turbulence parameters, one can obtain the turbulence levels corresponding to the dP/dt<sub>max</sub> which in turn corresponds to the K<sub>St</sub>-value described in the testes. The dP/dt is specified as simulation output, and the maximum value is obtained when running the various simulations in FLACS.

Results after performing a total of 9 simulations in the 60 m<sup>3</sup> vessel with closed vent, adjusting and logging the turbulence parameters, are presented in the Table 20 - Table 22. This investigation revealed that a characteristic velocity of 1 m/s, relative turbulence of 0.25 and turbulent length scale of 0.025 m were the initial turbulence levels corresponding best to the  $dP/dt_{max}$  equalling a  $K_{St}$ -value of 200 bar m/s. Presented in Figure 56 is a graphic illustration of the significance of initial turbulence parameters.

Table 20: Initial turbulence settings applied to the reference simulations.  $U$  set to 1 m/s,  $RTI$  set to 0.125,  $l_s$  varied

<b>Simulation No.</b>	113175	444175	222175
<b><math>K_{St}</math> [bar m/s]</b>	200 (175)	200 (175)	200 (175)
<b><math>U</math> [m/s]</b>	1	1	1
<b><math>RTI</math> [-]</b>	0,125	0,125	0,125
<b><math>l_s</math> [m]</b>	0,01	0,025	0,05
<b><math>(dP/dt)_{max}</math> [bar/s]</b>	35,572	47,712	63,122

Table 21: Initial turbulence settings applied to the reference simulations.  $U$  set to 1 m/s,  $RTI$  set to 0.25,  $l_s$  varied

<b>Simulation No.</b>	133175	144175	112175
<b><math>K_{St}</math> [bar m/s]</b>	200 (175)	200 (175)	200 (175)
<b><math>U</math> [m/s]</b>	1	1	1
<b><math>RTI</math> [-]</b>	0,25	0,25	0,25
<b><math>l_s</math> [m]</b>	0,01	0,025	0,05
<b><math>(dP/dt)_{max}</math> [bar/s]</b>	39,044	51,988	70,108

Table 22: Initial turbulence settings applied to the reference simulations.  $U$  set to 1 m/s,  $RTI$  set to 0.5,  $l_s$  varied

<b>Simulation No.</b>	333175	114175	111175
<b><math>K_{St}</math> [bar m/s]</b>	200 (175)	200 (175)	200 (175)
<b><math>U</math> [m/s]</b>	1	1	1
<b><math>RTI</math> [-]</b>	0,5	0,5	0,5
<b><math>l_s</math> [m]</b>	0,01	0,025	0,05
<b><math>(dP/dt)_{max}</math> [bar/s]</b>	43,832	58,71	75,265

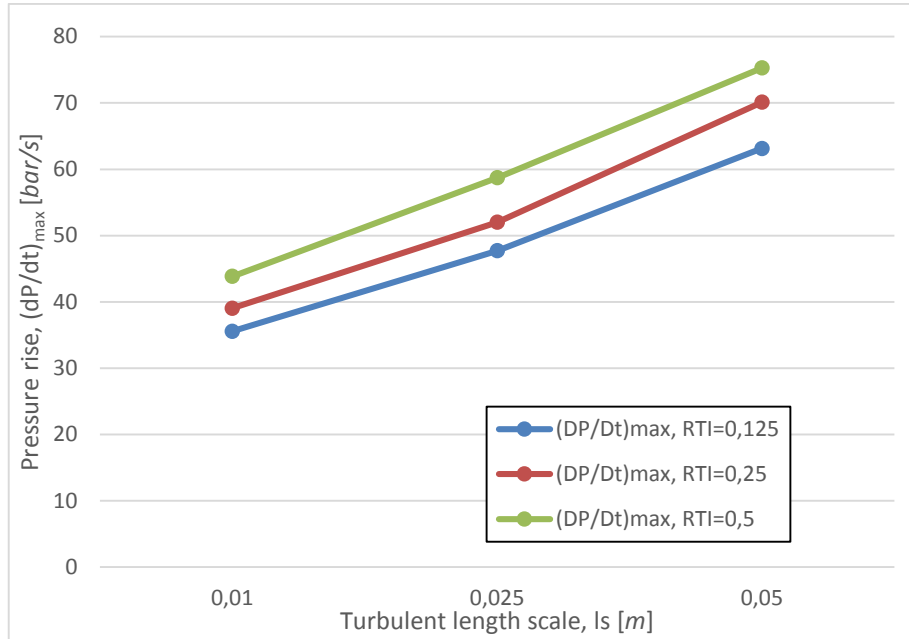


Figure 56: Effect of turbulence parameters on  $dP/dt_{max}$ , 60 m<sup>3</sup> vessel,  $K_{St}$  equal to 200 bar m/s

### Refined simulation results - 60 m<sup>3</sup>

Running the ordinary vented simulation scenario using the turbulence parameters corresponding to the  $dP/dt_{max}$  described above, gave a predicted internal pressure peak of 1137 mbar - still significantly higher than the experimental value of 700-750 mbar.

The continued deviation compared to experimental values might be an indication that incorrect initial turbulence is not the sole contributing factor to the differences in peak pressures. However, the method applied by Wirkner-Bott [5] to represent dusts of different characteristics introduces significant amounts of uncertainties regarding the nature of the dispersed dust cloud. In combination with the deviating pressure prediction, this might be an indication that the representation of the dust cloud in the simulation does not correspond to the characteristics of the cloud in the experiments. The assumption of the use of 500 g/m<sup>3</sup> as concentration in the dust cloud, might also be an additional source to the deviations in the predicted pressures.

When comparing the simulations in Table 20 - Table 22, one finds that even small adjustments to turbulence parameters result in noticeable variations to obtained  $dP/dt_{max}$ , especially when adjusting the turbulent length scale. Although accurate, these effects display a great sensitivity to variations, thus underlining the importance of an accurate representation of turbulence levels. Even though continued adjustments to the initial turbulence parameters could lead to a better correspondence with experimentally recorded values, this is not regarded as a suitable approach. Without any description of the actual turbulence levels present in the experiments such adjustments could be mere manipulations

of simulation settings leading to corresponding predictions, but in fact be an unrealistic representation of the experiments.

As the simulations applying turbulence values based on the investigation of corresponding  $dP/dt_{max}$  still over predicted the internal values significantly, an additional investigative simulation was performed. In this simulation the initial turbulence parameters were manipulated further, applying halved values for both the relative turbulence and the turbulent length scale while still maintaining the characteristic velocity. Running this simulation using characteristic velocity of 1 m/s, relative turbulence intensity of 0.125 and turbulent length scale of 0.0125 m, resulted in a predicted internal pressure peak of 634 mbar and an external pressure peak of 169 mbar. These predicted values are in much greater compliance to the experimentally recorded values. However, the initial turbulence represented by the applied turbulence parameters are found by continued manipulation of initial turbulence settings, and there is a great deal of uncertainty whether these are a realistic representation.

## **5.2.2 Results simulations of experiments by Colwell**

The first simulations representing the experiments by Colwell were based on experimental data obtained from here thesis [14] submitted as part of her Ph.D. Enclosed in the thesis was a considerable amount of experimental data including recordings from numerous tests. Combining these data with graphs, provided in the thesis, was regarded as a good basis for simulations.

### **Initial simulation results - 20 m<sup>3</sup>**

Initial simulations of the experiment of dust explosion carried out in a 20 m<sup>3</sup>, was run using simulation settings described in section 5.1.2. In Figure 57 and Figure 58 we can see that the predictions of both internal and external pressures are significantly lower than those obtained experimentally. An internal pressure peak of 49.0 kPa obtained from the simulations, compared to a peak of 80.6 kPa recorded in the experiments equals a deviation of approximately 40 %. The predictions of external pressures represent even larger percentage deviations with a calculated pressure of 0.9 kPa compared to 6.6 kPa in the experiments, equalling a deviation of approximately 86%. In the experiments the external pressure peak is registered at a distance of 5 m from the vent, while the simulations predict similar external peak pressures at two monitor points, these being at distances of 3.70 m and 5 m from the vent.

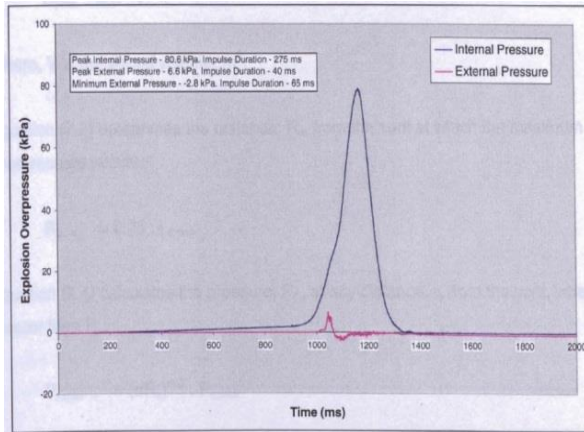


Figure 57: Experimental internal and external pressure, 20 m<sup>3</sup>, Colwell [14]

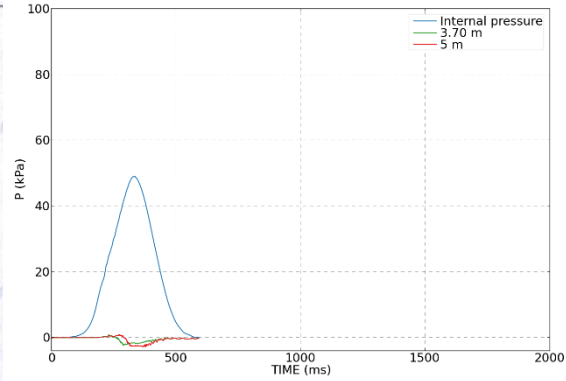


Figure 58: Simulated internal and external pressure, 20 m<sup>3</sup>

Comparing the graph displaying the predicted values obtained by simulation to those recorded experimentally reveal variations both in magnitude of pressure, and time of occurrence for pressure peaks. The difference in time of occurrence is not regarded as being of great significance due to the pressure recordings most likely being started prior to ignition of the dust cloud. It must however be noted that the internal pressure peak registered in the experiments is much sharper and of slightly shorter duration than the one obtained in the simulations. This can be an indication of the simulated explosion represents a scenario with a less reactive dust cloud.

### Improvement/refinement of specified scenario conditions - 20 m<sup>3</sup>

Some indicative simulations were performed to reveal the effects of initial turbulence on the predicted pressures. The same approach as used for simulations of Wirkner-Bott's experiments in the 60 m<sup>3</sup> vessel was adopted in an attempt to reproduce the initial turbulence resulting in a  $dP/dt_{max}$  corresponding to the  $K_{St}$ -value of the dust used in the experiments. The argument for applying the same approach, when the turbulence values obtained this way for the previous simulations did not result in prediction of corresponding values, is the reduced levels of uncertainties associated with the work of Colwell. In her thesis, she specifies the dust concentrations applied to the experiments and she does not use turbulence actively as a method for representation of dusts with different explosion properties ( $K_{St}$ -value).

Applying a  $K_{St}$  of 129 bar m/s and a volume of 20 m<sup>3</sup> when rearranging Eq.1.1, calculates to a maximum pressure rise as shown in the following:

$$(dP/dt)_{max} = \frac{K_{St}}{V^{1/3}} = \frac{129 \text{ bar m/s}}{(20\text{m}^3)^{1/3}} = 47.524 \text{ bar/s}$$

A total of 12 simulations were performed with the geometry of 20 m<sup>3</sup>, used in the experiments by Colwell, applying a closed vent opening. Adjustments to the turbulence parameters were logged, and



$dP/dt_{\max}$  were extracted as an output parameter calculated when running the simulations in FLACS. Turbulence settings and corresponding maximum rate of pressure rise are presented in the Table 23 - Table 26 below. A graphical presentation of the dependency is shown in Figure 59.

Table 23: Initial turbulence settings applied to the reference simulations.  $U$  set to 1 m/s, RTI set to 0.125,  $l_s$  varied

Simulation No.	200007	200008	200009
$K_{St}$ [bar m/s]	112	112	112
$U$ [m/s]	1	1	1
RTI [-]	0,125	0,125	0,125
$l_s$ [m]	0,025	0,05	0,1
$(dP/dt)_{\max}$ [bar/s]	34,006	45,835	58,979

Table 24: Initial turbulence settings applied to the reference simulations.  $U$  set to 1 m/s, RTI set to 0.25,  $l_s$  varied

Simulation No.	200001	200005	200006
$K_{St}$ [bar m/s]	112	112	112
$U$ [m/s]	1	1	1
RTI [-]	0,25	0,25	0,25
$l_s$ [m]	0,025	0,05	0,1
$(dP/dt)_{\max}$ [bar/s]	38,85	48,962	62,451

Table 25: Initial turbulence settings applied to the reference simulations.  $U$  set to 1 m/s, RTI set to 0.5,  $l_s$  varied

Simulation No.	200002	200003	200004
$K_{St}$ [bar m/s]	112	112	112
$U$ [m/s]	1	1	1
RTI [-]	0,5	0,5	0,5
$l_s$ [m]	0,025	0,05	0,1
$(dP/dt)_{\max}$ [bar/s]	45,337	55,097	67,56

Table 26: Initial turbulence settings applied to the reference simulations.  $U$  set to 1 m/s, RTI set to 1.0,  $l_s$  varied

Simulation No.	200010	200011	000002
$K_{St}$ [bar m/s]	112	112	112
$U$ [m/s]	1	1	1
RTI [-]	1.0	1.0	1.0
$l_s$ [m]	0,0125	0,025	0,05
$(dP/dt)_{\max}$ [bar/s]	46,144	53,641	63,276

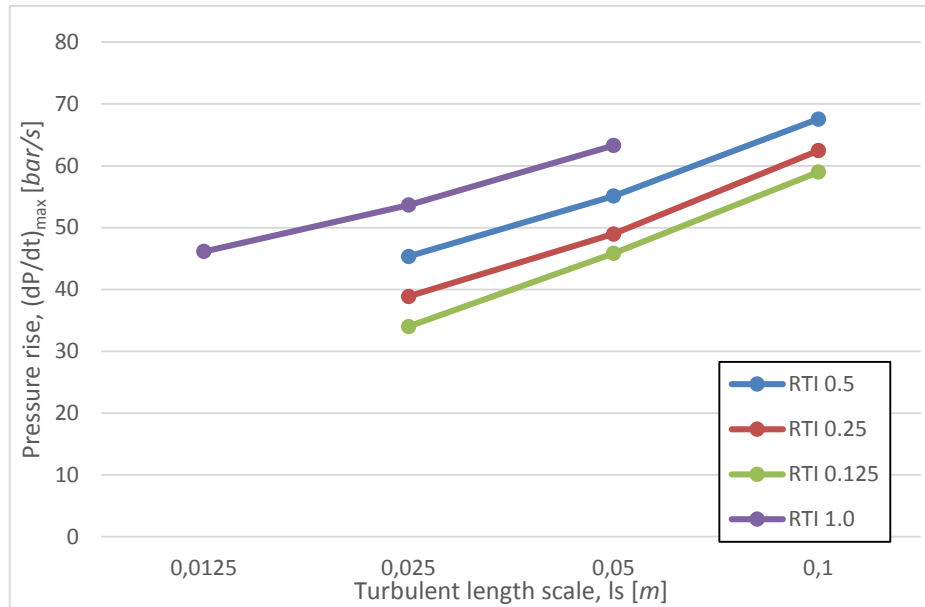


Figure 59: Effect of turbulence parameters on  $dP/dt_{max}$ , 20 m<sup>3</sup> enclosure,  $K_{St} = 129$  bar m/s

The turbulence parameters applied to reference simulation no 200010 in Table 26, were the ones corresponding best to the rate of pressure rise calculated to conform to the  $K_{St}$ -value of the dust used in the experiments.

Applying these values as settings for initial turbulence parameters, to a simulation of dust explosion in the 20 m<sup>3</sup> enclosure with a vent area of 1 m<sup>2</sup> did however not result in predicted peak pressures corresponding to those obtained experimentally. A predicted internal pressure peak of 117 mbar was of weak agreement compared to a recorded peak of 806 mbar in the experiments. The external peak pressure predicted to 14 mbar, also represented a significant deviation compared to 66 mbar registered experimentally.

As the simulations of the vented explosion in the 20 m<sup>3</sup> enclosure described above, was performed prior to the simulations described in section 4.2.3, the level of grid sensitivity was not yet realised. In light of the observed significance of even minor changes in the cell size, a final simulation was set up aiming to investigate similar sensitivities for the simulations of dust explosions in the 20 m<sup>3</sup> enclosure. This simulation applied an identical geometry and an identical extent of the grid, however the cell size applied to the core was 0.05 m. The scenario applied was the same as for the initial simulation, utilizing the turbulence settings of characteristic velocity 1 m/s, Relative Turbulence Intensity 3.5 and Turbulence length scale 0.05 m. These values were chosen as they resulted in the best correspondence to the peak pressures recorded experimentally when applied in prior simulations. Comparing the results of this simulation to the experimental values showed a much greater compliance. The predicted peak pressures were calculated to 864 mbar internally, and 16-33 mbar externally. Corresponding experimental values

were 806 mbar internal peak, and 66 mbar external peak. As this final simulation was performed at a later point in time than those discussed in section 4.2.3, the remaining time available did not allow for further investigation of influence of cell size and effect of variations in initial turbulence parameters. The increased correspondence achieved in this final simulation, in combination with the large dependency of initial turbulence discussed earlier, might be an indication that greater accuracy between predicted and recorded values is achievable. To obtain better agreement it is however necessary to perform more extensive grid sensitivity tests, while in possession of the correct values representing initial turbulence. It must be underlined that such values must represent the turbulence present in the experiments, and not just arbitrary values leading to pressure predictions corresponding to those recorded experimentally.

### **Initial simulation results - 40 m<sup>3</sup>**

The experiments with dust explosions in a volume of 40 m<sup>3</sup>, were conducted in an enclosure consisting of two adjoining enclosures of similar shape and size as the enclosure described above. With regards to the strong dependency of initial turbulence settings revealed when analysing simulations of experiments by Wirkner-Bott et al., and the prolonged computational time associated with simulations of larger volumes, the main approach to simulations in the enclosure of 40 m<sup>3</sup> was by application of the settings leading to the most agreeing predictions for the 20 m<sup>3</sup> enclosure. The simulation setting found to result in the most corresponding predictions for the volume of 20 m<sup>3</sup>, were the initial turbulence settings recommended by supervisor.

Applying these turbulence setting resulted in the pressure transcription presented in Figure 61. Comparing these predictions to the experimental recording presented in Figure 60 reveal a greater compliance than what observed for previous simulations. The peak internal pressure from the simulations is 38.9 kPa compared to 30 kPa for the experiments, representing an over prediction of 30 %. Prediction of the external pressure peak does not represent a similar level of compliance. The peak external pressure is calculated to 3.5 kPa, representing one level of magnitude lower than the 13.1 kPa recorded experimentally. Contrary to the simulations of the 20 m<sup>3</sup> enclosure, the predicted location of the external pressure peak corresponds to that registered experimentally.

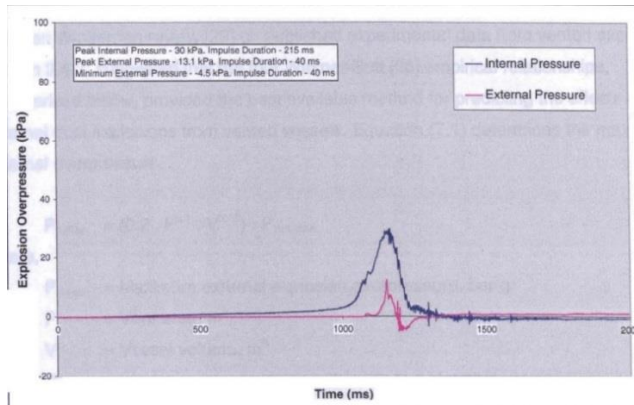


Figure 60: Experimental internal and external pressure, 40 m<sup>3</sup>, Colwell [14]

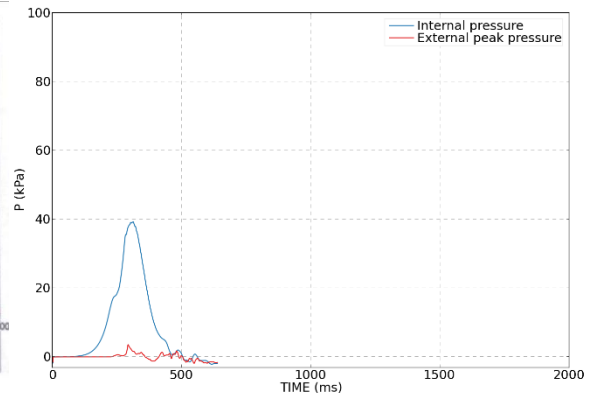


Figure 61: Simulated internal and external pressure, 40 m<sup>3</sup>

With regards to the pressure transcription presented in Figure 60 and Figure 61 one can detect similar pressure development trends for the internal pressure. The pressure-time-curves display comparable duration and rate of pressure increase. The small step, or temporary reduction in rate of pressure rise, is also present in the predicted pressure obtained by simulation. Not equally visible, is the simulated external pressure development displayed in Figure 61. Closer examination of the pressure development does reveal similar trends in the pressure development, however of significantly lower magnitude. The noticeable difference in time for initiation of pressure rise is also here believed to be a result of the experimental pressure recordings being initiated prior to ignition.

Similar investigation of initial turbulence parameters as those described for the enclosure of 20 m<sup>3</sup> has not been performed for the enclosure of 40 m<sup>3</sup>. This decision was made due to limitations in the amount of time available, and that this approach for identification of initial turbulence leading to more agreeing pressure predictions was deemed unsuccessful for prior simulations. Contributing to this decision is also the long computational time associated with simulations of larger volumes.

### 5.2.3 Key findings – dust explosions

Most experimental studies strive to ignite the dust/air mixture when the turbulence is at its lowest and when the cloud inside the enclosure is believed to be close to homogenous. In practical and physical situations, it is however neither likely, nor possible to achieve zero or insignificant turbulence while at the same time having the desired concentration inside the volume. Despite this no, or very few, scientific papers provide detailed data of the turbulence conditions within the enclosure prior to ignition. To represent a realistic scenario for the simulations, some level of initial turbulence has to be applied. As the dust cloud applied to the simulations described in section 5.2.1 and 5.2.2 was defined as a homogenous dust cloud covering the entire volume of the enclosures, the initial turbulence settings specified in the simulation scenarios were applied to the entire cloud. In most physical situations this

will be an inaccurate representation of the turbulence present inside the enclosure. Turbulence will in reality appear with variable local intensities and fluctuations, dependent on the shape of the geometry and the relevant location within that geometry. These local variations of turbulence are again dependent on the dispersion of the dust.

As described in section 5.2.1 and 5.2.2, several attempts have been made, trying to replicate initial turbulence settings leading to predictions corresponding to peak pressures recorded experimentally. Although unsuccessful, these attempts did reveal a significant sensitivity to even minor adjustments to the initial turbulence parameters. Indications observed in the attempts to reproduce pressure predictions corresponding to those recorded in the experiments, suggest that by manipulation of initial turbulence conditions one is at least able to reproduce the internal pressure. However, this is not regarded as an applicable approach. Continued manipulations of the internal pressure, aiming to reproduce the recorded internal pressure peaks is necessarily not a realistic approach to obtaining accurate simulations of the physical scenario in question. A better and more realistic method is by simulation of the dust dispersion, thus obtaining more precise values for initial turbulence levels, in turn representing a better basis for the explosion simulations. The possibility to simulate dispersion of dust is incorporated and available in FLACS, however to be able to perform such a simulation one is reliant on detailed descriptions of the dust dispersion system. For the experiments by Wirkner-Bott et al. [5] and Colwell [14], descriptions of the dispersion systems are available, but the level of detail, especially with regards to the dispersion nozzles, are not good enough for simulations without applying a fair bit of assumptions. As the argument for performing a dispersion simulation is to reduce uncertainties with regards to distribution and magnitude of turbulence, basing such a simulation on assumptions was not considered to be satisfactory.

The inability to define simulation scenarios and settings leading to a realistic representation of the experimental conditions indicates that the use of  $K_{St}$ -value, when presented on its own, is an insufficient measure for the reactivity of a dust cloud. It has been pointed out several times before that  $K_{St}$  only can be a valid measurement of the reactivity of a dust as long as the method for classification is standardized and reproducible [3]. To underline this insufficiency of  $K_{St}$  as a single nominator for expression of reactivity, we do not have to look further than to the article by Wirkner-Bott et al. [5], referred to many times in this thesis. In the experimental work described here, the two different levels of dust reactivity are represented by applying different time delays prior to ignition of clouds of the same dust. In that way allowing the turbulent dust/air mixture to calm, reducing the level of turbulence, in that way representing clouds of different reactivity. To ensure reproducibility of experimental work, a standardized definition of the  $K_{St}$ -value for the dust used should therefore be accompanied by detailed descriptions of the dispersion system used or descriptions of turbulence levels, thus allowing for a more precise representation of turbulence levels.

During the simulation and analysing of dust explosions, the deviations between simulated and experimental values were believed to be a consequence of different representation of initial turbulence parameters. The cell size was thought to be of influence, however due to the cell size applied being in correspondence with guidelines described in the FLACS Manual [18], and experiences of appropriate grid sizing for simulation of gas explosions, turbulence was accredited most influence. In light of the findings described in section 4.2.3, regarding the magnitude of grid dependency, the level of importance assigned to initial turbulence might need some revision. The level of turbulence prior to ignition is without a doubt of great importance, however the degree of sensitivity concerning grid and cell size had not been realized prior to the dust simulations. An investigative simulation applying a 0.05 core grid to the most agreeing simulation scenario for the 20 m<sup>3</sup> enclosure used by Colwell, indicates that further refinement of the applied core grid could lead to better correspondence between experimentally recorded and predicted values. Nonetheless, such continued grid refinement does need to be performed applying accurate representation of the dispersion process, in that way ensuring a realistic representation of the experimental conditions.

## 6 Conclusions

When using the Computational Fluid Dynamic simulator FLACS as a tool in the assessment of vented gas and dust explosions in empty geometries, the obtained predictions revealed quite varying levels of compliance compared to experimental results. The simulations were set up aiming to reproduce a realistic representation of the experimental conditions described for the physical tests. For most simulations, with an exception of experiments where acoustically enhanced combustion was present, the obtained predictions revealed a comparable pressure development to that recorded experimentally. The magnitude of predicted pressures did however not show good agreement for all of the simulations. Simulation settings giving the most agreeing predictions while at the same time representing a realistic scenario, where those using a geometry completely resolved on the grid and applying a core grid extended to include external regions in the direction of the flow. Extended core grid, and the application of a suitable cell size showed to be of particular importance with regards to an accurate prediction of the external phenomena associated with vented explosions. A realistic representation of the external explosion is in turn of great importance for the development of internal pressures. Consequently, the grid sensitivity tests revealed a strong grid dependency in precise predictions of both internal and external values.

The grid sensitivity tests also revealed a need for relatively small cell sizes in obtaining simulation results corresponding to explosion characteristics recorded during the experiments. The observed level of sensitivity to cell size was somewhat unexpected as applied core cell sizes in the various simulations were of little difference, and in compliance with recommendations in the FLACS Manual [18]. Despite this, significant differences were observed in the predicted values. Computational time associated with application of such fine grids, for geometries of sizes as those studied, causes significant time consumption running the simulations. Although inconvenient, such computational time might be manageable as long as the results are of satisfying accuracy. In other words, if similar simulations should be performed in commercial use, recommendations and guidelines must be precise enough to eliminate the need for elaborate grid sensitivity tests.

Most of the geometries evaluated in this thesis were of similar shape, however the proportions of the enclosures were not identical. Applying the same approach to the setup of grid dimensions therefore caused the various geometries to be resolved over an unlike number of grid cells. It was not possible to perform as extensive sensitivity tests for all the simulations as what was done for the most agreeing simulations. This was due to the long computation time associated with running simulations with geometries as those investigated while applying a very fine grid. The extent of the simulations performed as part of this thesis did therefore not serve as a sufficient basis for defining and proposing a common and satisfactory approach to the setup of the grid for scenarios as those investigated. It cannot be

disregarded that predictions of greater compliance to the experimental results might be achievable if further investigation and refinement of grid resolution and sizing was to be performed.

The lacking ability to reproduce acoustic waves, thus the inability to predict acoustically enhanced oscillatory combustion, was observed for several of the simulations. This type of combustion is not represented in all experimental scenarios involving gas. However, when present, the internal pressure peaks caused by such combustion are those of largest magnitude, thus representing the dimensioning over pressure. As a result, the lack to represent acoustically enhanced combustion must be regarded as an insufficiency, should the software be used for assessment of risks and hazards associated with vented gas explosions.

For simulations of dust explosions, the initial turbulence conditions were found to be of large importance for the predictions of explosion development and characteristics. As properties for turbulence conditions were not included in the description of the experimental work simulated, attempts were made to find a method of determining the turbulence conditions corresponding to the experiments. The methodology was however deemed unsuccessful when applied to the simulation investigated in this thesis. It was observed that even minor changes in the initial turbulence parameters gave changes in pressure development, thus underlining the importance of correct values in the representation of a realistic simulation scenario. The combination of strong grid dependency, and the lack of available descriptions of initial turbulence conditions for the experiments, complicated analysing and improvement of the simulations. Consequently, less accuracy was achieved for the dust explosion simulations. Investigative simulations did however indicate that corresponding predictions might be obtainable when adjusting the turbulence conditions and applying a suitable cell size.



# 7 Recommendations for further work

Should it be desirable to continue with investigations of the findings described in this thesis, it is recommended that such further studies are to be concentrated on the level of dependency to core cell size applied in the simulations. Initial work should be focused on simulations of vented gas explosions in enclosures of similar shapes as those used in this thesis, then proceed to investigate enclosures of other geometric configuration. The investigative simulation series should aim at developing a common approach for setting up a suitable grid resulting in accurate predictions. It is recommended that such an approach is proposed prior to attempts to further pursue and evaluate the case of vented dust explosions. This is due to the large effects of adjustments to the initial turbulence, and the increased complexity this represents in evaluation of sensitivity to adjustments in grid, should there be inaccuracies in the representation of initial turbulence.

Existing publications rarely include sufficient experimental data necessary for setting up simulation scenarios, thereby invoking the need for assumptions. This subsequently leads to uncertainties with regards to the accuracy of the simulations. Should a further study of the subject be performed, it would be recommended that this is to be based upon experimental work intended to serve as data basis for simulations. This is regarded as especially important in the case of dust simulations, as these proved to be sensitive to initial turbulence conditions. Should however, descriptions of turbulence conditions be excluded from the experimental data, it would be recommended to carry out a dispersion simulation, in that way hopefully obtaining more realistic initial conditions.

In an effort to improve and expand the applicability of the software it is recommended that a continued development is to be carried out, focusing on reducing the strong grid dependency observed in the simulations carried out in this thesis. A further recommendation is that the continued development of the software also should implement a solution allowing adequate representation of acoustic waves and the effects these can inflict on the applied simulations scenario. By implementing these improvements, the software would represent an even better tool in risk and safety assessments.

# References

- [1] Harrison, A.J. and J.A. Eyre, *External explosions as a result of explosion venting*. Combustion Science and Technology, 1987. **52**(1-3): p. 91-106.
- [2] Eckhoff, R.K., *Explosion hazards in the process industries*. 2005, Houston, Tex: Gulf Publishing.
- [3] Eckhoff, R.K., *Dust explosions in the process industries*. 3rd ed. ed. 2003, Amsterdam: Gulf Professional Publishing.
- [4] FlowSeal and Engineering. *Diagram, Pressure Characteristics of Vented Explosion*. 2015, <http://flowseal.co.za/explosionpanels3.php>. [cited 2016 18.03.2016].
- [5] Wirkner-Bott, S.S., M. Stock, *Flammen- und Druckwirkung bei Explosionsdruckentlastung*. VDI-Besichte, 1992. **975**: p. 185-305.
- [6] Verein Deutscher Ingenieure, V., *VDI 3673 Part 1 - Pressure venting of dust explosions*. 2002, Verein Deutscher Ingenieure.
- [7] European Committee for Standardization, C., *EN 14034-1 Determination of explosion characteristics of dust clouds - Part 1*. 2004.
- [8] European Committee for Standardization, C., *EN 14034-2 Determination of explosion characteristics of dust clouds - Part 2: Determination of the maximum rate of explosion pressure rise  $(dP/dt)_{max}$  of dust clouds*. 2006.
- [9] Crowhurst, D., Colwell, S.A., Hoare, D.P., *The external explosion characteristics of vented dust explosions*. IChemE Symposium Series 139, 1995: p. 79-96.
- [10] Cooper, M.G., M. Fairweather, and J.P. Tite, *On the mechanisms of pressure generation in vented explosions*. Combustion and Flame, 1986. **65**(1): p. 1-14.
- [11] Wingerden, K.v., *Counsel in connection with thesis*, M.-J. Klausen, Editor. 2015-2016.
- [12] van Wingerden, K., *On the venting of large-scale methane air explosions*. Loss Prevention and Safety Promotion in the Process Industries, 1989: p. 25-1 - 25-15.
- [13] van Wingerden, K., *Venting of Gaseous Explosions*, Master of Science thesis, *Faculteit der technische natuurkunde*. 1991, Technische Universiteit Delft.
- [14] Colwell, S., *The characterisation of vented dust explosions and their effect on structures*. Doctor of Philosophy thesis, 2000, South Bank University, London.
- [15] European Committee for Standardization, C., *BS EN 14491 Dust explosion venting protective systems*. 2012, BSI Standards Publication.
- [16] van Wingerden, K., *Prediction of pressure and flame effects in the direct surroundings of installations protected by dust explosion venting*. Journal of Loss Prevention in the Process Industries, 1993. **6**(4): p. 241-249.
- [17] Harmanny, A., *Pressure effects from vented dust explosions*. VDI-BERICHT nr. 1601, 2001: p. 539-550.
- [18] Gexcon AS, *FLACS v10.4 User Manual*.
- [19] Hagen, J.-T.G., *Counsel in connection with thesis*, M.-J. Klausen, Editor. 2015-2016.
- [20] Hisken, H., *Counsel in connection with thesis*, M.-J. Klausen, Editor. 2015-2016.
- [21] Mercx, W.P.M., C.M. van Wingerden, and H.J. Pasman, *Venting of gasous explosions*. Institution of Chemical Engineering Symposium, 1992.
- [22] Dragosavic, M.I., *Structural measures against natural-gas explosions in high-rise blocks of flats*. Heron, 1973. **19**(No. 4).
- [23] Narasimhamurthy, V.D., *Presentation on effect of geometry and grid on turbulence modelling - Commercial in confidence* 2015, Gexcon AS: Confidential - Unpublished.
- [24] Puttock, J., D. Chakraborty, and W. Farmayan, *Gas explosion modelling using PDRFoam*, in *International Symposium on Hazards, Prevention, and Mitigations of Industrial Explosions*. 2014.
- [25] Skjold, T., *Review of the DESC project*. Journal of Loss Prevention in the Process Industries, 2007. **20**(4): p. 291-302.